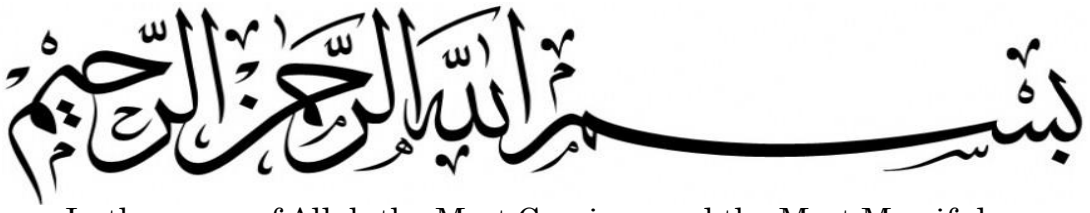

In the name of Allah the Most Gracious and the Most Merciful

Alteration in ambipolar characteristic of graphene after interaction with radical oxygen and ferritin

(ラジカル酸素およびフェリチンとの相互作用による
グラフェンのアンビポーラ特性変化)

Yana Mulyana

2016 年 3 月 17 日

奈良先端科学技術大学院大学

物質創成科学研究科　情報機能素子科学研究室

I bear witness that there is no God but Allah,
and I bear witness that Muhammad is His Messenger

Alteration in ambipolar characteristic of graphene after interaction with radical oxygen and ferritin

(ラジカル酸素およびフェリチンとの相互作用による
グラフェンのアンビポーラ特性変化)

LIST OF CONTENTS

LIST OF CONTENTS I

ACKNOWLEDGMENTS V

CHAPTER 1

Introduction 1

1.1. Background 2

1.2. Objectives 5

1.3. Outline 8

Reference 10

CHAPTER 2

Graphene and oxygen: oxidation of graphene and its thermal reduction 14

2.1. Background 14

2.2. UV/O_3-treatment 16

2.3. H_2/Ar-annealing 16

2.4. Preparation of graphene 17

2.5. Experiment 18

2.6. Result and discussion 20

2.6.1. XPS measurement 20

2.6.2. Ambipolar characteristics measurement 22

2.6.2.1. First redox reaction 22

2.6.2.2. Second redox reaction 26

2.6.3. Raman spectroscopy measurement 29

2.6.4. Contact resistance 31

2.7. Conclusion 32

2.8. Next task 33

References 34

CHAPTER 3

Graphene and oxygen: oxidation of graphene and its non-thermal reduction 37

3.1. Background 38

3.2. Experimental 40

3.3. UV/O_3-treatment and UV irradiation 42

3.4. Result and discussion 43

3.4.1. STM observation 43

3.4.2. XPS measurement 45

3.4.3. Electrical characteristics measurement 52

3.4.3.1. FET fabrication and electrical characterization setup 52

3.4.3.2. Ambipolar characteristics 54

3.4.3.3. Electron mobility and redox mechanism 56

3.4.4. Raman spectroscopy measurement 61

3.5. Conclusion 59

References 66

CHAPTER 4

Graphene and ferritin: construction of p-n junction on graphene 72

4.1. Background 73

4.2. Experiment 76

4.3. Result and discussion 79

4.3.1. Interaction between graphene and ferritin measured in water 79

4.3.1.1. Graphene and apoferritin in water 79

4.3.1.2. Graphene and iron-cored ferritin in water 84

4.3.2. Interaction between graphene and electron beam 88

4.3.3. Interaction between graphene and ferritin measured in vacuum 92

4.3.3.1. Graphene and apoferritin in vacuum 93

4.3.3.2. Graphene and iron-cored ferritin in vacuum 98

4.4. Conclusion 106

References 107

CHAPTER 5

Graphene and Escherichia coli: sensitivity of graphene 110

5.1. Background 110

5.2. Experiment 112

5.3. Result and discussion 113

5.4. Comparison with ferritin 118

5.5. Comparison with radical oxygen 120

5.6. Effect of electron beam irradiation 121

5.7. Conclusion 123

References 124

CHAPTER 6

General conclusion 125

6.1. Interaction with radical oxygen 125

6.2. Interaction with ferritin 126

6.3. Interaction with E. coli 127

6.4. Future task 127

Appendix 128

Acknowledgements

First of all, I would like to praise The Almighty Allah for guiding and establishing me to complete this work. All Praise is due to Allah سبحانه و تعالى, and may peace be upon the Last Prophet, Muhammad صلى الله عليه وسلم, his family, and his Companions. Secondly, I would like to thank both my parents for giving me the true foundation in education and life. This research was conducted with the supervision and the help of several individuals who in one way or another contributed and extended their valuable assistance in the preparation and completion of this research.

I would take this opportunity to express my sincere thanks to Professor Yukiharu Uraoka for providing me with all the necessary facilities and the continuous support of this study. I also place on record my sincere gratitude to Professor Ichiro Yamashita. I am extremely grateful and indebted to him for his patience, expert, immense knowledge and encouragement extended to me. His guidance helped me in all the time of research and writing of this thesis and other publications.

I would like to thank as well Associate Professor Yasuaki Ishikawa for his valuable advice, support and constant supervision and encouragement. I would also like to convey thanks to Associate Professor Takashi Tokuda for fruitful discussions and for giving me useful advice after every evaluation meeting.

My sincere thanks is extended to Assistant Professor Mutsunori Uenuma for numerous stimulating discussions, help with experimental setup and general advice. My sincere thanks also goes to all the members of Information Device Science Laboratory for their help and encouragement. I would like also to express my sense of gratitude to one and all who, directly or indirectly, have lent their helping hand in this study.

CHAPTER 1

Introduction

Experimental investigations regarding the interaction between graphene and oxygen; interaction between graphene and ferritin (spherical protein shell); and interaction between graphene and Escherichia coli (E. coli) are presented in this research. The interactions between graphene and three materials mentioned above are examined from graphene-based field effect transistor's (G-FET's) electrical characteristics point of view. This kind of investigations is a fundamental issue in fully understanding the electrical properties and bio-compatibility of graphene, which is essential in the realization of graphene-based electronics in the future.

Graphene is entirely made of carbon atom and known to be sensitive to charged materials. Therefore, graphene is expected to be a promising candidate for sensing device development, especially for bio-sensors since most of living organism are largely consisted of carbon atoms also. However, in the realization of graphene-based sensing electronics such as bio-sensor, some criteria like chemical stability; and sensitivity and bio-compatibility are ones of many criteria required to be fulfilled and systematically

studied. In this experimental investigation, both chemical stability; and sensitivity and bio-compatibility were evaluated by examining the alterations in ambipolar characteristic of graphene. The chemical stability of graphene was investigated by evaluating the alteration of graphene's ambipolar characteristic after being doped with radical oxygen and consecutively irradiated by high energy ultraviolet lights. In regard to sensitivity and bio-compatibility, the evaluation was performed by examining the alteration of graphene's ambipolar characteristic after the adsorption of bio-materials like ferritin and E. coli onto the graphene surface.

1.1. Background

Graphene is one-atom thick carbon layer whose atoms arranged in a regular hexagonal lattice. Graphene was deemed a merely academic material for many years.[1] Older theoretical prediction, presumed graphene would be unstable in reality due to thermal fluctuations.[2] This assumption was supported by various experiments with thin layer which became unstable as the thickness was decreased.[2] The fundamental works by Geim and Novoselov demonstrated the isolation of thin carbon films and eventually graphene by simply using scotch tape, widely known as the mechanical exfoliation

method,[3,4] and now graphene has emerged as a real sample. Recent progresses in researches of graphene have ignited intense activities to explore the electronic properties of this novel two-dimensional electronic system.[5] The impressive properties such as the linear energy dispersion relation near the charge neutrality point or the Dirac point in the electronic band structure, high transparency and flexibility, high field-effect charge mobility and carrier velocity at room temperature make graphene a possible candidate for novel electronic devices in the future.[6,7]

Valence and conduction in graphene are degenerated at 6 points located on the corners of the Brilloiun zone.[1] The Fermi surface in graphene is compacted to a zero dimension zone composed of 6 points on its Brillouin zone. Therefore, graphene is commonly known as semi-metal material or zero-gap semiconductor. The low energy dispersion near the Fermi level exhibits a circular conical shape.[1,4] As a result, charge carriers in graphene exhibit linear energy-momentum dispersion, as if they were massless relativistic particles. Charge carriers in graphene can behave as massless Dirac fermions with an effective Fermi velocity which is 300 times smaller than the speed of light.[4] That is way graphene-based devices have extremely high carrier mobility and can operate on a high frequency. This also makes graphene a reliable system for researching quantum

electrodynamics phenomena, a discipline of theoretical and experimental investigations which was previously limited to particle physics and cosmology investigation.

It is important to notice that many claims have been made for future application built out of graphene as well as of other well-known carbon nanostructure such as graphene oxide, graphene nano ribbon, carbon nano tube, fullerene and so on. However, most of the promise of these carbon materials have not been manufactured in form of real application yet. Some of the biggest challenges are the synthesis and modification of graphene, and the formation into atomically precise structures with high degrees of reproducibility. The most widely used method to synthesize graphene is chemical vapor deposition (CVD).[8] CVD method has many variation and is commonly applied to synthesize graphene on transition metal substrate such as copper, nickel, iridium and ruthenium, as well as on dielectric substrate such as sapphire and other various oxides.[8-13] On other hand, the graphene exfoliation from graphite bulk is an easy production and a low cost method. The variations of this technique include mechanical exfoliation, ultrasonic treatment in solution, intercalation step, and reduction process of graphene oxide.[3,14,15]

Besides its exceptional physical and electronic properties described above, being an extremely thin film, graphene is expected of being sensitive to electrical charged

stimulation as well as mechanical, physical and chemical stimulant. This property opens a new opportunity for graphene to be utilized as sensing material. Large surface-to-volume ratio, unique optical properties, excellent electrical conductivity, high carrier mobility and density, high thermal conductivity and many other properties can make graphene a very promising candidate a sensor material. The large surface area of graphene will enable the fabrication of wide detection area for desired targets, and exceptional conductivity is beneficial for conducting electrons between the target and electrode. Since graphene is entirely made of carbon atoms, it is expected to have a superior bio-compatibility, thus expected to be a suitable material for bio-sensor.

1.2. Objectives

Inspired by potential future application such ultra-high frequency transistor,[16] flexible displays, [17] solar cells, [18] and so on, a lot of research is being devoted to understand and modify the main physical properties of graphene. Generally, graphene can be mass-produced by CVD method of methane gas or by reducing graphene oxide which was obtained by chemically exfoliating natural graphite.[19] Similar to graphene, graphene oxide also offers a wide range of application possibilities e.g. on sensor technology,

energy-related material, biomedical use etc.[20] Since the epoxide bridge in graphene oxide has greater reactivity comparing to the firm chemical stability in sp^2 bond in graphitic structures of graphene, graphene oxide is also often used as a transitional phase in a series of chemical reactions to modify graphene with various functional groups.[21] Thus, judging from the close relationship between graphene and graphene oxide in term of fabrication, chemical and electrical characteristics, and application as well, we consider that it is very important thoroughly and systematically investigate the interaction between graphene and oxygen from chemical and electrical characteristics point of view. This is the motivation of our first investigation.

Second investigation dealt with the interaction between graphene and ferritin. Graphene is a very promising material to be used as sensing material, especially for bio-sensor. Graphene is extremely thin material, thus it makes graphene very sensitive to various impulses. Moreover, since graphene is entirely made of carbon atoms, it is expected to have a superior bio-compatibility, thus expected to be a suitable material for bio-sensor. However, to fully utilize the potential of graphene in the realization of graphene-based bio-sensors, it is considered essential to systematically investigate the interaction between graphene and bio-molecule.

In this investigation, as an instance of bio-molecule, spherical protein shell called ferritin was used. The structural stability, assembly properties, and capability to store a huge variety of cores make ferritin a promising element in nano-engineering.[22-30] Ferritin is entirely consisted of protein, and proteins are the key working molecules and building blocks in all living cells. Most of living organisms are largely composed of protein. Since the size of ferritin is around 12 nm, ferritins are barely observable through a scanning electron microscope (SEM), which makes ferritin relatively easy to utilize in nano-engineering fields. Recently, ferritin has been utilized in the construction of various nano-structure materials used in the fabrication of conducting, semiconducting, and magnetic nano-material. The structural stability, assembly properties, and capability to store a huge variety of cores make ferritin a promising element in nano-engineering for constructing advance electronics. [22-30] This is the reasons why the interaction between graphene and ferritin needs to be investigated, especially when it comes to the realization of organic electronics that are based on G-FET

The third investigation dealt with the interaction between graphene and E. coli. Some distinct variations of E. coli can cause serious food poisoning in their hosts, and are occasionally responsible for product recalls due to food contamination. The likely source of the E. coli is not the fruit & vegetable waste, but disposable diapers or human excretion

that are poorly treated in the mixed waste stream. As a first step in developing more sophisticated bio-sensors based on G-FET that can detect harmful organisms such as E. coli, the interaction between graphene and E. coli needs to be systematically investigated. This is the objective of the third investigation, which is to investigate the interaction between graphene and E. coli.

1. 3. Outline

In chapter 2, an experimental investigation regarding the interaction between graphene and oxygen is presented. In this chapter, changes in electrical properties of a graphene-based field-effect transistor (G-FET) after being oxidized and then consecutively reduced are discussed. The oxidation was performed through ultraviolet (UV)/ozone (O_3) treatment and the reduction of the resulted graphene oxide was conducted through H_2/Ar annealing. A decrease in carrier mobility was observed after oxidation. However, electrical properties recovered after reduction, indicating that oxidation with UV/O_3 treatment was thermally reversible.

Chapter 3 also deals with an experimental investigation regarding the interaction between graphene and oxygen. In this chapter, like in the previous chapter, changes in

electrical properties of a G-FET after being oxidized and then consecutively reduced are discussed. However, while the oxidation was performed through UV/O_3-treatment, like in the previous chapter, the reduction of the resulted graphene oxide was conducted through UV-irradiation. The electron mobility of G-FETs decreased after oxidation; however, it recovered after irradiating the oxidized G-FETs with UV-lights, indicating that GO was successfully reduced non-thermally through UV-irradiation. We concluded that UV/O_3-treatment produced chemically homogeneous GO which is non-thermally reversible through UV-irradiation, and changes in the electron mobility were non-thermally reversible also.

In chapter 4, an experimental investigation regarding the interaction between graphene and ferritin is presented. Native ferritins are negatively charged, however we found that native negatively-charged ferritins became positively-charged after performing electron beam (EB)-irradiation. We utilized this property to construct a p-n junction on G-FET. The produced G-FET can also operate through water-gate. We found also that EB-irradiation could remove the effect of charged impurity absorbed on graphene layer, thus the Dirac point was adjusted to gate voltage Vg = 0. The investigation of the interaction between graphene and bio-molecules such as ferritin is a fundamental issue in

understanding the bio-compatibility of G-FET, which is essential in the realization of graphene-based bio-sensors.

In chapter 5, the interaction between graphene and E. coli bacteria was discussed. The changes in ambipolar characteristics of six G-FETs before and after the adsorption of E. coli bacteria were evaluated. The Dirac point of all the devices shifted positively, indicating that E. coli was negatively charged and this particular negative charge caused the ambipolar curve to positively shift. The minimum shift of Dirac point was 20 V, and the maximum shift was beyond 40 V. The Dirac point shift of the remaining devices was around 30 V. We expected that these data would benefit the more systematic investigation of the sensitivity of biosensors based on G-FETs.

References:

1) P. R. Wallace, Phys. Rev. 71, 622 (1947).
2) Mermin, N. D. 1968. Crystalline order in two dimensions. Physical review 176: 250.
3) Novoselov, K. S.; Geim, A. K.; Morozov, S. V.; Jiang, D.; Zhang, Y.; Dobunos, S. V.; Grigorivera, I. V.; Firsov, A. A. Electric field effect in atomically thin carbon films. Science 2004, 306: 666.
4) Novoselov, K. S.; Geim, A. K.; Morozov, S. V.; Jiang, D.; Katsnelson, M. I.; Grigorivera, I. V.; Dobunos, S. V.; Firsov, A. A. Two-dimensional gas massless Dirac

fermions in graphene. Nature 2005, 438, 197-200.

5) Lin, Y. -M.; Dimitrakopoulos, C.; Jenkins, K. A.; Farmer, D. B.; Chiu, H. -Y.; Grill, A.; Avouris, P. 100-Ghz transistors from water-scale epitaxial graphene. Science 2010, 327, 662.

6) Kim, K. S.; Zhao, Y.; Jang, H.; Lee, S. Y.; Kim, J. M.; Kim, K. S.; Ahn, J. -H.; Kim, P.; Choi, J. -Y.; Hong, B. H. Large-scale pattern growth of graphene films for stretchable transparent electrodes. Nature 2009, 457, 706-710.

7) De Arco, L. G.; Zhang, Y.; Schlengker, C. W.; Ryu, K.; Thompson, M. E.; Zhou, C. Continuous, highly flexible, and transparent graphene films by chemical vapor deposition for organic photovoltaics. ACS Nano 2009, 4, 2865.

8) Li, X.; Cai, W.; An, J.; Kim, S.; Nah, J.; Yang, D.; Piner, R.; Velamakanni, A.; Jung, I.; Tutuc, E.; Banerjee, S. K.; Colombo, L.; Ruoff, R. S. Large-area synthesis of high-quality and uniform graphene films on copper foils. Science 2009, 324, 1313-1314.

9) Li, X.; Magnuson, C. W.; Venugopal, A.; An, J.; Suk, J. W.; Han, B.; Borysiak, M.; Cai, W.; Velamakanni, A.; Zhu, Y.; Fu, L.; Vogel, E. M.; Voelkl, E.; Colombo, L.; Ruoff, R. S. Graphene films with large domain size by a two-step chemical vapor deposition process. Nano Letters 2010, 10 (11), 4328-4334.

10) Hamilton, J. C.; Blakely, J. M. Carbon segregation to single crystal surfaces of Pt, Pd and Co. Surface Science 1980, 91 (1), 199-218.

11) Wu, W.; Liu, Z.; Jauregui, L. A.; Yua, Q.; Pillai, R.; Cao, H.; Bao, J.; Chen, Y. P.; Pei, S. -S. Wafer-scale synthesis of graphene by chemical vapor deposition and its application in hydrogen sensing. Sensor and Actuators B 2010, 150, 296-300.

12) Obraztsova, A. N.; Obraztsova, E. A.; Tyurnina, A. V.; Zolotukhin, A. A. Chemical vapor deposition of thin graphite films of nanometer thickness. Carbon 2007, 45, 2017-2021.

13) Yu, Q.; Lian, J.; Siriponglert, S.; Li, H.; Chen, Y. P.; Pei, S. -S. Graphene segregated on Ni surfaces and transferred to insulators. Applied Physical Letters 2008, 93, 113103-1-3.

14) Hernandez, Y.; Nicolosi, V.; Lotya, M.; Blighe, F. M.; Sun, Z.; De, S.; McGovern, I. T.; Holland, B.; Byrne, M.; Gun'Ko, Y. K.; Boland, J. J.; Niraj, P.; Duesberg, G.; Satheesh, K.; Goodhue, R.; Hutchison, J.; Scardaci, V.; Ferrari, A. C.; Coleman, J. N. High-yield production of graphene by liquid-phase exfoliation of graphite. Nature Nanotechnology 2008, 3, 563-568.

15) Zhu, J. New solutions to a new problem. Nature Nanotechnology 2008, 3, 528-529.

16) Wu, Y.; Lin, Y.; Bol, A. A.; Jenkins, K. A.; Xia, F.; Farmer, D. B.; Zhu, Y.; Avouris, P. High-frequency, scaled graphene transistors on diamond-like carbon. Nature 2011, 472, 74–78.

17) Polat, E. O.; Balci, O.; Kakenov, N.; Uzlu, H. B.; Kocabas, C.; Dahiya, R. Synthesis of large area graphene for high performance in flexible optoelectronic devices. Scientific Reports 2015, 5, 16744.

18) Park, H.; Rowehl, J. A.; Kim, K. K.; Bulovic, V.; Kong, J. Doped graphene electrodes for organic solar cells. Nanotechnology 2010, 21, 50.

19) Yu, Q.; Lian, J.; Siriponglert, S.; Li, H.; Chen, Y. P.; Pei1, S. -S. Graphene Segregated on Ni Surfaces and Transferred to Insulators. Appl. Phys. Lett. 2008, 93, 113103.

20) Chung, C.; Kim, Y. -K.; Shin, D.; Ryoo, S. -R.; Hong, B. H.; Min, D. -H. Biomedical Applications of Graphene and Graphene Oxide. Acc. Chem. Res. 2013, 46, 2211-2224.

21) Shen, B.; Zhai, W.; Tao, M.; Lu, D.; Zheng, W. Chemical Functionalization of Graphene Oxide toward the Tailoring of the Interface in Polymer Composites. Composites Science and Technology 2013, 77, 87-94.

22) Xu, D.; Watt, G. D.; Harb, J. N.; Davis, R. C. Electrical Conductivity of Ferritin Proteins by Conductive AFM. Nano Lett. 2005, 5 (4), 571–577.

23) Yamashita, I.; Iwahori K.; Kumagai S. Ferritin in the field of nanodevices. Biochim Biophys Acta. 2010, 1800 (8), 846-857.

24) Okuda, M.; Iwahori, K.; Yamashita, I.; Yoshimura, H. Fabrication of nickel and chromium nanoparticles using the protein cage of apoferritin. Biotech. Bioeng. 2003, 84 (2), 187-194.

25) Wong, K.; Mann, S. Biomimetic synthesis of cadmium sulfide-ferritin nanocomposites. Adv. Mater. 1996, 8, 928.

26) Awschalom, D. D.; Smyth, J. F.; Grinstein, G.; DiVincenzo, D. P.; Loss, D. Macroscopic quantum tunneling in magnetic proteins. Phys. ReV. Lett. 1992, 68 (20), 3092-3095.

27) Hilty, S.; Webb, B.; Frankel, R. B.; Watt, G. D. Iron core formation in horse spleen ferritin: Magnetic susceptibility, pH, and compositional studies. J. Inorg. Biochem. 1994, 56 (3), 173-185.

28) Tejada, J.; Zhang, X. X.; del Barco, E.; Hernandez, J. M. Macroscopic Resonant Tunneling of Magnetization in Ferritin. Phys. Rev. Lett. 1997, 79 (9), 1754-1757.

29) Harris, J. G. E.; Grimaldi, J. E.; Awschalom, D. D.; Chiolero, A.; Loss, D. Excess

Spin and the Dynamics of Antiferromagnetic Ferritin. Phys. Rev. B 1999, 60 (5), 3453-3456.

30) Mamiya, H.; Nakatani, I.; Furubayashi, T. Reexamination of macroscopic quantum tunnelling observed in ferritin: magnetic field dependence of magnetic relaxation. Supperlattices Microstruct. 2002, 32 (4-6), 179-186.

CHAPTER 2

Graphene and oxygen:

Oxidation of graphene and its thermal reduction

In this chapter, changes in electrical properties of a bilayer graphene-based field-effect transistor (G-FET) after being oxidized through ultraviolet (UV)/ozone (O_3) treatment are presented. A decrease in conductivity and carrier mobility was observed after oxidation. However, electrical properties recovered after annealing oxidized G-FET with H_2/Ar, indicating that oxidation with UV/O_3 treatment was thermally reversible. Raman spectroscopy was conducted to verify that no defects were introduced after oxidation. The existence of chemical bonds between oxygen and graphene was confirmed from the X-ray photoelectron spectroscopy. Moreover, we found that graphene's sheet resistance increased after oxidation. Nevertheless, contact resistivity at graphene-Au/TiN electrode interface remained unchanged.

2.1. Background

Graphene holds great promise to be applied in next-generation electronics because of its exceptional physical and electronic properties i.e. high field-effect charge mobility as high as 15,000 cm^2/Vs at room temperature.[1–3] Significant research activities in the field of chemical

functionalization of graphene have been actively pursued in efforts to explore and modify its properties. [4,5] An alternative approach has recently been reported for oxidizing graphene using reactive atomic oxygen in an ultrahigh vacuum to form chemically homogeneous and thermally reversible graphene oxide (GO).[6] Indeed, the chemical functionalization of graphene can be a way of improving the performance of graphene-based devices,[7–9] and ultraviolet (UV)/ozone (O_3) treatment is considered to be a promising route to enhance the weak chemical reactivity of graphitic structures.[10–12] Nevertheless, changes in the electrical properties of graphene after being oxidized are still seldom studied and remain to be fully investigated.

Changes in electrical properties of bilayer graphene, such as its conductivity and carrier mobility, after being oxidized through UV/O_3 treatment and the mechanism are presented. The electrical properties of graphene were evaluated by measuring the current-gate voltage (I_d-V_g) characteristics of graphene-based field-effect transistors (G-FETs). The thermal reversibility of the oxidation process was also investigated by conducting H_2/Ar anneal treatment. Raman spectroscopy measurements were carried out after each process of oxidation and reduction to find whether the processes introduced any significant defects into graphene lattice. The existence of chemical bonds between oxygen and carbon atoms (C-O) in graphene layer was proven by performing X-ray Photoelectron Spectroscopy (XPS) measurements of chemically vapor deposited (CVD)-graphene. Finally, graphene's sheet resistance and contact resistance at graphene-electrode interface were examined using the transfer length method (TLM).[13]

2.2. UV/ O_3-treatment

UV/ O_3 treatment is commonly performed by placing samples on a hot plate in a chamber where the samples are irradiated with ultraviolet light. Simultaneously, O_3 gasses are introduced into the chamber and exhausted. In this experiment, the UV/ozone treatment was performed using Samco UV-1 cleaning system where the graphene-based FET was treated for 3 minutes and the hot plate temperature was set to 25^{o}C. In this equipment, oxygen gasses are channeled into the chamber at a flow rate of 0.5 L/min and simultaneously two types of ultraviolet light with wavelengths of 184.9 nm and 253.7 nm are produced from a low pressure mercury lamp. Ultraviolet rays with a wavelength of 184.9 nm decompose one O_2 molecule into two more reactive O atoms. With a certain probability, one O atom can react with one O_2 molecule to form one O_3 molecule. However, ultraviolet rays with a wavelength of 253.7 nm decompose one O_3 molecule into three more O atoms so that eventually reactive O atoms are produced inside the chamber.

2.3. H_2/Ar annealing

H_2/Ar annealing is commonly performed by placing samples inside a tube furnace where the samples are heated under a reducing atmosphere. Simultaneously H_2 and Ar gasses are introduced into the chamber and exhausted. Actively reducing gas such as H_2 is introduced in

order to create a reducing atmosphere and inert gas such as Ar is introduced in order to prevent reaction between the samples and oxygen. In this experiment, H_2/Ar annealing was performed on KOYO KTF030N1/035N1 annealing furnace in which the graphene-based FET was annealed at a temperature of $300^{O}C$ for 2 hours and H_2 and Ar gasses are simultaneously channeled into the tube furnace at a flow rate of 200 sccm.

2.4. Preparation of graphene

In this study, graphene was prepared by using a mechanical exfoliation technique, shown in Fig. 1, well known as the scotch tape method which was invented by Andre Geim and Konstantin Novoselov.[14] The method is as follows:

i. Place a thin graphite flake onto adhesive scotch tape surface.

ii. Take the two edges of the scotch tape and fold them together, thereby causing the whole piece of tape to stick to each other.

iii. Peel the folded tape, and repeat the process several times, until a faint gray cloud can be observed on the tape.

iv. Place the tape with thin graphite on SiO_2/Si wafer and gently rub the tape using an electric toothbrush for three minutes so that the graphene layer is transferred onto SiO_2 surface.

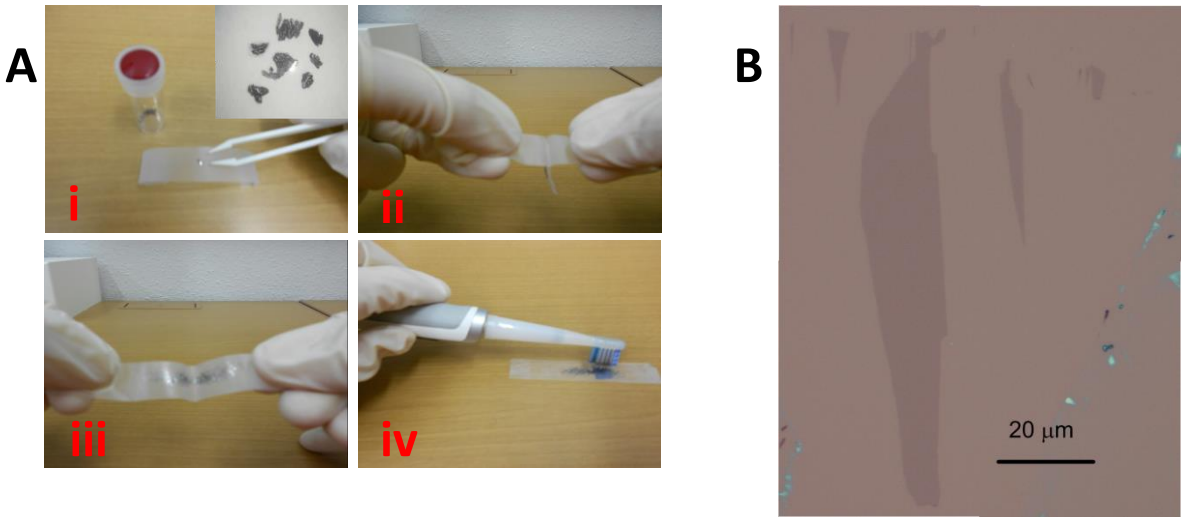

Fig. 1. Mechanical exfoliation technique well known as the scotch tape method (A) and optical microscope image of graphene prepared by the scotch tape method (B). The contrast between reflected light from the graphene and the substrate in optical microscope images increases as the layer number increases

2.5. Experiment

A bilayer G-FET that was 10 μm long and 3 μm wide was used in this experiment. The bilayer graphene was transferred onto a 100-nm SiO_2/p^+-Si substrate using the micromechanical cleavage of Kish graphite.[14] The number of layers was determined by optical contrast and Raman spectroscopy.[15] The G-FET was fabricated by using photolithography to print source/drain patterns onto both ends of the graphene layer and depositing Au/TiN (100/50 nm)

metals with a process of electron beam vapor deposition followed by a lift-off process in acetone for 10 min. A bottom-gate was constructed by attaching a Cu plate onto the bottom of SiO_2/Si substrate using silver paste, after lower SiO_2 layer of the substrate was removed with buffered hydrofluoric acid solution. Electrical characterization was carried out under vacuum conditions of 4.6 x 10^{-5} Pa using a nano-probing microscopy (Hitachi NE4000).

The G-FET was oxidized with UV/O_3 treatment and then reduced by H_2/Ar annealing. The UV/O_3 treatment was performed using a UV/O_3 cleaning system where the G-FET was treated for 3 min and the hot plate temperature was set to 25ºC. Oxygen gasses in this equipment were channeled into the chamber at a flow rate of 500 cm^3/min and two types of UV light with wavelengths of 184.9 nm and 253.7 nm were simultaneously produced from a low pressure mercury lamp so that reactive oxygen atoms were eventually produced inside the chamber. The H_2/Ar anneal treatments were undertaken in a tube annealing furnace in which the G-FET was annealed at a temperature of 300ºC for 2 h and H_2 and Ar gasses were simultaneously channeled into the tube furnace at a flow rate of 200 cm^3/min. Actively reducing gas such as H_2 was introduced to create a reducing atmosphere and inert gas such as Ar was introduced to prevent reactions between the samples and oxygen. Raman spectroscopy measurements were carried out after each process to determine whether the oxidation and reduction processes had introduced any significant defects into graphene lattice using ~1 mW of 514.5 nm light from an Ar laser.[16,17] The beam's spot size was ~1 μm.

Another experiment in which XPS spectra of oxidized CVD-graphene were measured was conducted to investigate whether oxygen atoms chemically reacted with carbon atoms of graphene. Since the area of graphene exfoliated with micromechanical cleavage was too small to be measured in the XPS spectrometer,[14] CVD-graphene, which is graphene grown on Cu foil with CVD and has a relatively large area, was used in this experiment. The oxidized CVD-graphene was then annealed with H_2/Ar and its XPS spectra were measured. The pass energy was 40 eV and the anode HT was 15 kV. The step energy resolution was ~20 meV. The contact resistance and sheet resistance of graphene before and after oxidation were determined using the TLM.[13] Three-layered graphene with four Au/TiN-electrodes was used in these measurements.

2.6. Result and discussion

The feasibility of redox reaction of graphene was evaluated from XPS, Raman spectroscopy, electrical properties and electrical characteristics of G-FET point of view.

2.6.1. XPS measurement

The XPS spectra of pristine CVD-graphene after oxidation and reduction are shown in Fig. 2, where an additional peak emerged as a result of oxidation. This peak can be attributed to the C-O bond from its energy binding.[18] This may be evidence that reactive oxygen atoms

chemically reacted with carbon atoms of graphene during UV/O_3 treatment to form epoxide groups, resulting in a GO layer. Other oxygen functional groups were not detected from this XPS measurement. The peak vanished after H_2/Ar annealing, indicating that C-O bonding had broken and CVD-graphene layer recovered to its pristine order as a result of reduction done by H_2/Ar annealing.[6]

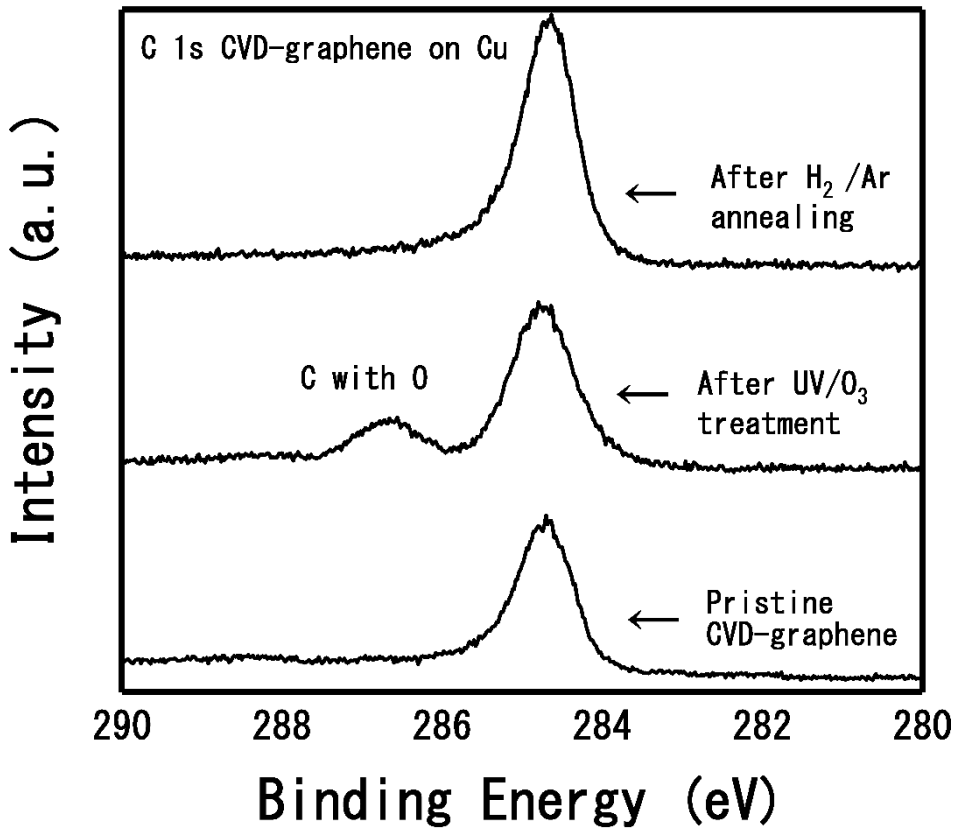

Fig. 2. C 1s XPS spectra of pristine CVD-graphene after being oxidized and then annealed.

The Hummers method is widely used for oxidizing graphene. Aggressive acidic treatments are used in this method, resulting in a chemically inhomogeneous surface with a range of oxygen functional groups, such as carboxylic, hydroxyl and carbonyl groups, and structural defects that degrade the charge mobility and compromise its usability in high-performance devices.[6,19] On the other hand, oxidation by UV/O_3 treatment produced reversible and homogeneous GO with only functional group of epoxide without any structural defects. Several ways of reducing GO have been reported, including that in which excimer laser was used. However, because of the high fluence, excimer laser radiation fragmented graphene sheets into smaller flakes.[19] On the contrary, reduction of GO through H_2/Ar annealing can still maintain graphene layer perfectly intact without any structural defects.

2.6.2. Ambipolar characteristics

To provide a deeper insight into the reversibility of redox reaction on graphene, electrical characterization was performed after conducting redox reaction on the G-FET twice.

2.6.2.1. First redox reaction

The G-FET's I_d-V_g characteristics after the first oxidation through UV/O_3 treatment are plotted in Fig. 3. Prior to that, the G-FET was cleaned through H_2/Ar annealing. The ambipolar curve shifted downward after oxidation, from curve No. 1 to No. 2, suggesting decreased

conductivity. The carrier mobility slightly decreased from 2500 to 2100 cm^2/Vs, indicated by the decreased curve slope. These values are comparable to the variations in the carrier mobility of bilayer graphene, ranged between 1500 and 4000 cm^2/Vs, reported by Novoselov et al.[3] and Nagashio et al.[15] A positive shift in the Dirac point can be observed and could be attributed to charged impurities that physically adhered to graphene surface during UV/O_3 treatment. It is probable that the impurities were negatively charged by considering that it was a positive shift. However, after annealing the oxidized G-FET with H_2/Ar, the ambipolar curve almost perfectly recovered to the state before oxidation, as indicated by curve No. 3. The carrier mobility recovered to 2400 cm^2/Vs, 96% of its previous level, and the minimum conductivity recovered to almost 100% of its previous level. This high (more than 90%) recovery of carrier mobility and minimum conductivity could be an assessment of thermally reversibility of oxidation through UV/O_3 treatment.

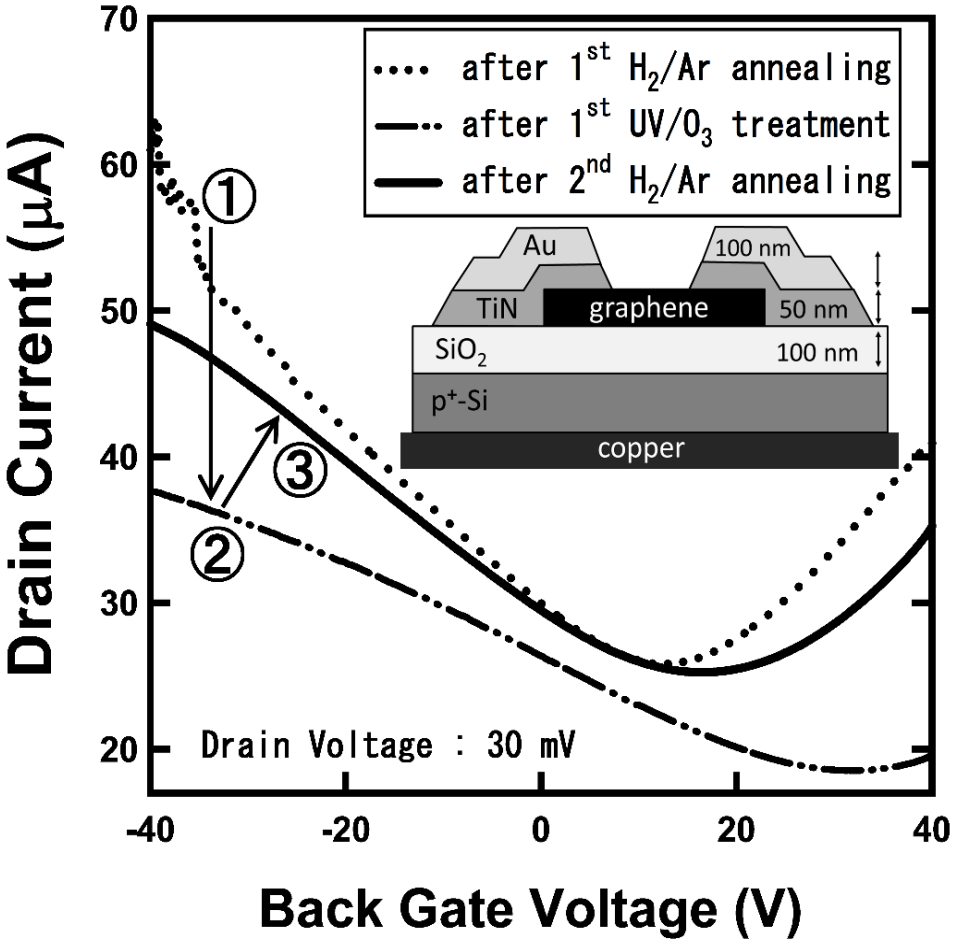

Fig. 3. Graphene-based FET's I_d-V_g characteristics after first oxidation and reduction process. Inset shows device structure.

UV/O_3 treatment could cause reactive oxygen atoms to chemically react with carbon atoms in the graphene to form oxide groups by taking into account the results of XPS measurements of oxidized CVD-graphene.[18] It appears that in this reaction a certain number of π electrons of graphene were used in the formation of C-O bond. On the other hand, during reductive H_2/Ar annealing, hydrogen reacted with chemically doped oxygen atoms to form H_2O, which were eventually exhausted, and caused C-O bonds to break, leaving the π electrons

unbound. In the formation of C-O bonds, as a result of oxidation, a number of π electrons were used in the chemical bonding and yet bound. This forced those π electrons to stop functioning as charge carriers, eventually causing a decline in the number of charge carriers. Since π electrons, which act as charge carriers, are responsible for electrical conductivity of graphene,[2] the decline in number of charge carriers resulting in the decreased conductivity. Therefore, oxidation caused a decrease in the number of charge carrier and hence in conductivity which was indicated by the downshift of ambipolar curve. Since not all of the π electrons were used in C-O bonds, the ambipolar characteristics of graphene can still be observed after oxidation. Nevertheless, subsequent reduction caused C-O bonds to break, leaving those π electrons unbound, and hence restored the number of charge carrier as well as ambipolar transfer characteristic to its pristine level.

It seems likely that after oxidation, the formation of C-O bond obstructed the path of charge carrier and hence increased carrier scattering in graphene. Since charge mobility is directly affected by various scattering, the increased scattering eventually suppressed the charge mobility of G-FET. Nonetheless, subsequent reduction caused C-O bonds to break, clearing the oxidized path of charge carrier, and hence recovered the charge mobility of G-FET to its pristine level. The recovery of conductivity was comparable to the increase in conductivity by two orders of magnitude upon reduction of GO through excimer laser irradiation reported by Kumar et al.[20] Then, it is also reported that the conductivity of metal-decorated graphene is much higher

than that of graphene.[20] Furthermore, besides the difference in conductivity, GO and reduced GO have also different optical behaviors. It has been reported that under irradiation with different light sources, GO exhibited yellow emission, meanwhile reduced GO exhibited blue emission.[21]

2.6.2.2. Second redox reaction

The G-FET's I_d-V_g characteristics after the second oxidation are plotted in Fig. 4. Prior to that, H_2/Ar annealing was repeated to clean the graphene's surface. As indicated by curve No. 1, the Dirac point was observed near zero back-gate voltage, suggesting that most charged impurities that physically adhered to graphene surface were cleaned. After the second oxidation, exactly like after the first one, the ambipolar curve shifted downward from curve No. 1 to No. 2, indicating decreased conductivity from 3000 to 2500 cm^2/Vs. Moreover, a positive shift in the Dirac point due to negatively charged impurities, similar to that found after the first oxidation, was observed. However, after keeping the device inside the vacuum chamber (4.6 x 10^{-5} Pa) for 24 h, the I_d-V_g curve horizontally shifted back to near zero back-gate voltage, from curve No. 2 to No. 3, indicating that the impurities were swept. The carrier mobility during this shifting remained at a level of 2500 cm^2/Vs.

It seems reasonable to assume that the impurities, did not chemically react with carbon atoms of graphene, and only physically adhered to the surface instead. If the impurities had chemically reacted with carbon atoms, this would have caused a decline in the number of charge carriers which decreases the conductivity. If that were the case, conductivity would have recovered, and vertical shift would have been observed, as the impurities vanished (from curve No. 2 to No. 3). Additionally, further studies are needed to identify the charged impurities and to determine details of their profiles.

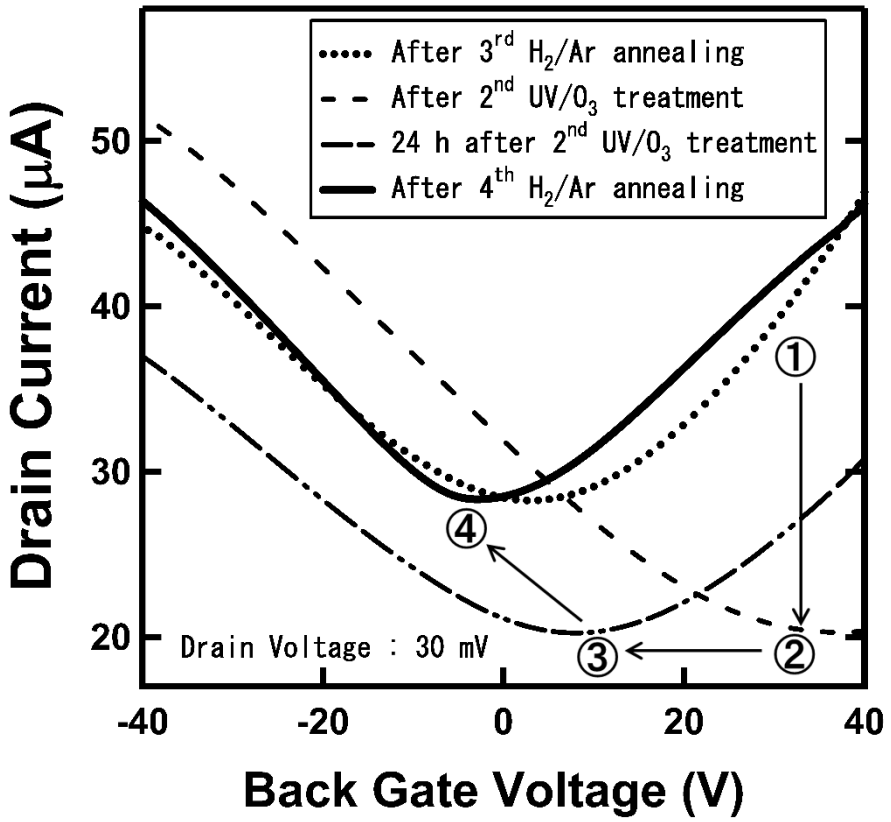

Fig. 4. Graphene-based FET's I_d-V_g characteristics after second oxidation and reduction process.

However, in the case of oxygen-doped graphene, oxygen atoms chemically reacted with carbon atoms and the chemical bonds were stable. That may explain the fact that even after the oxygen-doped G-FET had been kept for more than 24 h inside the vacuum chamber, the electrical conductivity did not recover by itself. Nonetheless, after the oxygen-doped G-FET had been annealed with H_2/Ar, the ambipolar curve almost perfectly recovered to its state before oxidation, as indicated by curve No. 4. The carrier mobility recovered to its previous level of 3000 cm^2/Vs. This may assess that oxidation through UV/O_3 treatment is thermally reversible, even after being done for multiple turns.

TABLE I. Changes in G-FET characteristic

Sequential order	Process	μ [a] (cm^2/Vs)	$V_{G\text{-}min}$ [b] (V)	$I_{D\text{-}min}$ [c] (A)	I_G [d] (A)
1	1st annealing [e]	2500	13.2	25.8	10^{-12}
2	1st oxidation	2100	31.8	18.5	10^{-12}
3	2nd annealing [f]	2400	16.2	25.3	10^{-9}
4	3rd annealing [e]	3000	3.0	28.3	10^{-9}
5	2nd oxidation	2500	8.4	20.2	10^{-9}
6	4th annealing [f]	3000	-1.8	28.3	10^{-9}

[a] μ is carrier mobility.

[b] $V_{G\text{-}min}$ is back-voltage at minimum conductivity, i.e. Dirac point.

[c] $I_{D\text{-}min}$ is drain current at minimum conductivity.

[d] I_G is maximum leakage current.

e) This is done for cleaning purpose.

f) This is done to reduce oxidized graphene

2.6.3. Raman spectroscopy measurement

The Raman spectra of pristine graphene after oxidation and reduction are given in Fig. 5, where no distinct peaks in the D band feature of graphene can be observed. Since the D band is defect-induced band,[16,17] this suggests that oxidation and reduction did not introduce any significant crystalline defects into graphene layers, even after annealing at 300ºC for 2 h. This could indicate that the decrease in conductivity was not caused by any defects in the structure of the graphene's crystal. All measurement results are summarized in Table I and II.

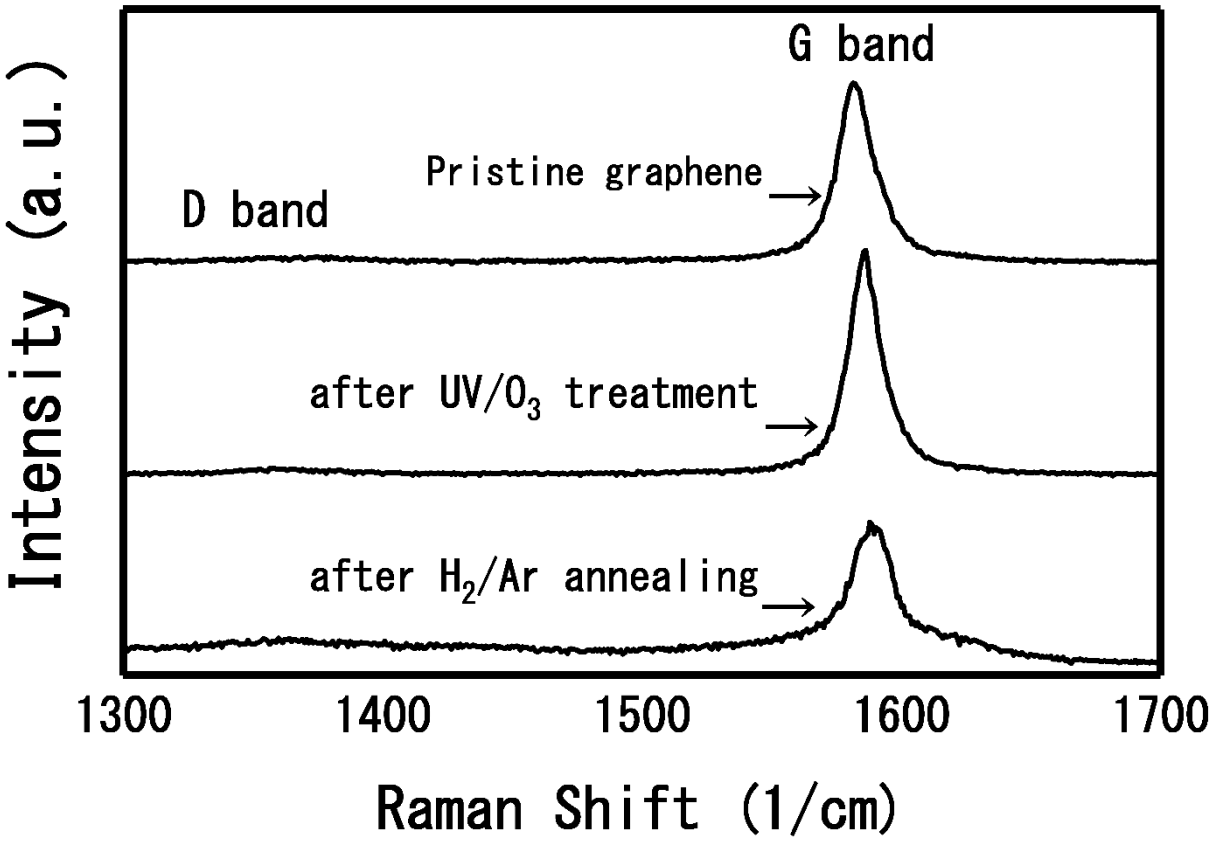

Fig. 5. Raman spectra of pristine graphene after being oxidized and then reduced.

TABLE II. Changes in XPS and Raman spectroscopy features

Sequential order	Process	Concentration [g]		D/G [i]
		C-C [h] (%)	C-O [h] (%)	(a.u.)
1	Pristine graphene [j]	100	0	0
2	After oxidation	81	19	0
3	After reduction	97	3	0

[g] Concentration was quantified by C-C and C-O peak area.

[h] Binding energy position is 284.8 eV for C-C and 286.4 eV for C-O.

[i] The degree of lattice defect was quantified by the area ratio of D band and G band in Raman spectroscopy.

[j] CVD-graphene was used in XPS and mechanically exfoliated graphene was used in Raman measurement.

2.6.4. Contact resistance

The contact resistance at the Au/TiN electrode-graphene interface before and after oxidation that was determined by TLM,[13] are plotted in Fig. 6. The contact resistance at metal-graphene interface (2Rc) before oxidation, 950±170 Ω, or after oxidation, 1100±120 Ω, did not differ significantly, indicating that oxidation did not increase the contact resistance. Nonetheless, the sheet resistance of graphene layer increased by ~20 Ω/μm after oxidation. This is comparable to the decreased conductivity of the G-FET after oxidation. Therefore, it is reasonable to conclude that changes in I_d-V_g characteristics are not caused by any change in the electrode-graphene interface, but are instead related to the change in graphene's sheet resistance. It appears that contact resistivity at the electrode-graphene interface of Au/TiN, i.e., ~3500 Ωμm, is more versatile than that of conventional materials such as Au/Cr or Au/Ti, which both are approximately ~10,000 Ωμm.[22] In fact, contact resistivity at the electrode-graphene interface of Au/TiN could compete with that of Ni, which is ~2000 Ωμm.[13] It seems that Au/TiN has something to offer considering that it is chemically inert and the adhesion with SiO_2 is excellent compared to that of Ni.[23]

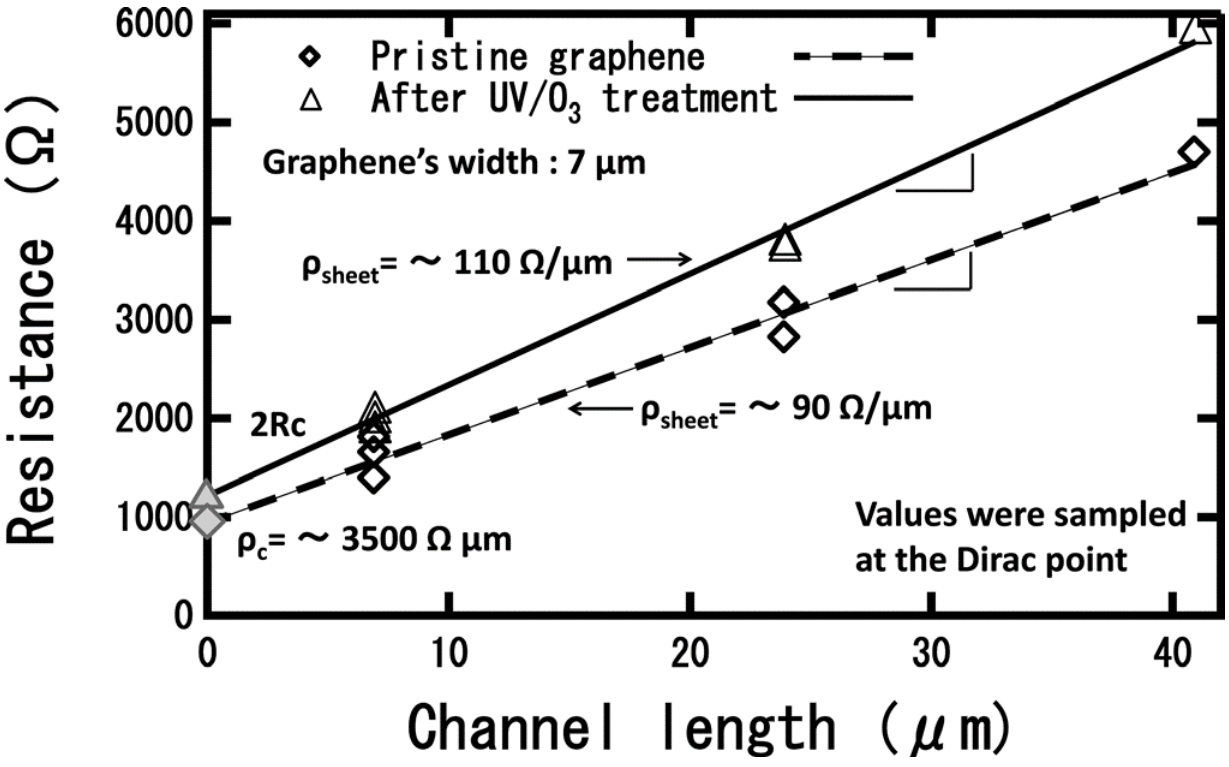

Fig. 6. Result of TLM measurement before and after oxidation process.

2.7. Conclusion

In summary, the changes in electrical properties of graphene after being oxidized through UV/O_3 treatment were investigated. Reactive oxygen atoms chemically reacted with carbon atoms of graphene, which was confirmed from the XPS spectra. The conductivity of the graphene layer decreased as a result of oxidation. The electrical characteristics such as conductivity and carrier mobility recovered to the level before oxidation after annealing the oxidized graphene with H_2/Ar, suggesting that the oxidation of graphene with UV/ozone

treatment is thermally reversible. The oxidation did not change the contact resistance at the Au/TiN electrode-graphene interface. The thermal reversibility of the redox reaction may suggest possibilities for applications to a nonvolatile memory and reconfigurable electric circuit.

2.8. Next task

To investigate whether the oxidation of graphene via UV/ O_3 treatment is also thermally reversible for single layer graphene, H_2/Ar annealing of oxidized single layer graphene was conducted. The UV/ O_3 treatment and H_2/Ar annealing were performed under the same condition. As shown in Fig. 7, the G-FET's mobility and conductivity decreased after being oxygen-doped via UV/ O_3 treatment, and the I-V characteristic of the graphene FET did not recover after being annealed. This result suggests that the oxidation of graphene via UV/ozone treatment is not thermally reversible for single layer graphene. Another further investigation is needed to develop a method for reducing single layer graphene oxide and in the same time recovering the decreased electron mobility without introducing significant damaged to the G-FET. This kind of investigation will be covered in the next chapter.

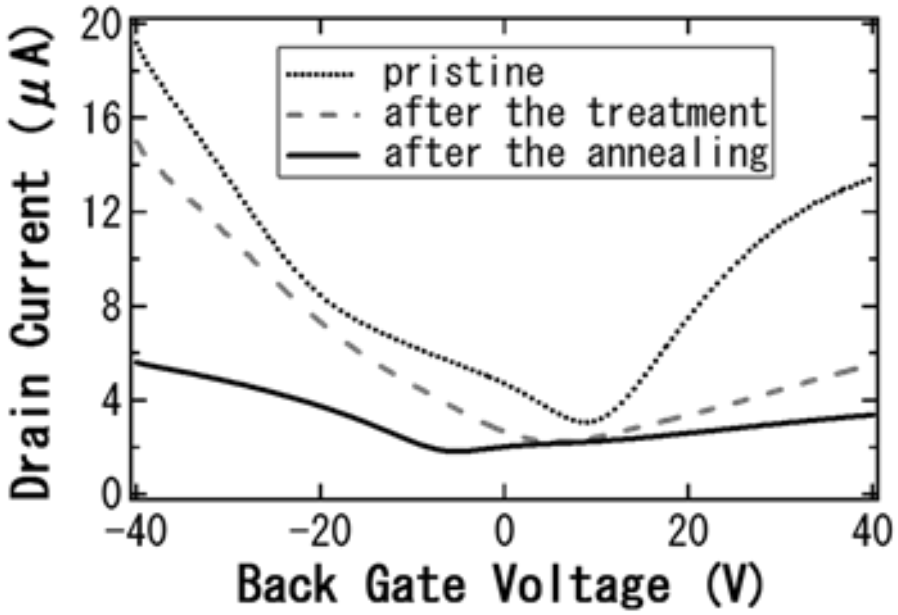

Fig. 7 I-V characteristic of single layer graphene FET during redox process.

References:

1) K. S. Novoselov, A. K. Geim, S. V. Morozov, D. Jiang, Y. Zhang, S. V. Dubonos, I. V. Grigorieva, and A. A. Firsov, Science **306**, 666 (2004).

2) P. R. Wallace, Phys. Rev. **71**, 622 (1947).

3) S. V. Morozov, K. S. Novoselov, M. I. Katsnelson, F. Schedin, D. C. Elias, J. A. Jaszczak, and A. K. Geim, Phys. Rev. Lett. **100**, 016602 (2008).

4) A. H. Castro Neto, F. Guinea, N. M. R. Peres, K. S. Novoselov, and A. K. Geim, Rev. Mod. Phys. **81**, 109 (2009).

5) Y. -M. Lin, A. V. -Garcia, S. –J. Han, D. B. Farmer, I. Meric, Y. Sun, Y. Wu, C. Dimitrakopoulos, A. Grill, P. Avouris, and K. A. Jenkins, Science **332**, 1294 (2011).

6) Md. Zakir Hossain, James E. Johns, K. H. Bevan, H. J. Karmel, Y. T. Liang, S. Yoshimoto, K. Mukai, T. Koitaya, J. Yoshinobu, M. Kawai, A. M. Lear, L. L. Kesmodel, S. L. Tait, and M. C. Hersam, Nat. Chem. **4**, 305 (2012).

7) M. Y. Han, B. Oezyilmaz, Y. Zhang, and P. Kim, Phys. Rev. Lett. **98**, 206805 (2007).

8) M. Shan, Q. Xue, N. Jing, C. Ling, T. Zhang, Z. Yan, and J. Zheng, Nanoscale **4**, 5477 (2012).

9) A. Hirsch, J.M. Englert, and F. Hauke, Acc. Chem. Res. **46**, 87 (2013).

10) G. Lee, B. Lee, J. Kim, and K. Cho, J. Phys. Chem. **113**, 14225 (2009).

11) S. Huh, J. Park, Y. S. Kim, K. S. Kim, B. H. Hong, and J. –M. Nam, ACS Nano **5**, 9799 (2011).

12) S. Zhao, S. P. Surwade, Z. Li, and H. Liu, Nanotechnology **23**, 355703 (2012).

13) K. Nagashio, T. Nishimura, K. Kita, and A. Toriumi, Jpn. J. Appl. Phys. **49**, 051304 (2010).

14) P. Blake, E. W. Hill, A. H. Castro Neto, K. S. Novoselov, D. Jiang, R. Yang, T. J. Booth, and A. K. Geim, Appl. Phys. Lett. **91**, 063124 (2007).

15) K. Nagashio, T. Nishimura, K. Kita, and A. Toriumi, Appl. Phys. Express **2**, 025003 (2009).

16) M. A. Pimenta, G. Dresselhaus, M. S. Dresselhaus, L. G. Cancado, A.Jorio, and R. Saito, Phys. Chem. Chem. Phys. **9**, 1276 (2007).

17) D.Graf, F. Molitor, K. Ensslin, C. Stampfer, A. Jungen, C. Hierold, and L. Wirtz: Nano Lett. **7**, 238 (2007).

18) N. Leconte, J. Moser, P. Ordejón, H. Tao, A. Lherbier, A. Bachtold, F. Alsina, C.M.S. Torres, J. -C. Charlier, and S. Roche: ACS Nano **4**, 4033 (2010).

19) P. Kumar, B. Das, B. Chitara, K. S. Subrahmanyam, K.Gopalakrishnan, S. B. Krupanidhi, C. N. R. Rao, Macromol. Chem. Phys. **213**, 1146 (2012).

20) P. Kumar, K. S. Subrahmanyam, C. N. R. Rao, Mater. Express **1**, 252 (2011).

21) K. S. Subrahmanyam, P. Kumar, A. Nag, C.N.R. Rao, Solid State Communications 150, 1774 (2010).

22) K. Nagashio, T. Nishimura, K. Kita, and A. Toriumi, Appl. Phys. Lett. **97**, 143514 (2010).

23) C.N. Kirchner, K. H. Hallmeier, R. Szargan, T. Raschke, C. Radehaus, and G. Wittstock, Electroanalysisme **19**, 1023 (2007).

CHAPTER 3

Graphene and oxygen:

Oxidation of graphene and its non-thermal reduction

In this chapter, we present alternative methods to oxidize graphene layer through ultraviolet (UV)/ozone (O_3)-treatment resulting in chemically homogeneous graphene oxide (GO) and then to reduce GO through UV-irradiation. Both UV/O_3-treatment and UV-irradiation were performed at room temperature in atmospheric pressure for only several minutes and did not involve any wet chemical treatments. The quantity of doped oxygen, determined using X-ray photoelectron spectroscopy, increased after oxidation and decreased after reduction. The quantity of doped oxygen reached its maximum which was around 20 % (approximately one oxygen atom in every five or six carbon atoms) after performing UV/O_3-treatment for 6 to 10 min. Conducting UV/O_3-treatment for around 6 or 10 min resulted in chemically homogeneous GO surface with only oxygen epoxide groups on graphene surface. Performing UV/O_3-treatment beyond 15 min as well as multiple turns of UV/O_3-treatment could lead to the formation of defects and carbonyl groups on graphene lattice. The oxygen quantity gradually decreased after conducting 6-min UV-irradiation several times, indicating that the resulting GO

was successfully reduced. How the doped oxygen atoms distributed on graphene surface were directly investigated using scanning tunneling microscopy. Moreover, changes in electrical properties of three identical single-layer graphene field-effect transistors (G-FETs) after being oxidized through UV/O_3-treatment were investigated. The electron mobility of G-FETs decreased after oxidation; however, it recovered after irradiating the oxidized G-FETs with UV-lights, indicating that GO was successfully reduced non-thermally through UV-irradiation. The reversibility in electron mobility was confirmed even after conducting redox processes twice. Furthermore, the reversibility of oxidation was also verified from graphene lattice disorder point of view using Raman spectroscopy. We concluded that UV/O_3-treatment produced chemically homogeneous GO which is non-thermally reversible through UV-irradiation, and changes in the electron mobility were non-thermally reversible also.

3.1. Background

Because of its exceptional electron mobility, graphene holds great promise to be applied in future ultrafast electronics.[1,2] Moreover, its thinness and flexibility make graphene a promising candidate for applications in sensing devices as well as in transparent flexible thin film electronics and thermoelectric applications.[1,2] Zhang et al. have reported that based on

calculation using molecular dynamics simulation, thermal transport property of graphene can be tailored through oxygen functionalization.[3] The simulation results have provided fundamental insight on how to precisely control thermal property of graphene for thermal management and thermoelectric applications.[3] Generally, graphene can be mass-produced by chemical vapor deposition CVD of methane gas or by reducing graphene oxide which was obtained by chemically exfoliating natural graphite.[4] Similar to graphene, graphene oxide also offers a wide range of application possibilities e.g. on sensor technology, energy-related material, biomedical use etc.[5] Since the epoxide bridge in graphene oxide has greater reactivity comparing to the firm chemical stability in sp^2 bond in graphitic structures of graphene, graphene oxide is also often used as a transitional phase in a series of chemical reactions to modify graphene with various functional groups.[6] Hou et al. have reported that the doping of heteroatoms could improve the ability of graphene to intercalate more lithium ions, enhance the conductivity of graphene and facilitate the transport of electrons and ions. This would eventually improve the performance of graphene as anode for lithium ion batteries significantly.[7]

Therefore, research in oxidation and reduction of graphene as well as research in more advance chemical functionalization of graphene are actively being pursued for further enhancement and deeper exploration of the properties of graphene.[8,9] Due to the weak chemical reactivity of graphitic structures, oxidation of graphene is commonly performed using a variety

of strong acids, despite requiring several hours for completion and resulting in graphene surface with chemically inhomogeneous functions such as hydroxyl and carboxyl groups besides the oxygen epoxide group.

3.2. Experimental

Reduction of graphene oxide (GO) also can be done chemically by utilizing hydriodic acid or by conducting annealing treatment in ultra-high vacuum (UHV) environtment.[10-16] Hossain et al. presented an alternative approach for oxidizing epitaxial graphene by supplying atomic oxygen in UHV.[15] Atomic oxygen is produced by cracking O_2 molecules on a hot (1500℃) tungsten filament under UHV conditions. This oxidation is shown to be fully reversible by annealing at temperatures as low as 260℃.[15] Lin et al. have reported the fabrication of superior capacitance from functionalized graphene prepared by controlled reduction of GO using solvothermal method. GO dispersed in dimethylformamide was thermally treated at a moderate temperature (150℃), which allows a fine control of the density of functionalities.[17] However, these types of method consume a large amount of energy and time, besides resulting in chemically inhomogeneous graphene oxide, especially for oxidation by wet chemical treatments.[10-17] Consequently, any possibilities of alternative methods to produce chemically homogeneous graphene oxide with oxygen epoxide group only on its

surface and to obtain pristine graphene surface from graphene oxide are required to be systematically studied.

Here, we presented simpler, faster and more cost-effective ways to oxidize graphene layer through UV (ultraviolet)/O_3 (ozone)-treatment and reduce the resulting GO through UV-irradiation. The objectives are to investigate whether UV/O_3-treatment could be a feasible method to produce chemically homogeneous GO with only oxygen epoxide group on its surface, and whether UV-irradiation could be a feasible method to non-thermally reduce GO, and to confirm whether or not the changes in electrical properties after oxidation is reversible. Both oxidation and reduction were performed in a very short period of time (several minutes) at room temperature in atmospheric pressure and did not involve any chemicals. X-ray photoelectron spectroscopy (XPS) measurements were conducted to determine the quantity of doped oxygen atom on graphene layer after oxidation and to investigate any changes in oxygen quantity after reduction. Scanning tunneling microscopy (STM) measurements were performed to directly observe how the doped oxygen atoms were distributed on graphene surface. Moreover, changes in electrical properties of three identical single-layer graphene field-effect transistors (G-FETs) after redox processes were also investigated and Raman spectroscopy measurements were carried out after each process to evaluate lattice disorder of graphene crystalline after oxygen atoms were doped on the surface. Prezhdo et al. have stated that seeking fundamental information of graphene and functionalized graphene through physical chemistry perspectives

such as synthesis, structure, spectroscopy and electron-transport like we tried to present in this work has been at the forefront of disseminating basic understanding of graphene as the parent structure of fullerenes, carbon nanotubes and nanofibers.[18]

3.3. UV/O_3-treatment and UV-irradiation

In this study, oxidation of graphene was conducted through UV/O_3-treatment resulting in GO and subsequent reduction of GO was conducted through UV-irradiation. In the UV/O_3-treatment here, oxygen gasses were channeled into a chamber where CVD-graphene was placed inside at a flow rate of 0.5 L/min and then ozonized using an ozone generator while simultaneously two types of UV-lights with wavelengths of 184.9 and 253.7 nm were produced from a low pressure mercury lamp to continuously generate reactive radical oxygen atoms. These radical oxygen atoms will eventually react with carbon atoms in graphene and form epoxide groups on the graphene surface.

Both UV/O_3-treatment and UV-irradiation were done for only several minutes using the same light source and conducted at room temperature in atmospheric pressure on UV-1 cleaning system from SAMCO Incorporation. The sample stage where graphene films and G-FETs sat on was not heated. The only difference between UV/O_3-treatment and UV-irradiation is that in UV-irradiation no ozone was supplied.

3.4. Result and discussion

The feasibility of redox reaction of graphene was evaluated from STM observation, XPS, Raman spectroscopy, electrical properties and electrical characteristics of G-FET point of view.

3.4.1. STM observation

The STM measurements were carried out at room temperature in a vacuum chamber with base pressure below 10^{-4} Pa, using a tunneling current of 2.0 nA and a sample bias of 0.8 V. We used E-sweep scanning probe microscopy from SII Nanotechnology Incorporation to conduct the STM measurements and KRATOS-165 spectrometer from Shimazu Corporation to conduct the XPS measurements. In the XPS measurements, the pass energy was 40 eV, the anode high-tension was 15 kV, and the step energy resolution was 10 meV with a dwell time of 500 msec for each step. In every measurement, each sample was scanned for five times, and the XPS spectra were obtained by computing the mean value from each scanning. Peak areas were calculated by fitting the spectra into Gaussian (60%) and Lorentzian (40%) functions. The goodness of fit was evaluated using the coefficient of variation of the root mean square error (CV-RMSE), and this CV-RMSE was used for error estimation included in Figures 2 and 3 (half value of CV-RMSE was used in calculation of the error bars in Figure 3). The less great the CV-RMSE is, the more accurate the fitting is. Since the area of graphene exfoliated from graphite was too small to be measured by XPS spectrometer,[19] and since it is very difficult to

observe the exfoliated graphene with STM instrument, CVD-graphene, graphene which is grown on Cu foil with CVD method and has relatively large area,[3,19,20] was used in the STM and XPS measurements.

STM topography of pristine graphene and after being oxidized through UV/O_3-treatment for 6 min are shown in Figure 1. To observe how the doped oxygen atoms were distributed, STM observations were performed on 4 random different spots. As can be seen in this figure, pristine graphene films were flat, and in some spots, ripples were observed. To the contrary, in the resulting GO there were some mountain-like peaks scattered over the graphene surface, indicating the existence of oxygen, and some of them flocked and formed areas looked like mountain range.[15] Moreover, each oxygen atom has identical appearance which might indicate the homogeneity of epoxide group on graphene surface.[15] Since O_2 and O_3 gasses were supplied from the top part of the chamber and the location of light source is above the sample stage, as shown in Figure 1(B), it appears that the radical oxygen atoms were doped only on the top surface of graphene layer. The contrast showed in STM topography was related to the difference in height. On the other hand, XPS measurements were conducted to accurately determine whether or not the doped element was indeed oxygen. That would be determined from the binding energy of detected peak position from the XPS obtained. The results of the XPS measurement will be discussed in more detailed manner in the next section.

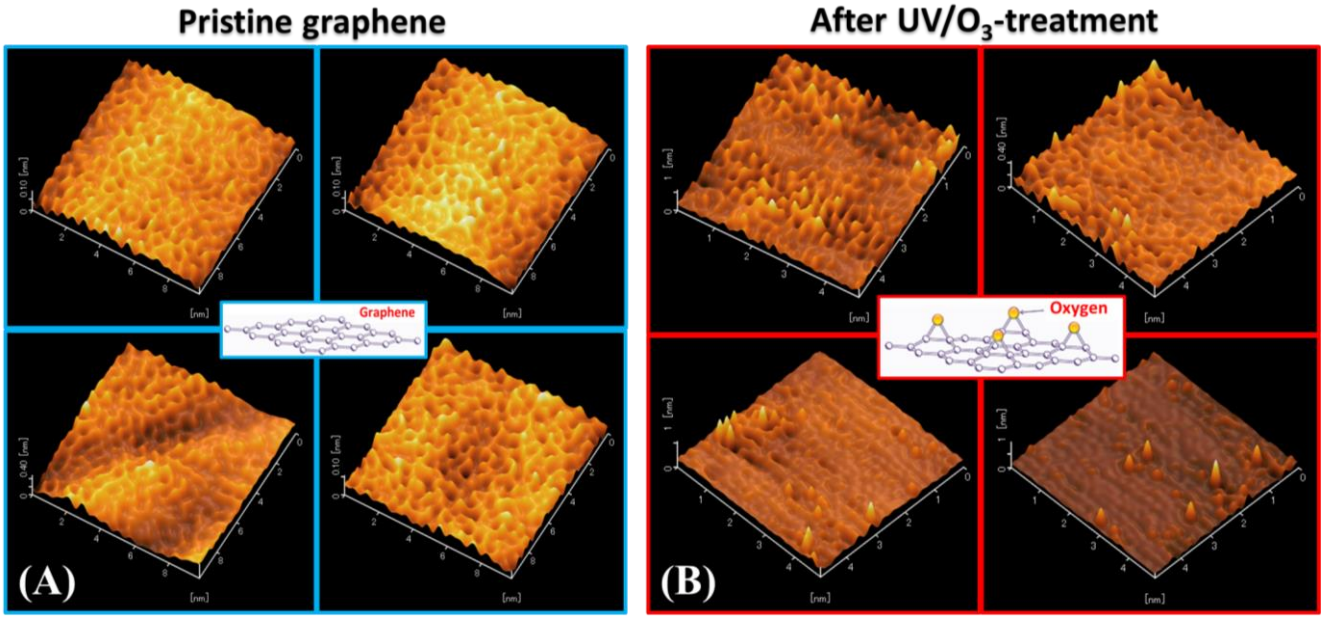

Figure 1. STM topography of pristine CVD-graphene on copper foil **(A);** and that after being oxidized through UV/O_3-treatment for 6 min **(B)**. STM observations were performed on four random different spots, in order to observe how doped oxygen atoms were distributed on graphene surface.

3.4.2. XPS measurement

XPS spectra of pristine graphene are shown in Figure 2(A-inset) where we found only one peak at 284.7 (standard deviation: ± 0.2) eV originated from carbon-carbon single bond (C-C bond). XPS spectra of graphene after 6-min UV/O_3-treatment are shown in Figure 2(A) where we found only two peaks, one of C-C bond and the other at 286.5 (± 0.2) eV originated from carbon-oxygen single bond (C-O bond).[13,21,22] Since we did not find any peaks of other functional groups besides C-O bond or epoxide groups, this might indicate the existence of homogeneous oxygen epoxide groups on the surface of graphene layer. The C-O peak might

also suggest that the radical oxygen atoms chemically reacted with carbon atoms of graphene during UV/O_3-treatment.

Nevertheless, after conducting UV/O_3 treatment for 15 min, as shown in Figure 2(B) we found another peak at 288.6 ($\pm$ 0.3) eV originated from C=O bond or carbonyl groups, besides C-C and C-O bond.[13,21,22] Since a carbon atom has four valence electrons and three out of four are used in the covalent bonds with three neighboring carbon atoms in graphene lattice,[23] the formation of carbon-oxygen double bond (C=O bond) might indicate the introduction of lattice defect.

In order to know the UV/O_3-treatment time dependence of doped oxygen quantity, the treatment time was arranged from 3 to 30 min and the results of subsequent XPS measurement are shown in Figure 2(C) and Figure 3(A). The complete XPS measurement results are presented in section B of the appendix. The oxygen quantity, counted from the peak area, reached the maximum which was around 20% (approximately one oxygen atom in every five or six carbon atoms) while keeping lattice defects at negligible level after conducting UV/O_3-treatment for between 6 and 10 min. Performing UV/O_3-treatment beyond 15 min could lead to the formation of carbonyl groups on graphene surface which was indicated by the detection of C=O bonds in the XPS measurements. Although the sample stage was not heated, we found that the temperature of sample stage increased up to 40 centigrade after conducting UV/O_3-treatment for 30 min which possibly was caused by the energy of UV lamps. This might suggest

that the prolonged UV/O_3-treatment time could increase the temperature of sample stage and subsequently force carbon atoms of graphene to form carbon dioxides, leaving holes in graphene layer which eventually lead to the introduction of defects onto graphene lattice. Another plausible explanation is that 15% of the UV-lights used in the experiment had a wavelengths of 184.9 nm and this energy had enough energy to break the C-C bond in graphene. The formation of holes in graphene lattice is displayed in STM images provided in section A of the appendix. Denis et al. have reported that structural defects play a key role in the chemistry and physics of graphene. Their presence reduces the Young modulus and Poisson ratio, induce magnetism, and alter the chemical reactivity of graphene.[24]

The oxygen quantity, counted from the peak area of the XPS spectra, reached the maximum which was around 20% after conducting UV/O_3-treatment for 6 min, as shown in Figure 2(C) and Figure 3(A). Areas of 600 μm in diameter were the subject of this XPS measurement. An oxygen concentration of 20% means approximately one oxygen atom in every five or six carbon atoms. Four random points on the surface of the produced GO after the treatment were observed using STM, and the observed STM topography was shown in Figure 1(B). Areas of 5 x 5 nm were the subject of this STM observation. As can be observed from Figure 1(B), some points had more than one oxygen atom in every five carbon atoms, and some points had less than one oxygen atom in every six carbon atoms. However, when it was observed from a greater perspective, for instance from areas of 600 μm in diameter as conducted

using XPS measurement, the overall oxygen concentration of the produced GO was around 20%, as shown in Figure 2(C) and Figure 3(A).

Furthermore, in order to know the UV/O_3-treatment number dependence of doped oxygen quantity, 3-min UV/O_3-treatment was conducted for six times and the results of XPS measurement are shown in Figure 2(D) and Figure 3(B). The oxygen quantity tended to increase after repeating UV/O_3-treatment, however, C=O bonds were formed right after the second treatment and its number raised as the repetition increased, suggesting the formation of lattice defect, as shown in section A in the appendix. This might suggest that the C=O bonds were easily formed after conducting UV/O_3-treatment on oxidized graphene surface. The results of conducting 6-min UV/O_3-treatment once and 3-min UV/O_3-treatment twice were not necessarily the same. Heating the sample stage while conducting oxidation would result lattice defect in graphene crystalline as shown in section A in the appendix.

The reduction process of GO through UV-irradiation is shown in Figure 2(E). Each UV-irradiation was performed for 6 min using the same UV-lights used in UV/O_3-treatment. The quantity of doped oxygen in GO decreased with no C＝O peaks observed after conducting 6-min UV-irradiation several times, as shown in Figure 2(E), suggesting that GO was reduced without introducing any significant lattice defects. This might suggest that since the bond energy of C-C (473 kJ/mol) in graphene is greater than C-O (358 kJ/mol),[25,26] the energy of UV-rays could cause the chemical bonds of C-O to break but still leaving the C-C bonds intact.

This is possibly what made reduction through UV-irradiation feasible. The changes in oxygen quantity after two consecutive redox processes are summarized in Figure 3(C) where we found that multiple cycles of oxidation through UV/O_3-treatment and reduction through UV-irradiation on graphene were feasible.

Additionally, as can understood from complete XPS measurement results presented in section B of the appendix, prolonged UV/O_3-treatment could lead to the formation of carbonyl groups on graphene surface which was indicated by the detection of C=O bonds in the XPS measurements. However, the detection of C=O did not necessary mean that the lattice defects or permanent holes, which could not be recovered, had been formed on graphene layer, because after conducting reduction through UV-irradiation the peak area of C=O bond decreased, as indicated by the XPS measurement result, suggesting that the C=O bonding had been broken due to UV-irradiation.

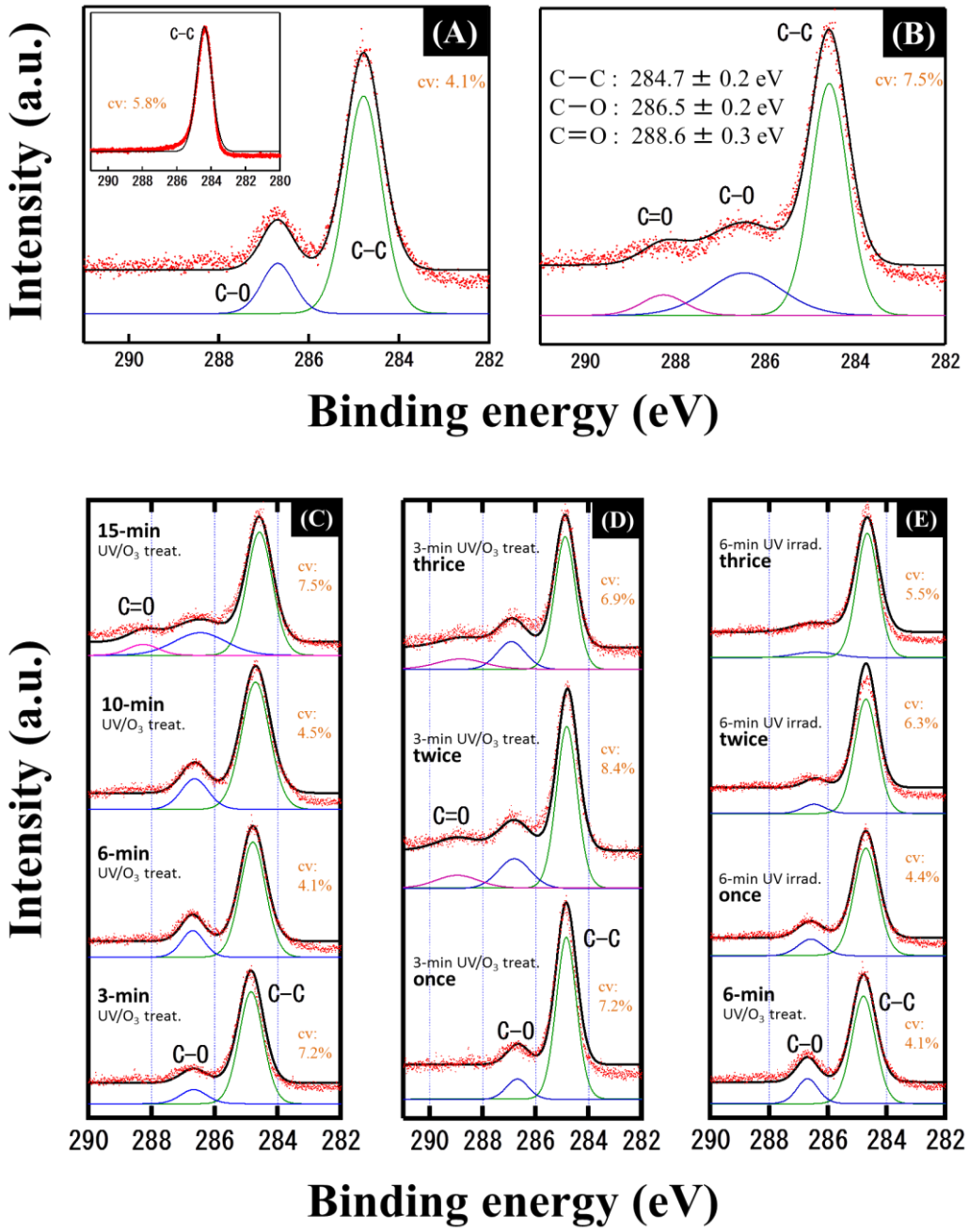

Figure 2. XPS spectra of CVD-graphene after 6-min UV/O_3-treatment **(A)**, **A-inset** shows XPS spectra of pristine graphene**,** and after 15-min UV/O_3-treatment **(B)**; UV/O_3-treatment time dependence **(C)** and UV/O_3-treatment number dependence of doped oxygen quantity **(D)**; and XPS spectra of graphene oxide after conducting 6-min UV-irradiation several times **(E)**. CV-RMSE (cv) was used an indicator for the goodness of fit and as well as error estimation.

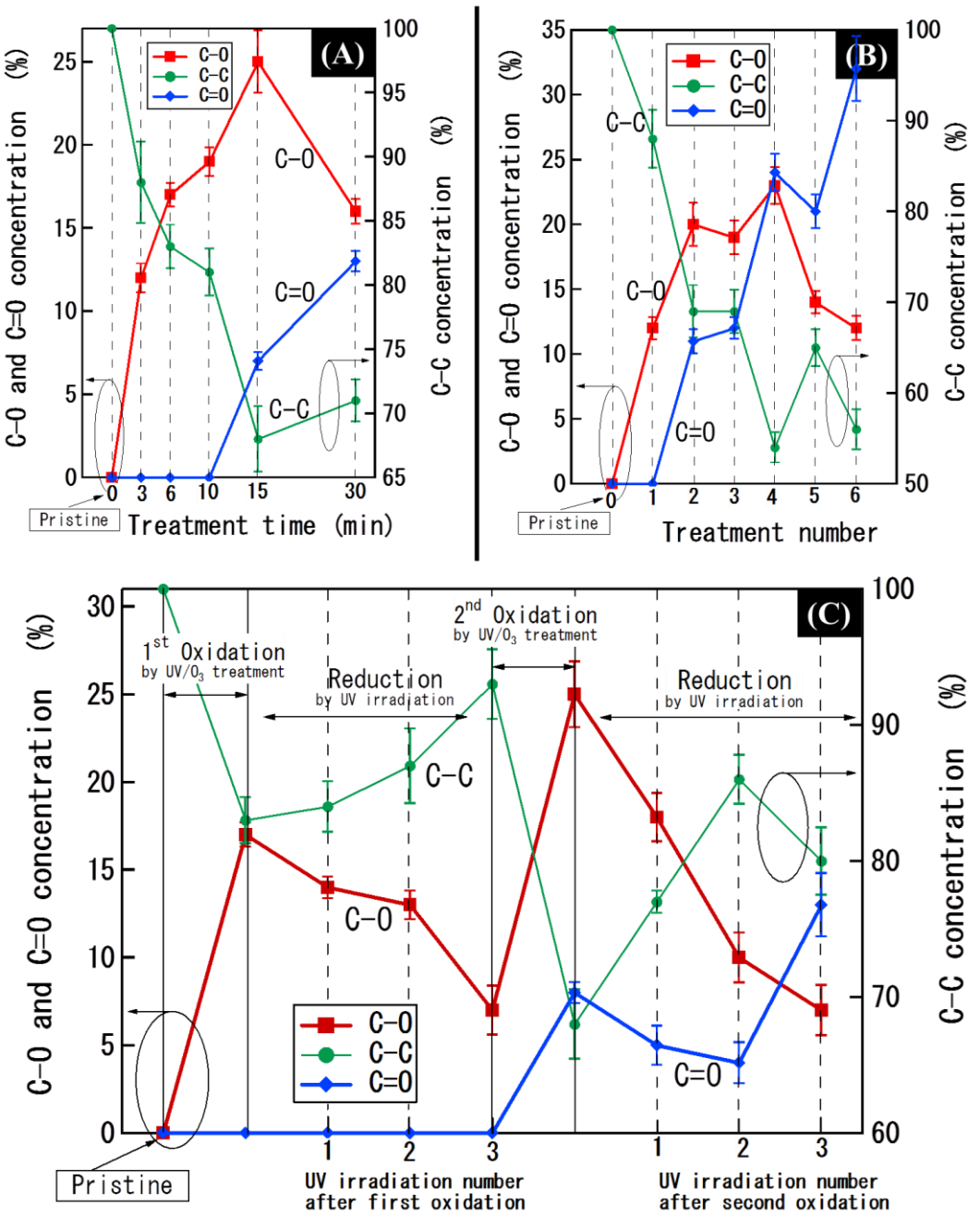

Figure 3. UV/O_3-treatment time dependence **(A)** and UV/O_3-treatment number dependence **(B)** of doped oxygen quantity; and quantity of doped oxygen after two cycles of oxidation and reduction process **(C)**. Calculations were done based on area of peaks detected in XPS spectra.

3.4.3. Electrical characteristics measurement

In this section, G-FET fabrication process and experimental setup, the changes in ambipolar characteristics of graphene during redox reaction, and the relation between electron mobility and the mechanism of redox reaction on graphene will be discussed.

3.4.3.1. FET fabrication and electrical characterization setup

The feasibility of oxidation and reduction were also examined from electrical characteristics points of view and three identical single-layer G-FETs were used in this evaluation. The fabrication processes and structure of (bottom-gated) G-FETs used in this study are shown in Figure 4. The G-FETs were fabricated from single-layer graphene films on 100-nm SiO_2/p^+-Si substrates (Figure 4(A)). The graphene films were exfoliated using the micromechanical cleavage method of kish graphite.[19] The number of layer was determined by optical contrast and Raman spectroscopy.[20] The Raman spectra (2D band, G band and D band) of the G-FETs are provided in section C of the appendix (Figures C-1 to C-3; the intensity of defect-derived D band increased after two cycles of redox process, however the sharpness of 2D band, which indicates that the graphene film is one layer, remained unchanged). The electrodes were formed through a chain of procedures of photolithography to print source/drain patterns onto the both ends of graphene layer (Figure 4(B)), and then deposition of Au/Cr (100/50 nm) metals with electron beam vapor deposition technique followed by a lift-off

process in acetone for 10 min (Figure 4(C)). The bottom-gate was constructed by attaching Cu plate onto the bottom of SiO_2/Si substrate using silver paste, after removing the lower SiO_2 layer of substrate with buffered hydrofluoric acid solution. Electrical characterizations of G-FETs were performed under a vacuum condition of 4.6 x 10^{-5} Pa using NE4000 nano probing microscopy from Hitachi.

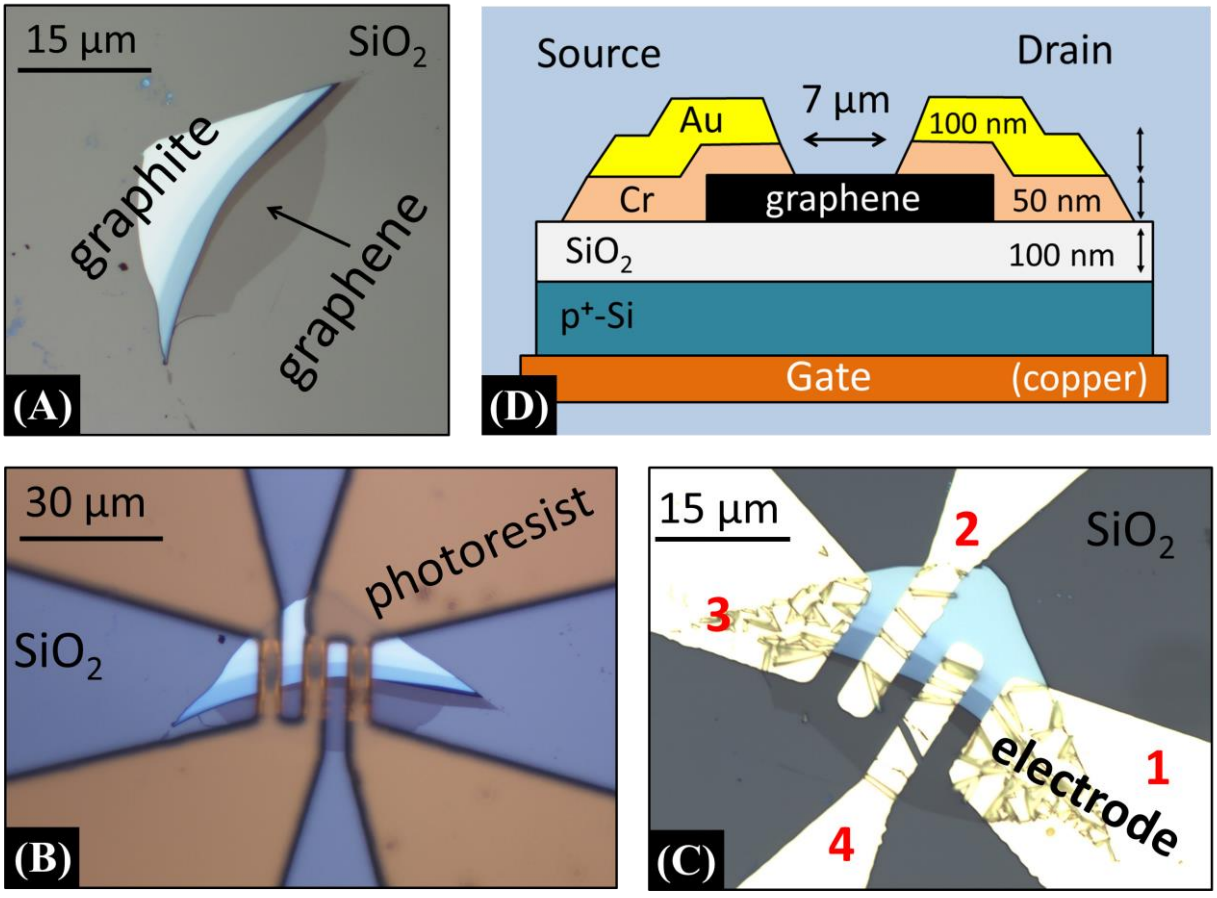

Figure 4. Graphene layer exfoliated from kish graphite using micromechanical cleavage method on SiO_2/Si substrate **(A),** graphene film was single layer and adjoining a graphite flake; source/drain patterns printed onto graphene layer using photolithography **(B)**; Au/Cr (100/50 nm) electrode deposited on graphene layer using electron beam vapor deposition technique **(C)**,

four electrodes were formed and proper combinations of two electrodes were used as source/drain; and structure of fabricated graphene-based FET **(D)**. Note that there is an opening or a gap at electrode 4. Source/drain combinations of electrode 1-4, 2-4 and 3-4 exhibited ambipolar characteristics of graphene, indicating that drain current flowed on graphene layer. However, other combinations which were electrodes 1-2, 1-3 and 2-3 did not exhibit ambipolar characteristics of graphene, indicating that drain current flowed through graphite.

3.4.3.2. Ambipolar characteristics

Transfer characteristics of G-FETs after two cycles of redox processes are plotted in Figure 5 and the changes in electron mobility during these processes are summarized in Figure 6. The exact values of electron mobility plotted in Figure 6 are provided in section C of the appendix. Each oxidation was performed through 3-min UV/O_3-treatment and each reduction was conducted through 3-min UV-irradiation. The slope of ambipolar curves in all G-FETs decreased after oxidation during the first redox process as shown in Figure 5, indicating the decreased electron mobility. However, significant recoveries of the ambipolar curve slope were observed after UV-irradiation, indicating that GO was reduced and the electron mobility recovered. The reversibility in electron mobility were observed in all G-FETs.

Changes in the behavior of ambipolar curves and electron mobility of G-FETs after the second redox process were identical to the first one. The ambipolar curves significantly recovered to nearly pristine state after conducting UV-irradiation three times. Nonetheless,

excessive UV-irradiation could cause re-oxidation or defect introduction. The reversibility in electron mobility were observed in all G-FETs even after the second cycle of redox process. It seems likely that the electron mobility reversibility could be observed even after multiple cycles of UV/O_3-treatment and UV-irradiation. The changes in electron mobility after two cycles of redox process are summarized in Figure 6. This non-thermal reversibility in G-FETs mobility we confirmed here in this study was relevant to its thermal counterpart by H_2/Ar-anneal treatment discussed in the previous chapter.[16] These results are also compatible with work reported by Eda et al. which stated that with extensive reduction GO prepared by a modified Hummers method underwent insulator-semiconductor-semimetal transitions, and the improvement of electron mobility was also confirmed.[27]

Additionally, as can be understood from Figure 5, another conductivity dip beside the main Dirac point or intrinsic Dirac point was observed in some G-FETs. Since the position of this conductivity dip was in the positive side of gate voltage, the conductivity dip might be caused by negatively charged impurities which are physically adhered to graphene surface during the redox processes, and then formed another Fermi level other than the intrinsic Fermi level, depending on the amount of negatively charged impurities which were adhered.[33] The formation of multiple Dirac point on G-FET will be also discussed in the next chapter.

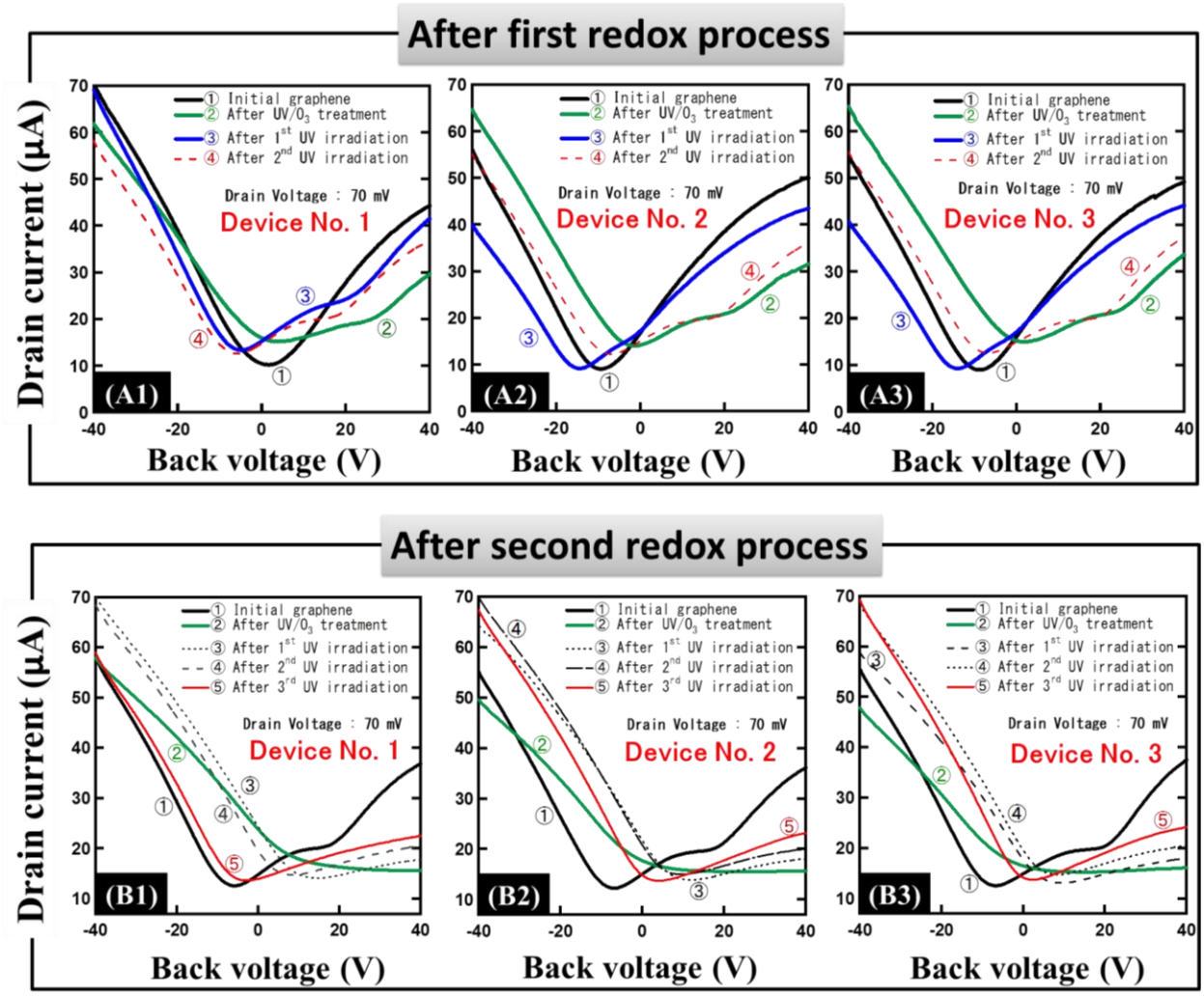

Figure 5. Transfer characteristics of three identical single-layer graphene-based FETs after first **(A1-3)**; and second cycle of oxidation through UV/O_3-treatment and reduction through UV-irradiation **(B1-3)**. Source/drain combinations of device No. 1, 2 and 3 were respectively combinations of electrodes 1-4, 2-4 and 3-4 shown in Figure 4(C).

3.4.3.3. Electron mobility and redox mechanism

In each carbon atom of graphene, three out of four valence electrons are used in the covalent bonds with three neighboring carbon atoms, they are called the σ-electrons and the covalent bonds are called the σ-bonds or indeed the C-C bonds. Thus, each carbon atom has

one electron, called the π-electron, which can move free around graphene layer, and act as electron carrier. The π-electrons located near the six individual corners in the first Brillouin zone of graphene, known as Dirac point in graphene, have zero effective mass or massless. This occurs because the energy and momentum relation is linear for electrons with low energies located near the Dirac points. These electrons are known as Dirac fermions, or Graphinos, and are responsible for the high electron mobility.[23] When the reactive radical oxygen atoms were doped onto graphene layer during UV/O_3-treatment, each of them used two free π-electrons from two carbon atoms to satisfy the octet configuration and form epoxide bridges. However, they did not need to break σ-bonds nor use σ-electrons to satisfy the octet configuration. It seems likely that the formation of epoxides or C-O bonds obstructed the path of electron carrier and hence increased electron scattering in graphene. Since electron mobility is directly affected by various scattering, the increased scattering eventually suppressed the electron mobility of G-FETs. That is possibly why the electron mobility decreased after oxidation.

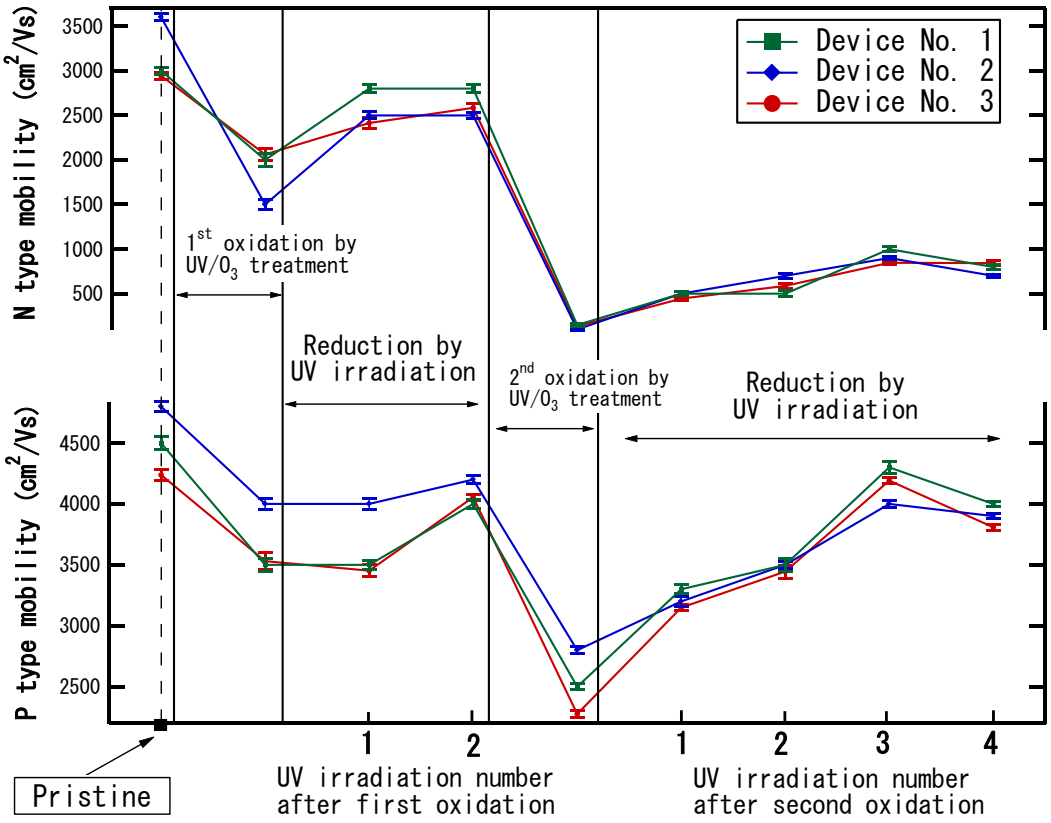

Figure 6. Electron mobility of three identical graphene-FETs after two cycles of oxidation through UV/O_3-treatment and reduction through UV-irradiation. Source/drain combinations of device No. 1, 2 and 3 were respectively combinations of electrodes 1-4, 2-4 and 3-4 shown in Figure 4(C). Error bars indicate standard error.

Because the bond energy of C-O (358 kJ/mol) is weaker than that of C-C (473 kJ/mol) in graphene,[25,26] when GO was UV-irradiated, the UV energy broke the C-O bonds, clearing the oxidized or obstructed path of electron carriers but still leaving the C-C bonds intact. Therefore, the electron mobility of G-FETs could recover to the pristine state after reduction through UV-irradiation. In the formation of C-O bonds, a number of free π-electrons were used in the C-O chemical bonding and then they were bound so that they could not act as electron

carriers. However, when the C-O bonds broke, apparently those π-electrons were freed again. Additionally, during these redox processes, seemingly σ-electrons and σ-bonds (or C-C bonds) were not involved, thus no significant lattice defects were introduced to the graphene crystalline. The non-involvement of σ-electrons and σ-bonds (or C-C bonds) during the redox processes apparently might make an important contribution to the reversibility of electron mobility even to the near pristine level.

The displacements of Dirac point (point of minimum conductivity) in ambipolar curves during each redox process observed in Figure 5 are summarized in Table 1. The Dirac points tended to shift positively after oxidation and negatively after reduction. These horizontal displacements of Dirac point might be attributed to the electrons surrounding the doped oxygen nucleus creating local negative charge, or to any charged impurities physically adhered to graphene surface during the redox processes. The Dirac points tended to shift upward after oxidation, indicating the increased conductivity, and tended to shift downward after reduction. These vertical displacements of Dirac points might be attributed to the reduced metal-graphene contact resistivity after oxidation causing an increase in electrical conductivity.[28]

As can be seen from the electrical characteristics shown in Figure 5, even at pristine condition, an electron-hole asymmetry or conductance asymmetry was observed. This phenomenon could be attributed to the role of metal contact in G-FET, as reported by Huard et al. which states that the asymmetry originates from the pinning of the charge density below the

metal/graphene interface.[32] That is probably the reason, why after conducting oxidation the G-FETs exhibited p-type like characteristics, which is because conductance asymmetry had already existed even at pristine stage and this conductance asymmetry became more obvious after oxidation, eventually exhibiting a p-type like characteristic.

Ambipolar characteristics of several G-FETs with various metal contacts measured in this experiment are shown in the section F in the appendix. Moreover, further study needs to be conducted to verify the authenticity of p-type like characteristics, since the equipment used in this experiment can only apply a gate voltage of ± 40 V.

Table 1. Position of Dirac point during redox process

Process	Back-gate Voltage (V)			Drain current (μA)		
Device No.	1	2	3	1	2	3
Initial graphene	1.6	-9.2	-8.4	10.2	9.1	9.0
First redox:						
$UV/0_3$-treatment	3.0	-1.8	1.8	15.1	14.0	15.0
1st UV-irradiation	-4.1	-14.2	-13.8	13.4	9.2	9.3
2nd UV-irradiation	-5.4	-6.8	-6.6	12.7	12.3	13.6
Second redox:						
$UV/0_3$-treatment	40.0	24.6	14.8	15.7	15.5	15.3
1st UV-irradiation	14.6	12.4	8.8	14.1	13.9	13.1

2nd UV-irradiation	7.6	9.2	8.2	14.7	15.0	14.8
3rd UV-irradiation	-3.2	4.0	2.0	13.7	13.8	13.7
4th UV-irradiation	14.7	10.8	9.8	13.7	13.5	13.5

3.4.4. Raman spectroscopy measurement

The feasibility of redox process through these methods was also examined from lattice disorder point of view using Raman spectroscopy. The Raman spectroscopy measurements of exfoliated graphene on 100-nm SiO_2/Si substrate were conducted to give us also direct comparison to the changes in electrical characteristics of G-FETs, discussed in the previous section, which were also fabricated from exfoliated graphene. Wang et al. have reported that the Raman features of monolayer exfoliated graphene are independent from the substrate used. In other words, the effect of substrate on the atomic/electronic structures of graphene is negligible for exfoliated graphene. On the other hand, epitaxial monolayer graphene on SiC substrate is also investigated in which a significant blueshift of Raman bands is observed. This could be attributed to the interaction of the graphene sheet with the substrate, resulting in the change of lattice constant and also the electronic structure.[29] Therefore, we could conclude that conducting Raman spectroscopy measurements using exfoliated graphene on SiO_2/Si substrate is probably reasonable.

There are three major band in Raman spectroscopy of graphene, which are G band, D band and 2D band. G band is related with the graphitic structure of graphene, and 2D band is related with the number of layer. In this section, we focused on D band which is related to the degree of defect in graphene lattice. The intensity or peak area of D band increases in the presence of lattice disorder or defect. [30,31] The complete measurement and analysis results are provided in section D of the appendix. We used NRS-2100 Raman spectrometer from JASCO Corporation to conduct the Raman measurements. The Raman spectroscopy measurements were conducted using 1 mW of 514.5 nm light from an argon (Ar) laser. The beam's spot size was around 1 μm and exposure time for every measurement was 500 sec. Since the spot size was relatively small enough, graphene exfoliated from kish graphite was able to be used in this measurement.[30,31] In every measurement, each sample was scanned for five times with a scanning time of 100 sec for each scanning, and the Raman spectra were obtained by computing the mean value from each scanning. The complete measurement results, including more detailed analysis results such as full width at half maximum (FWHM), are provided in section D of the appendix. Since the computation of peak area slightly differed depending on where we determine the start and end points of the band peak, each peak area calculation was repeated on different start and end points for five times.

The changes in degree of lattice disorder, which were calculated from the ratio of peak area of defect-induced D band and graphite-originated G band in Raman spectroscopy,[30,31] are

plotted in Figure 7. In this evaluation, three single-layer graphene films exfoliated from kish graphite were used (Figure 7),[19] and each UV/O_3-treatment and UV-irradiation were performed for 3 min. As shown in Figure 7, the lattice disorder increased after oxidation, since a certain number of oxygen was doped onto graphene lattice. Nevertheless, it gradually decreased after reduction through several UV-irradiations suggesting that the oxygen quantity decreased and GO was successfully reduced. The exact values of D/G band intensity ratio are stated in Table D-I of the appendix. We also found that seemingly there was a similar tendency occurred with the FWHM and the peak position of the G band which comply with the oxidation and reduction process as shown in Table D-II and D-II in section D of the appendix.

It seems likely that when the radical oxygen atoms reacted with carbon atoms and formed epoxide bridges on the graphene surface during UV/O_3-treatment, although it did not necessary introduce lattice defects on the graphene surface, the formation of epoxide groups would certainly increase the degree of lattice disorder. Therefore, the peak area of D band increased after oxidation through UV/O_3-treatment. However, when GO was UV-irradiated, it appears that the UV energy broke the C-O bonds, but still leaving C-C bonds intact and then eventually the degree of lattice disorder decreased. This might possibly happen because the bond energy of C-O (358 kJ/mol) is weaker than that of C-C (473 kJ/mol).[25,26] Moreover, during these redox processes, seemingly σ-electrons and σ-bonds (C-C bonds) were not involved. Hence, the oxygen atoms were feasibly de-doped without causing significant lattice defects.

We conducted also an additional experiment where an exfoliated graphene film was UV/O_3-treated for 6 min, and then the oxidized graphene was reduced by performing 6-min UV-irradiation several times. The complete measurement and analysis results are provided in section E of the appendix. In this additional experiment, the treatment time (6 min) was twice longer than treatment time of the experiment of the three exfoliated graphene films (3 min), yet the tendency after oxidation and reduction process was similar. The D/G band intensity ratio increased from zero to 1.39 ± 0.04, meaning that the D band had larger area than the G band. This may indicate that by conducting UV/O_3-treatment for 6 min the quantity of oxygen as well as degree of lattice disorder were greater than 3-min UV/O_3-treatment. Nevertheless, the D/G band intensity ratio decreased after performing 6-min UV-irradiation several times, indicating that the oxidized graphene was successfully reduced.

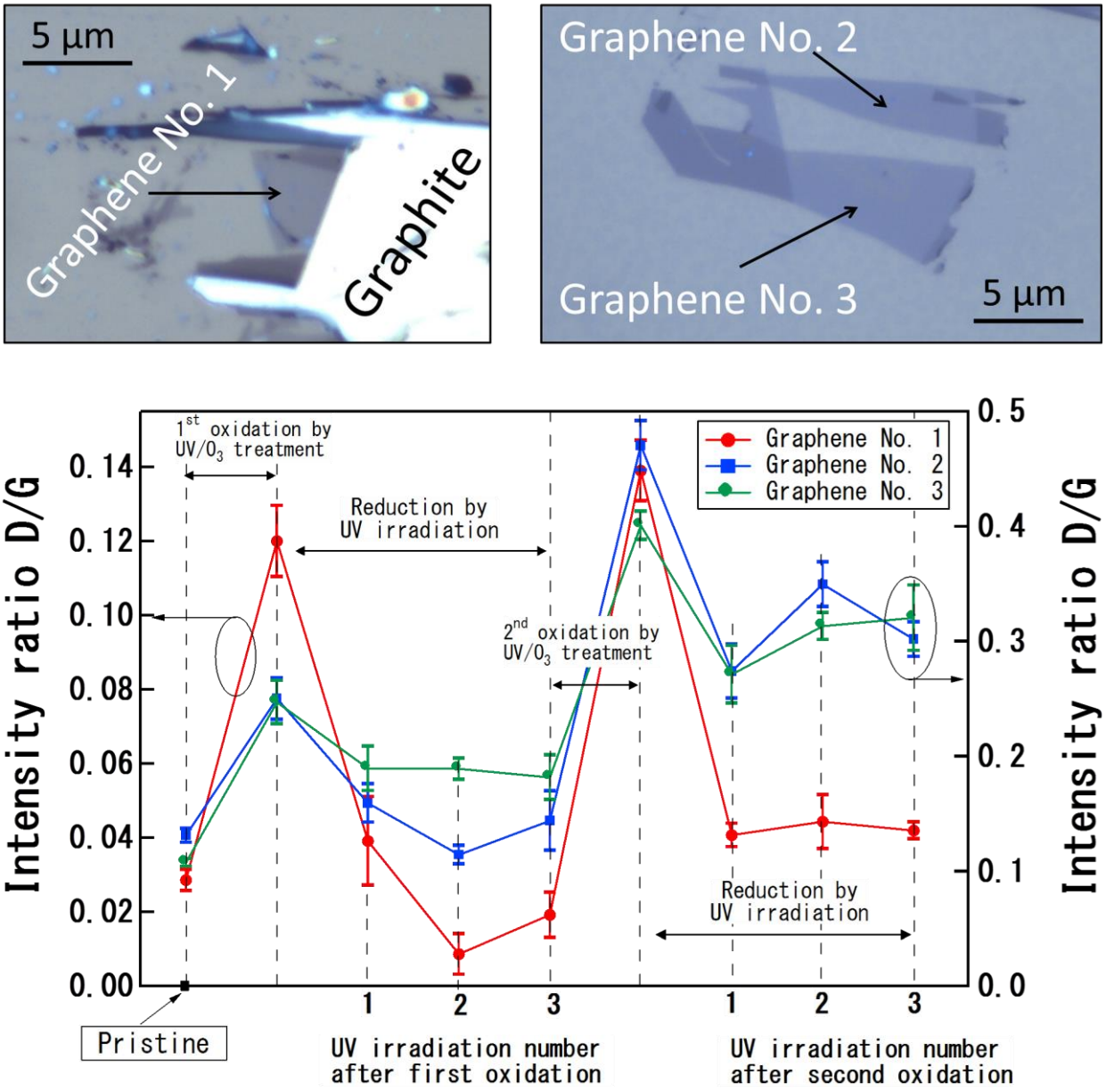

Figure 7. D/G band intensity ratio of Raman spectroscopy of exfoliated graphene after two cycles of oxidation through UV/O_3-treatment and reduction through UV-irradiation. Upper figures show graphene films used in Raman spectroscopy measurement. Error bars indicate standard deviation.

3.5. Conclusion

In summary, from the results of XPS measurements, we found that the doped oxygen atoms chemically reacted with carbon atoms in graphene and the quantity of doped oxygen reached its maximum which was around 20 % (approximately one oxygen atom in every five or six carbon atoms) after performing UV/O_3-treatment for 6 to 10 min. Conducting UV/O_3-treatment for around 6 or 10 min resulted in chemically homogeneous GO surface with only oxygen epoxide groups on graphene surface. Performing UV/O_3-treatment beyond 15 min as well as multiple turns of UV/O_3-treatment could lead to the formation of lattice defects and carbonyl groups on graphene surface. The oxygen quantity gradually decreased after conducting 6-min UV-irradiation several times, indicating that the resulting GO was successfully reduced. Hence, UV/O_3-treatment produced chemically homogeneous GO surface with oxygen epoxide groups only, and this could be reduced non-thermally through UV-irradiation. Moreover, we have confirmed that the changes in G-FETs electron mobility were non-thermally reversible even after multiple cycles of redox process and the reversibility was consistent with its thermal counterpart by H_2/Ar-anneal treatment discussed in the previous chapter.[16] All the data of XPS, Raman spectroscopy and electrical characteristics measurements supported each other, although the reversibility was not 100%. This might possibly occur because a certain degree of

lattice defect was introduced during the oxidation, moreover re-oxidation and the introduction of defect might also be involved during the reduction.

The re-oxidation and the introduction of defect could be improved through several method, for instance by utilizing a UV light source which is only strong enough to break the bond energy between oxygen atoms in O_3 (around 143 kJ/mol), but weaker than the bond energy between carbon atoms in graphene (473 kJ/mol) to prevent the formation of defect during the oxidation. Moreover, during the reduction an appropriate UV light source which is only strong enough to break the C-O bond energy (358 kJ/mol), but weaker than the bond energy between carbon atoms in graphene (473 kJ/mol) is required. Additionally, to prevent the re-oxidation, the reduction process should be performed in vacuum environment or by simultaneously supplying reduction agent such as H_2 gas while conducting irradiation through UV-irradiation. However, although those improvement can be expected, there are also some downsides to be considered. For example, because the apparatus used in the experiment was not equipped with H_2 gas channeling system, to modify the system or to do the UV-irradiation inside vacuum chamber would increase the cost eventually.

Furthermore, these methods are simpler, faster and more cost-effective than any other methods utilizing hydriodic acid or anneal treatment in UHV.[10-16] Thus, we concluded that UV/O_3-treatment and UV-irradiation might be prominent candidates to be used in oxidation and reduction, and furthermore on more advance chemical functionalization of graphene. In

addition, we hope that these findings would contribute to research on controlling electrical properties of graphene and development of graphene-based information processing and storage technology as well as sensing devices.

References:

1) Novoselov, K. S.; Geim, A. K.; Morozov, S. V.; Jiang, D.; Zhang, Y.; Dubonos, S. V.; Grigorieva, I. V.; Firsov, A. A. Electric Field Effect in Atomically Thin Carbon Films. *Science* **2004**, *306*, 666-669.

2) Morozov, S. V.; Novoselov, K. S.; Katsnelson, M. I.; Schedin, F.; Elias, D. C.; Jaszczak, J. A.; Geim, A. K. Giant Intrinsic Carrier Mobilities in Graphene and Its Bilayer. *Phys. Rev. Lett.* **2008**, *100*, 016602.

3) Zhang, H.; Fonseca, A. F.; Cho, K. Tailoring Thermal Transport Property of Graphene through Oxygen Functionalization. *J. Phys. Chem. C* **2014**, *118 (3)*, 1436–1442.

4) Yu, Q.; Lian, J.; Siriponglert, S.; Li, H.; Chen, Y. P.; Pei1, S. -S. Graphene Segregated on Ni Surfaces and Transferred to Insulators. *Appl. Phys. Lett.* **2008**, *93*, 113103.

5) Chung, C.; Kim, Y. -K.; Shin, D.; Ryoo, S. -R.; Hong, B. H.; Min, D. -H. Biomedical Applications of Graphene and Graphene Oxide. *Acc. Chem. Res.* **2013**, *46*, 2211-2224.

6) Shen, B.; Zhai, W.; Tao, M.; Lu, D.; Zheng, W. Chemical Functionalization of Graphene Oxide toward the Tailoring of the Interface in Polymer Composites. *Composites Science and Technology* **2013**, *77*, 87-94.

7) Hou, J.; Shao, Y.; Ellis, M. W.; Moored, R. B.; Yie, B. Graphene-based Electrochemical Energy Conversion and Storage: Fuel Cells, Supercapacitors and Lithium Ion Batteries. *Phys. Chem. Chem. Phys.* **2011**, *13*, 15384-15402.

8) Hirsch, A.; Englert, J. M.; Hauke, F. Wet Chemical Functionalization of Graphene. *Acc. Chem. Res.* **2013**, *46*, 87-96.

9) Georgakilas, V.; Otyepka, M.; Bourlinos, A. B.; Chandra, V.; Kim, N.; Kemp, K. C.; Hobza, P.; Zboril, R.; Kim, K. S. Functionalization of Graphene: Covalent and Non-Covalent Approaches, Derivatives and Applications. *Chem. Rev.* **2012**, *112*, 6156-6214.

10) Hummers Jr., W. S.; Offeman, R. E. Preparation of Graphitic Oxide. *J. Am. Chem. Soc.* **1958**, *80*, 1339-1339.

11) Marcano, D. C.; Kosynkin, D. V.; Berlin, J. M.; Sinitskii, A.; Sun, Z.; Slesarev, A.; Alemany, L. B.; Lu, W.; Tour, J. M. Improved Synthesis of Graphene Oxide. *ACS Nano* **2010**, *4*, 4806-4814.

12) Eigler, S.; Grimm, S.; Enzelberger-Heim, M.; Müllerb, P.; Hirscha, A. Graphene Oxide: Efficiency of Reducing Agents. *Chem. Commun.* **2013**, *49*, 7391-7393.

13) Zangmeister, C. D. Preparation and Evaluation of Graphite Oxide Reduced at 220 °C. *Chem. Mater.* **2010**, *22*, 5625-5629.

14) Stankovich, S.; Piner, R. D.; Chen, X.; Wu, N.; Nguyen, S. T.; Ruoff, R. S. Stable Aqueous Dispersions of Graphitic Nanoplatelets via the Reduction of Exfoliated Graphite Oxide in the Presence of Poly(sodium 4-styrenesulfonate). *J. Mater. Chem.* **2006**, *16*, 155-158.

15) Hossain, Md. Z.; Johns, J. E.; Bevan, K. H.; Karmel, H. J.; Liang, Y. T.; Yoshimoto, S.; Mukai, K.; Koitaya, T.; Yoshinobu, J.; Kawai, M.; Lear, A. M.; Kesmodel, L. L.; Tait, S. L.; Hersam, M. C. Chemically Homogeneous and Thermally Reversible Oxidation of Epitaxial Graphene. *Nat. Chem.* **2012**, *4*, 305-309.

16) Mulyana, Y.; Horita, M.; Ishikawa, Y.; Uraoka, Y.; Koh, S. Thermal Reversibility in Electrical Characteristics of Ultraviolet/Ozone-treated Graphene. *Appl. Phys. Lett.* **2013**, *103*, 063107.

17) Lin, Z.; Liu, Y.; Yao, Y.; Hildreth, O. J.; Li, Z.; Moon, K.; Wong, C. Superior Capacitance of Functionalized Graphene. *J. Phys. Chem. C*, **2011**, *115 (14)*, 7120–7125.

18) Prezhdo, O. V.; Kamat, P. V.; Schatz, G. C. Virtual Issue: Graphene and Functionalized Graphene. *J. Phys. Chem. C*, **2011**, *115 (8)*, 3195–3197.

19) Blake, P.; Hill, E. W.; Castro-Neto, A. H.; Novoselov, K. S.; Jiang, D.; Yang, R.; Booth, T. J.; Geim, A. K. Making Graphene Visible. *Appl. Phys. Lett.* **2007**, *91*, 063124.

20) Nagashio, K.; Nishimura, T.; Kita, K.; Toriumi, A. Mobility Variations in Mono- and Multi-Layer Graphene Films. *Appl. Phys. Express* **2009**, *2*, 025003.

21) Shang, J.; Ma, L.; Li, J.; Ai, W.; Yu, T.; Gurzadyan, G. The Origin of Fluorescence from Graphene Oxide. *Scientific Reports* **2012**, *2*, 792.

22) Jeong, H.-K.; Noh, H.-J.; Kim, J.-Y.; Jin, M. H.; Park, C. Y.; Lee, Y. H. X-Ray Absorption Spectroscopy of Graphite Oxide. *Europhys. Lett.* **2008**, *82*, 67004.

23) Wallace, P. R. The Band Theory of Graphite. *Phys. Rev.* **1947**, *71*, 622.

24) Denis, P. A.; Iribarne, F. Comparative Study of Defect Reactivity in Graphene. *J. Phys. Chem. C*, **2013**, *117 (37)*, 19048–19055.

25) Glockler, G. Carbon–Oxygen Bond Energies and Bond Distances. *J. Phys. Chem.* **1958**, *62*, 1049-1054.

26) Brenner, D. W.; Shenderova, O. A.; Harrison, J. A.; Stuart, S. J.; Ni, B.; Sinnott, S. B. A Second-Generation Reactive Empirical Bond Order (REBO) Potential Energy Expression for Hydrocarbons. *J. Phys.: Condens. Matter* **2002**, *14*, 783-802.

27) Eda, G.; Mattevi, C.; Yamaguchi, H.; Kim, H. K.; Chhowalla, M. Insulator to Semimetal Transition in Graphene Oxide. *J. Phys. Chem. C*, **2009**, *113 (35)*, 15768–15771.

28) Li, W.; Liang, Y.; Yu, D.; Peng, L.; Pernstich, K. P.; Shen, T.; Walker, A. R. H.; Cheng, G.; Hacker, C. A.; Richter, C. A.; Li, Q.; Gundlach, D. J.; Liang, X. Ultraviolet/Ozone Treatment to Reduce Metal-Graphene Contact Resistance. *Appl. Phys. Lett.* **2013**, *102*, 183110.

29) Wang, Y. Y.; Ni, Z. H.; Yu, T.; Shen, Z. X.; Wang, H. M.; Wu, Y. H.; Chen, W.; Wee, A. T. S. Raman Studies of Monolayer Graphene: The Substrate Effect. *J. Phys. Chem. C*, **2008**, *112 (29)*, 10637–10640.

30) Pimenta, M. A.; Dresselhaus, G.; Dresselhaus, M. S.; Cancado, L. G.; Jorio, A.; Saito, R. Studying Disorder in Graphite-based Systems by Raman Spectroscopy. *Phys. Chem. Chem. Phys.* **2007**, *9*, 1276-1290.

31) Graf, D.; Molitor, F.; Ensslin, K.; Stampfer, C.; Jungen, A.; Hierold, C.; Wirtz, L. Spatially Resolved Raman Spectroscopy of Single- and Few-Layer Graphene. *Nano Lett.* **2007**, *7*, 238-242.

32) Huard, B.; Stander, N.; Sulpizio, J. A.; Goldhaber-Gordon, D. Evidence of the role of contacts on the observed electron-hole asymmetry in graphene. *Physical Review B* **2008**, 78, 121402.

33) Chiu, H. -Y.; Perebeinos, V.; Lin, Y. -M.; Avouris, P. Controllable p-n Junction Formation in Monolayer Graphene Using Electrostatic Substrate Engineering. *Nano Lett.* **2010**, 10 (11), 4634–4639.

CHAPTER 4

Graphene and ferritin:

Construction of p-n junction on graphene

We found an alternative way to construct a stable p-n junction on graphene-based field effect transistor (G-FET) through physical adsorption of ferritin (spherical protein shell). The produced G-FET can also operate through water-gate. We found that native negatively-charged ferritins became positively-charged after performing electron beam (EB)-irradiation. We utilized this property to construct a p-n junction on G-FET. We found also that EB-irradiation could remove the effect of charged impurity adsorbed on graphene layer, thus the Dirac point was adjusted to gate voltage Vg = 0.

In semiconductor paradigm, p-n junctions are formed by joining n-type and p-type semiconductor materials, and that is also the definition on p-n junction in general, including semiconductor material and semi-metal material such as graphene.[1,2] P-type and n-type materials have different Fermi levels, and after joining both n-type and p-type materials to form p-n junction, the constructed p-n junction has a single constant Fermi level at equilibrium state.[1,2] This concept applies on both semiconductor materials and

graphene. However, since they have different band structures, p-n junction of semiconductor and p-n junction of graphene do not necessarily exhibit the same transfer characteristic. In case of graphene, p-type and n-type G-FET is constructed by performing a process of adsorption of negatively or positively charged-dopant onto graphene layer respectively. The formation of p-type G-FET is indicated by the location of Dirac point in ambipolar characteristic which is in positive side of gate voltage, and in case of n-type G-FET, the location of Dirac point is in the negative side of gate voltage. Therefore, the formation of p-n junction of G-FET is indicated when two Dirac points were observed in ambipolar characteristic at the same time.[3-13]

4.1. Background

Graphene is entirely made of carbon atom and known to be sensitive to charged materials. Therefore, graphene is expected to be a promising candidate for sensing device development, especially for bio-sensors since most of living organism are largely consisted of carbon atoms also. However, in the realization of graphene-based sensing electronics, a criterion sensitivity and bio-compatibility are ones of many criteria required to be fulfilled and systematically studied. In this investigation, as an instance of bio-

molecule, spherical protein shell called ferritin was used. The structural stability, assembly properties, and capability to store a huge variety of cores make ferritin a promising element in nano-engineering.[14-17] Ferritin is entirely consisted of protein, and proteins are the key working molecules and building blocks in all living cells.

While the interaction between graphene and ferritin being investigated, we found that the ambipolar characteristics of the G-FETs used in the experiment were modulated into the ambipolar characteristic of peculiar G-FET with p-n junction on its graphene layer. On the other hand, to realize more complex and sophisticated graphene-based electronics, understanding of the basic nature of p-n junctions in graphene and their production are crucial. It has been reported that p-n junctions in graphene could lead to unique phenomena such as fractional quantum Hall transport,[3,4] Klein tunneling,[5] quantum point contacts,[6] quantum dots,[7] and planar electron Veselago lens and prism used for focusing electron flow.[8] Wilmart et al. have conducted simulations showing that graphene transistors with p-n junctions have a significant switching capability.[9] Several methods for creating p-n junctions on graphene have been reported; such as, through chemically doping with polyethylene imine and diazonium salts used as complementary molecular dopants,[10] using high-resolution resist material like hydrogen silsesquioxane

(HSQ) as complementary dopants,[11] by constructing double gates below and on top of the graphene layer,[4,8,12] or through electrostatic modification of gate insulators.[13]

In this study, we present a unique approach to the creation of a p-n junction on graphene-based field effect transistors (G-FET) through physical adsorption of a protein-based bio-supramolecule called ferritin. The ferritin used in this study is a spherical protein shell consisting of 24 subunits or peptide chains, arranged in F432 symmetry, forming a hollow sphere with an outer diameter of 12 nm and a shell thickness of 2 nm in a water environment.[14-17] Ferritin is capable of storing iron oxide and thus plays a key role in iron metabolism. Ferritin is ubiquitously found in humans, vertebrates and invertebrates, higher plants, fungi, and bacteria and has been a subject of research because of its unique electrochemical, magnetic and assembly properties.[14-17] Recently, ferritin has been utilized in the construction of various nano-structure materials used in the fabrication of conducting,[18] semiconducting,[19] and magnetic nano-material.[20-24] The structural stability, assembly properties, and capability to store a huge variety of cores make ferritin a promising element in nano-engineering.[16-24] By combining G-FET with ferritin, we were able to form a reversible p-n junction on graphene, which can be activated through electron beam (EB)-irradiation and deactivated by supplying water. We also confirmed that the p-n junction was stable. Moreover, investigation of the interaction

between graphene and bio-molecules such as ferritin is a fundamental issue in understanding the bio-compatibility of G-FET, which is essential in the realization of graphene-based bio-sensors. As shown in this study, judging from the electrical characteristics of G-FET, the produced p-n junction was stable even when the electric field was applied through a water-gate, and this could compensate for the lack of stability of recently developed MoS_2 nanosheet-based FET biosensors, especially when operated in a water environment.[30] In this paper, along with the formation of p-n junctions on G-FET, the interactions between graphene and ferritin, characterized both in water and vacuum environments, are elaborated. The interaction of graphene and electron beam is also presented as a reference.

4.2. Experimental

In the fabrication process of G-FET, the graphene films were exfoliated on a 100-nm SiO_2/p^+-Si substrate using the micromechanical cleavage method of kish graphite.[25-27] The electrodes were formed through a chain of procedures of photolithography to print source/drain patterns onto both ends of the graphene layer, and then deposition of Au/Cr (100/50 nm) metals with electron beam vapor deposition technique followed by a lift-off

process in acetone for 10 min.[26,27] We used two types of ferritin: apoferritin or empty ferritin, and ferritin with iron oxide cores (iron-cored ferritin).[13-17] The outer and inner diameters of the ferritin are approximately 12 and 7 nm, respectively. Interactions between graphene and ferritins were investigated by examining the changes in transfer characteristic or ambipolar curves of G-FET after protein adsorption.

Earlier studies have reported that zeta potential of ferritin differs according to the pH of its solution, and the ambipolarity of G-FET also differ when solution with various pH value was dropped onto the graphene layer.[13-17] In order to investigate the interaction between graphene and ferritin without any pH influence from the solution which would affect the ambipolarity of the G-FETs, firstly the interaction between graphene and ferritin was investigated under neutral pH environment or under deionized pure water. The result of investigation between graphene and ferritin in wet environment is very important in the development of graphene-based devices which operate under wet environment such as bio-sensor. However, in order to expand the significance of this study to the more generalized electronic application system, the investigation of interaction between graphene and ferritin in vacuum environment was also performed using a nano probing microscope. This equipment allows us to conduct electrical characterization and scanning electron microscope (SEM) observation concurrently. The

electron beam from this SEM was expected to affect the nature of ferritin and the ambipolarity of G-FET. Therefore, the interaction between graphene and ferritin before and after being exposed to the electron beam was also performed. The investigation in atmospheric environment was not performed due to the impurity contained in the air that would deteriorate the electrical characteristic of G-FET.

Firstly, change in electrical ambipolar characteristics after apoferritin adsorption when the electric field was applied through the water-gate was studied. The ambipolar characteristic of G-FET is a modulation of drain current obtained when a constant drain-source voltage and a variable gate voltage are applied concurrently. Fig. 1-A shows a schematic drawing of the setup for G-FET ambipolar characteristic measurements. 0.3 μL of aqueous solution of 1 mg/mL apoferritin was dropped on graphene and apoferritins were let adsorb onto the graphene surface. The remaining water was used as a liquid gate and ambipolar characteristics were measured. The water evaporated within several minutes during the electrical measurement. At this point, another 0.3 μL of aqueous ferritin solution was dropped and the measurement was repeated. This procedure was repeated several times. The number of ferritins presumably increased as the intermittent apoferritin solution drop and dry process was repeated.

4.3. Result and discussion

The discussion will encompass the interaction between graphene and ferritin measured in water and vacuum environment, and also the interaction between graphene and EB-irradiation.

4.3.1. Interaction between graphene and ferritin measured in water

The interaction between graphene and both apoferritin and iron-cored ferritin will be discussed from the electrical characteristic point of view in the next two sections. The electrical characteristics were measured under water environment.

4.3.1.1. Graphene and apoferritin in water

The changes in ambipolar curves or transfer characteristics after dropping the ferritin solution several times are shown in Fig. 1-B, in this measurement the electric field was applied through the water-gate. The ambipolar characteristics of pristine G-FET, before the dropping of apoferritin solution (shown in dark blue) and the characteristics after the first drop (shown in grey) did not show a major difference, suggesting that a small amount of apoferritin adsorbed onto the graphene surface of has little to no effect. However, the

ambipolar characteristics changed gradually and drastically after intermittent ferritin solution dropping and drying, which must have created an apoferritin layer on the graphene surface. As can be seen in the figure, the slope of the ambipolar curve became steeper as the number of drops increased. It is possible that the electron mobility of G-FET increased after each drop. Furthermore, the Dirac point shifted toward positive direction after each drop, and additional depression in conductivity or local minimum value other than the main Dirac point was observed after the 4^{th} drop (plotted in light blue dots) where the liquid-gate voltage was approximately or less than -1.5 V.

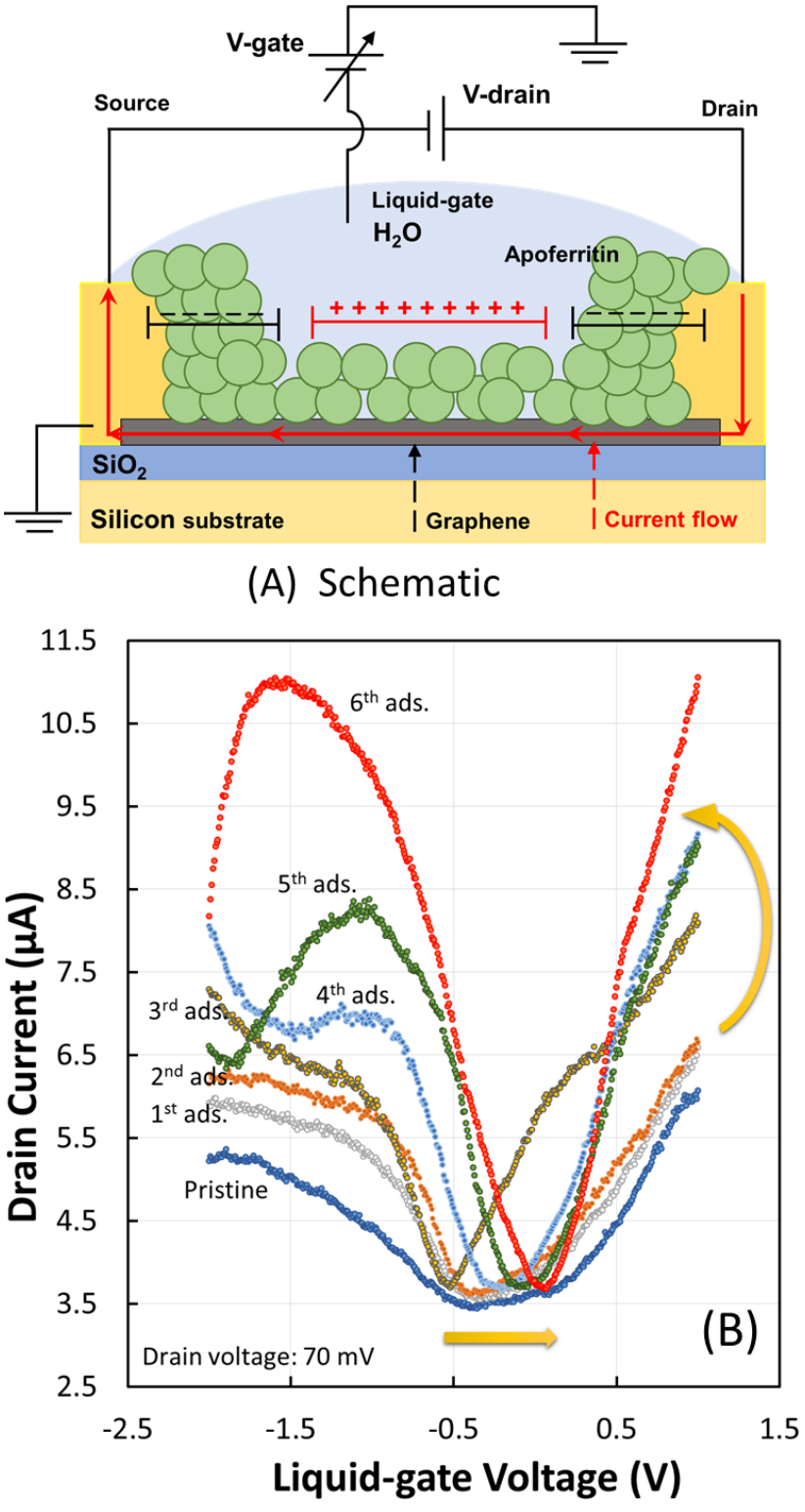

Fig. 1. Schematic of measurement setup when electric field was applied through water-gate **(A)**; and changes in G-FET ambipolar characteristics after apoferritin adsorption **(B)**.

The gradient of ambipolar curve increased after each adsorption, indicating increased electron mobility. The formation of second Dirac point can be observed after the 4th adsorption.

The increased mobility could be attributed to the accumulated apoferritins forming a kind of protective layer on the top of the graphene surface. This protective layer would likely reduce the electron scattering, eventually increasing the electron mobility. The increased electron mobility increased the conductivity of G-FET itself, as indicated by the increment of drain current in the saturation region. The Dirac point, i.e. the minimum conductivity point, shifted positively indicating that apoferritin was seemingly negatively charged in H_2O. Yamashita et al. reported that apoferritin is negatively charged around a neutral pH.[17,24,28] It is known that when negatively charged materials are adsorbed on graphene, the Dirac point shifts positively or toward the positive voltage side, because it provides an extra negative electric field. An additional amount of positive electric field is necessary for counterbalance. Furthermore, as confirmed by Ohno et al., after introduction of negatively charged bio-molecules onto graphene, the Dirac point shifted positively.[29]

The formation of another conductivity dip in ambipolar characteristics, which can be observed after the 4th adsorption of apoferritin, is likely related with the formation of p-n junction. The formation of this conductivity dip or the second Dirac point was clearly observed in the experiments involving iron-cored ferritin (Fig. 2 and 5).The formation of p-n junctions was discussed in detail by Farmer, Brenner and Chiu et al. [9,10,12] The two Dirac points are the sign of the formation of p-n junction in graphene. The p-n junction is formed on graphene when positively and negatively charged material are locally adsorbed on the graphene surface at the same time. This may explain the formation of the conductivity dip by taking into consideration that apoferritins are negatively charged in the water and the ferritin-family protein adsorbed on a substrate, once dried, became positively charged in the water, as reported by Yamada et al.[30] The history of "dried or not" makes apoferritins exhibit different electrostatic effects, positive and negative charge effects under water, and form p-n junction. A part of the apoferritins was dried during consecutive electrical measurements and became positively charged. On the other hand, other apoferritins remained negatively charged. This locally distributed negatively and positively charged apoferritin micro-lump leads to the formation of p-n junctions on graphene. Ferritins accumulated around the contact regions between graphene and electrode metals were considerably denser than ferritins adsorbed on the graphene surface

(Fig. 5-F), so that, it is likely that apoferritins in those regions were kept wet, even when ferritins on the graphene were dried.

4.3.1.2. Graphene and iron-cored ferritin in water

The changes in G-FET ambipolar characteristics after dropping 0.3 μL of aqueous solution of iron-cored ferritin on the graphene layer are shown in Fig. 2-B. Two Dirac points were clearly observed after the adsorption of iron-cored ferritin, indicating the formation of p-n junctions on the G-FET. The formation of p-n junctions through iron-cored ferritin adsorption was even more obvious than that of apoferritin. The figure illustrates that in addition to an increased electron mobility and shifted Dirac point, a significant increase in electrical conductivity was observed for the iron-cored ferritin. This is likely due to a certain degree of drain current flowing through the iron-cores accumulating at the corners of the contact between the graphene and electrodes (Fig. 5-F), avoiding the high contact resistivity between graphene and metal,[13] as illustrated in Fig. 2-D.

As can be seen from Fig. 2-B, the formation of another minimum value other than the main Dirac point was observed directly after the second drop of iron-cored ferritin,

indicating p-n junction formation. In both apoferritin and iron-cored ferritin cases, the emergence of p-n junction became more obvious as the number of adsorption increased, as can be compared from Fig. 1 and Fig. 2. However, in the case of iron-cored ferritin, the formation of p-n junctions happened faster and more distinct than that of apoferritin. A conductivity plateau was observed next to the main Dirac point following the first drop of iron-cored ferritin aqueous solution. From that conductivity plateau, the formation of the second Dirac point was distinctly observed after the second drop, and the depth of the second Dirac point increased as the number of drops increased. This suggests that there is another factor contributing to the faster p-n junction formation other than dried ferritin. Iron-cored ferritins seem to make aggregates more compared to apoferritin, however the cause of which is not yet known well. This tendency might increase the adsorption of ferritin.

The emergence of Dirac point in transfer characteristic of G-FET, or the lowest conductivity point, is related to the formation of Dirac point in the band structure. P-type and n-type G-FET have different Fermi levels, where the former has higher Fermi lever than the latter, as shown in Fig. 2 (C). In other way, the Dirac point of p-type G-FET is located in higher energy level than the other. When these p-type and n-type G-FET were conjugated, a new G-FET with band structure that possess two Dirac point was

constructed. That is why p-n junction on G-FET has two Dirac points in its transfer characteristic. Although, the modified G-FET in this experiment seems to have n-p-n junction, as shown in Fig. 2 D, the transfer characteristics did not exhibit three Dirac points, because apparently the two n-type regions had Dirac points with the same energy level, meaning that there were only two Dirac points in the band structure, one from the p-type region and the other from the two n-type region.

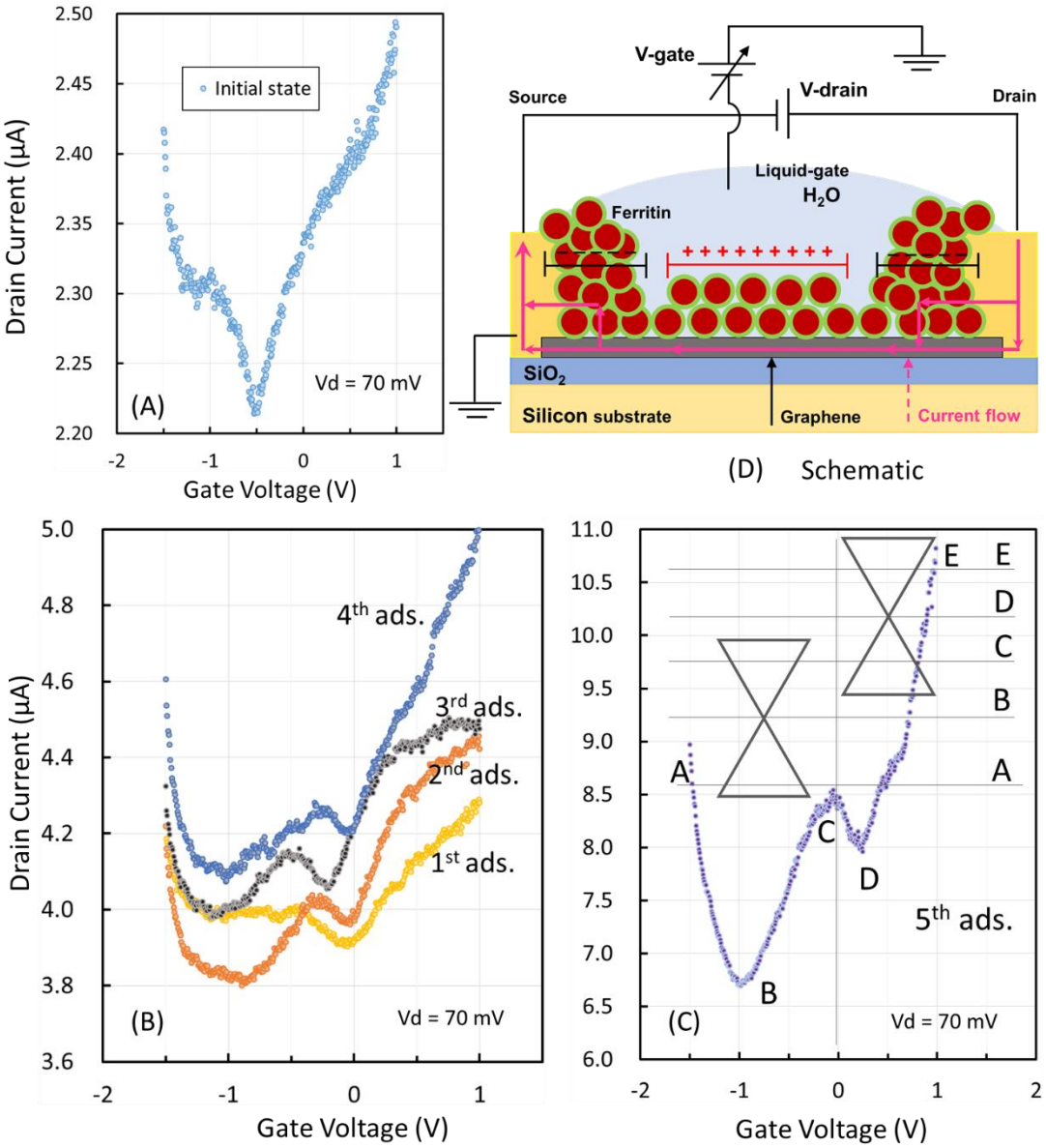

Fig. 2. Changes in ambipolar characteristics of G-FET measured after iron-cored ferritin adsorption, electric field was applied through water-gate. Ambipolar curve of pristine G-FET **(A)**; after 1st to 4th adsorption **(B)**; after 5th adsorption of iron-cored ferritin **(C)**; and schematic of iron-cored ferritin adsorption and measurement setup **(D)**. The formation of p-n junction on G-FET can be confirmed from the emergence two Dirac points, as the signature of a p-n junction **(C)**.

4.3.2. Interaction between graphene and electron beam

The interaction between graphene and electron beam was also studied under a vacuum environment. Electrical characterizations were performed under a vacuum condition of 4.6 $x10^{-5}$ Pa using a NE4000 nano probing microscope from Hitachi. Here, the silicon substrate was functioning as a back gate and SiO_2 as gate insulator. This equipment allows us to conduct electrical characterization and scanning electron microscope (SEM) observation concurrently. The EB-irradiations were performed by the SEM under the following conditions: (1) the irradiation time was 10 sec, (2) the irradiation area was 10 x 10 μm, (3) the emission current was 10 μA, and (4) the accelerating voltage was 1 kV.

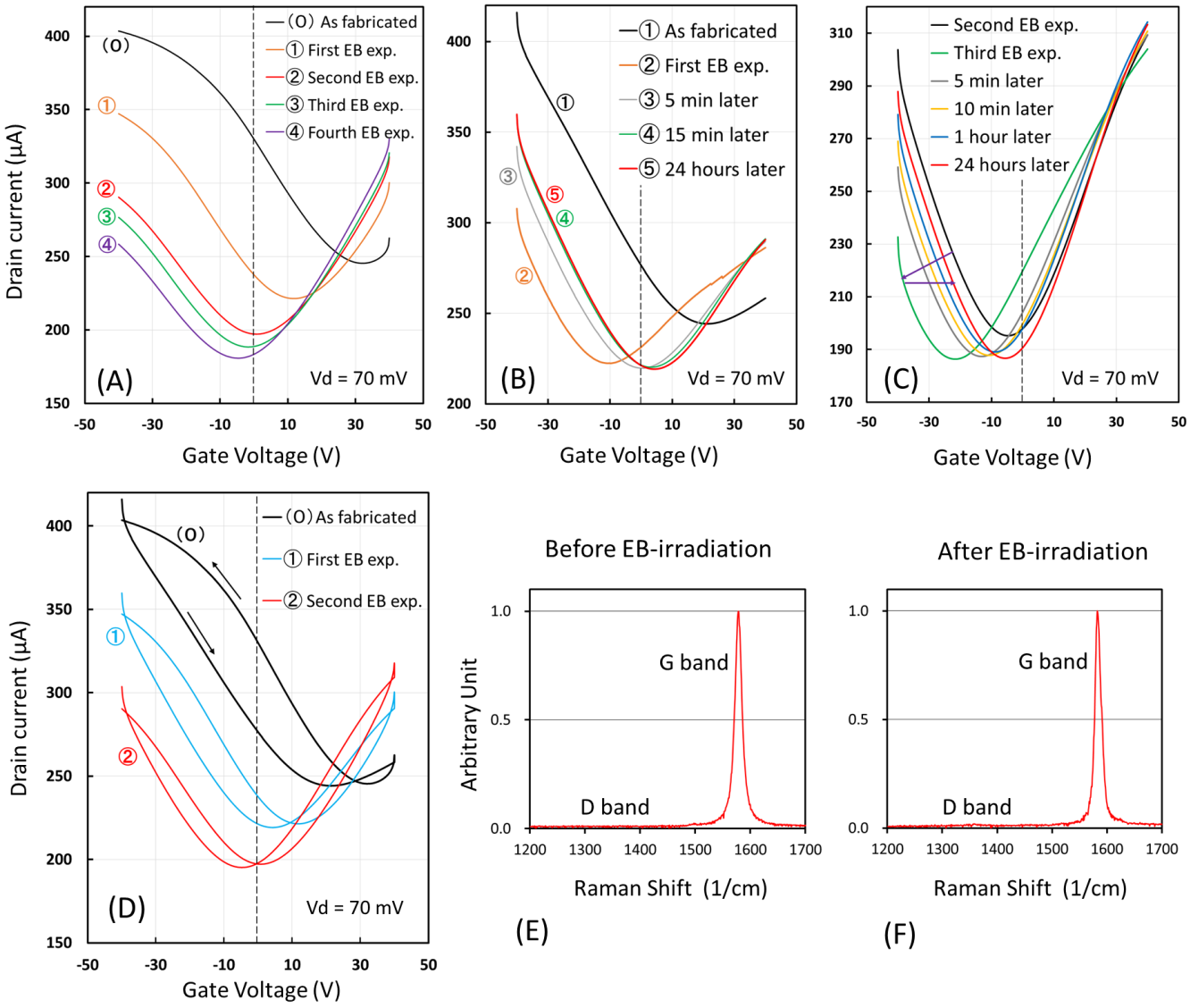

Fig. 3. Changes in ambipolar characteristics of G-FET measured in vacuum environment after performing EB-irradiation several times **(A)**; detail changes of ambipolar curves through time after 1st **(B)**; and 3rd EB-irradiation **(C)**; narrowed hysteresis width after performing EB-irradiation **(D)**; Raman spectroscopy of graphene layer before **(E)**; and after performing EB-irradiation **(F)**. EB-irradiation caused the Dirac point to shift to gate voltage Vg = 0 and to narrow the hysteresis width, indicating that EB-irradiation could remove the charged impurity adsorbed on graphene layer. As can be understood from defect induced D band in Raman spectra **(E, F)**, located at 1350 cm^{-1}, EB-irradiation did not introduce any significant lattice defects.

The changes in G-FET ambipolar characteristics after several EB-irradiations are shown in Fig. 3-A. The Dirac point of ideal G-FETs, or G-FETs with a negligible amount of charged impurity on the graphene surface, is located at gate voltage Vg = 0, however, since typical G-FETs unintentionally have a substantial amount of positively charged impurity, the Dirac point of fabricated G-FETs is typically located to some extent away from gate voltage Vg = 0, at the high-voltage side, as confirmed in Fig. 3-A. After performing EB-irradiation several times, the Dirac point gradually shifted close to gate voltage Vg = 0, as plotted in Fig. 3-A. This suggests that EB-irradiation cleaned the charged impurities of graphene surface. This is supported by the fact that the hysteresis width became gradually narrower after EB-irradiations (Fig. 3-D). The location of the Dirac point near Vg = 0 V along with a very small hysteresis indicates the absence of negatively charged impurities on the graphene surface after EB-irradiation several times. Another plausible explanation is that the EB-irradiation might cause the negatively charged impurities to lose electrons and be neutralized, eventually shifting the Dirac point to gate voltage Vg = 0.

When the initial position is away from Vg = 0 toward the positive voltage side, the behavior of the Dirac point displacement by EB-irradiation is shown in Fig. 3-B. EB-irradiation caused the Dirac point to shift broadly to the negative voltage side. Within 15 min the Dirac point shifted back very close to gate voltage Vg = 0, and this last re-shifting was permanent, remaining stable even after 24 hours. The negative shift of the Dirac point away from Vg = 0 suggests that positively charged substances were physically adsorbed onto the graphene surface. However, based on the result that the Dirac point shifted back to Vg = 0, it is reasonable to assume that those positively charged substances were naturally removed from the graphene surface under the low pressure of the vacuum environment.

When the initial position of the Dirac point is around Vg = 0, indicating the graphene surface was free of charged impurities, EB-irradiation caused the Dirac point to shift broadly to the negative voltage side, as shown in Fig. 3-C. Within 10 min, however, the Dirac point shifted back to Vg = 0. This suggests that EB-irradiation might cause a certain amount of positively charged impurity to be physically adsorbed on the graphene surface temporarily. Conversely, EB-irradiation may cause the graphene layer to lose some of its electrons which would lower the Fermi level and eventually shift the Dirac point

negatively. This state did not remain for a long period, possible because additional electrons were injected from metal electrode region to the graphene layer.

Raman spectroscopy measurements were also performed before and after the EB-irradiation to examine whether it introduced crystalline defects into the graphene lattice. As confirmed in Fig. 3-E and F, the D band peak, which is the lattice defect induced band located at 1350 cm^{-1}, was not detected even after conducting EB-irradiation several times. This indicates that the EB-irradiation performed in this study did not introduce any crystalline defect. This may be explained by the short irradiation time (10 sec) and very low accelerating voltage (1 kV). Following results described above, it could be concluded that EB-irradiation is a prominent way to clear or neutralize the negatively charged impurity and adjust the position of the Dirac point back to gate voltage Vg = 0.

4.3.3. Interaction between graphene and ferritin measured in vacuum

The interaction between graphene and both apoferritin and iron-cored ferritin will be discussed from the electrical characteristic point of view in the next two sections. The electrical characteristics were measured under vacuum environment.

4.3.3.1. Graphene and apoferritin in vacuum

Thirdly, the change in electrical characteristics after ferritin adsorption was measured under vacuum environment. For comparison, both apoferritin and iron-cored ferritin were used. The changes in G-FET ambipolar characteristics after apoferritin adsorption measured under vacuum environment are shown in Fig. 4-A to D. 0.3 μL of aqueous solution of apoferritin with a concentration of 1 mg/mL was dropped onto the graphene layer and then the device was placed inside a sample case for 30 min so that the water evaporated and the apoferritins were physically adsorbed onto the graphene layer. After apoferritin adsorption, as shown in the figures, the Dirac points tended to positively shift, indicating that the apoferritins were negatively charged. This result is consistent with some reports by Harisson, Yamashita and Kumagai et al. stating that native ferritins are negatively charged.[15,17,28] However, after conducting EB-irradiation on the adsorbed apoferritins, the Dirac point shifted negatively and this negative shift seems to be permanent even after 24 hours. It may be reasonable to assume that most of the apoferritins lost some of their electrons due to EB-irradiation and became positively charged, leading to the negative shift of the Dirac point. It has also been reported by

Shimaya and Li et al. that conducting EB-irradiation to semiconductor and insulator materials could cause them to be positively charged.[31,32]

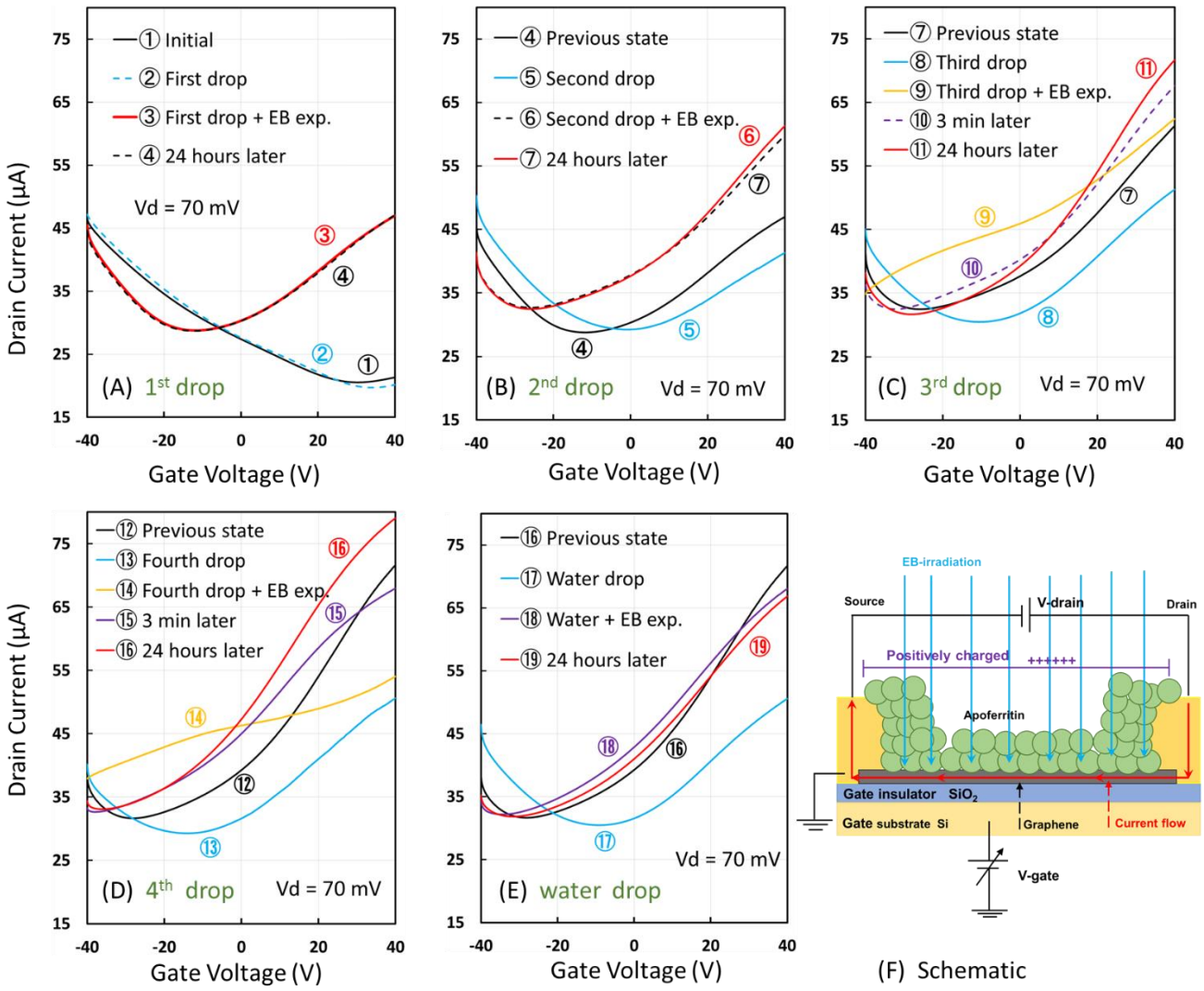

Fig. 4. Changes in ambipolar characteristics of G-FET measured under vacuum environment after adsorption of apoferritin several times **(A)** to **(D)**; and after water supply **(E)**; schematic of apoferritin adsorption and the measurement setup **(F)**. Native ferritins are negatively charged so the Dirac point positively shifted, however after conducting EB-irradiation the Dirac point shifted negatively, indicating that the

apoferritin became positively charged. Water also had apparently an important role in restoring the ferritin electrostatic **(E)**.

Dropping the apoferritin aqueous solution was repeated several times and after each dropping, changes in the behavior of ambipolar characteristics displayed the same tendency. After another dropping of the solution, the Dirac point shifted positively, possibly implying that a certain amount of negatively charged native apoferritins were newly added and possibly the positively charged apoferritin, which were adsorbed before, accepted electrons from the solvent or water molecules and eventually were naturalized or even partially became negatively charged again or recovered like the native apoferritin. However, after conducting EB-irradiation consecutively, the Dirac point shifted negatively and this negative shift seems to be permanent even after 24 hours, as shown in Fig. 4-A to D. The position of the Dirac point increasingly shifted negatively as the number of drops increased or presumably as the number of adsorbed apoferritins increased. After repeating the procedure of dropping aqueous solution of apoferritin and consecutively conducting EB-irradiation for four times, the position of the Dirac point shifted significantly from gate voltage Vg = 30 V to Vg = -39 V, as can be compared

from lines No. 1 (Fig. 4-A) and 16 (Fig. 4-D). In this case, it seems probable that since most of apoferritin were uniformly (positively) charged, the p-n junction was not formed.

Furthermore, in order to confirm that the water might be involved in the electrostatic charge of ferritin, 0.3 μL of pure water was dropped onto positively charged apoferritin adsorbed on a graphene layer and the apoferritin were consecutively EB-irradiated. As revealed in Fig. 4-E, the Dirac point shifted positively after dropping the water suggesting that a certain amount of positively charged apoferritins accepted electrons from the water molecules and became possibly naturalized or even became negatively charged close to the condition of native apoferritins which are also negatively charged. After conducting EB-irradiation consecutively, similar to the case of newly dropping aqueous solution of apoferritins, the Dirac point shifted negatively. These results show a strong possibility that the electrostatic charge of ferritin could be recovered simply by supplying water molecules.

This negative shift seems to be permanent even after 24 hours, and the adsorbed ferritin were not rinsed out even after pure water cleanses. Therefore, it is reasonable also to assume a possibility the existence of electrostatic of the adsorbed ferritins in vacuum, besides that the adsorbed ferritins were electrically charged up. It was confirmed from the

K-AFM image of ferritin after being EB-irradiated, shown in section H in the appendix, that the surface charge of EB-irradiated ferritin was positive indeed.

Additionally, it was found also that after conducting EB-irradiation the ambipolar curve shifted negatively to a significant extent so that the Dirac point was not observable, as plotted in yellow lines at Fig 4-C and 4-D (lines No. 9 and 14). However, after re-conducting the electrical characterization, the ambipolar curve re-shifted back again so that the Dirac point was barely observed around gate-voltage Vg = 37 - 39 V. It could be speculated that after conducting EB-irradiation, ferritins lost theirs electrons in great numbers thus causing them to be positively charged, which eventually caused the ambipolar curve to shift negatively. However, during the first electrical characterization after EB-irradiation, a certain amount of ferritin areas were recharged or resupplied by electrons which caused them to be less positively charged causing the ambipolar curve to re-shift positively. That may explain why the Dirac point was observed after the second measurement. Another plausible explanation is that the EB-irradiation might cause a certain amount of positively charged impurity to be physically adsorbed on the graphene surface temporarily, causing the ambipolar curve to negatively shift further. However these were not permanently adsorbed thus they were possibly removed after minutes inside the vacuum chamber.

4.3.3.2. Graphene and iron-cored ferritin in vacuum

The changes in the ambipolar characteristics of G-FET after iron-cored ferritin adsorption measured in vacuum environment are shown in Fig. 5. The experimental procedure was similar to that of apoferritin. 0.3 μL of aqueous solution of iron-cored ferritin with a concentration of 1 mg/mL was dropped onto the graphene layer. The device was then placed inside a sample case for 30 min so that the water evaporated and the iron-cored ferritins were physically adsorbed onto the graphene layer. This procedure was repeated three times. As shown in Fig 5-A line No.2, after the first drop of iron-cored ferritins, the ambipolar curve shifted positively to Vg = 12 V and its slope significantly increased. This positive shift suggests that the adsorbed native iron-cored ferritins were negatively charged. The increased slope indicates that the electron mobility of G-FET increased.

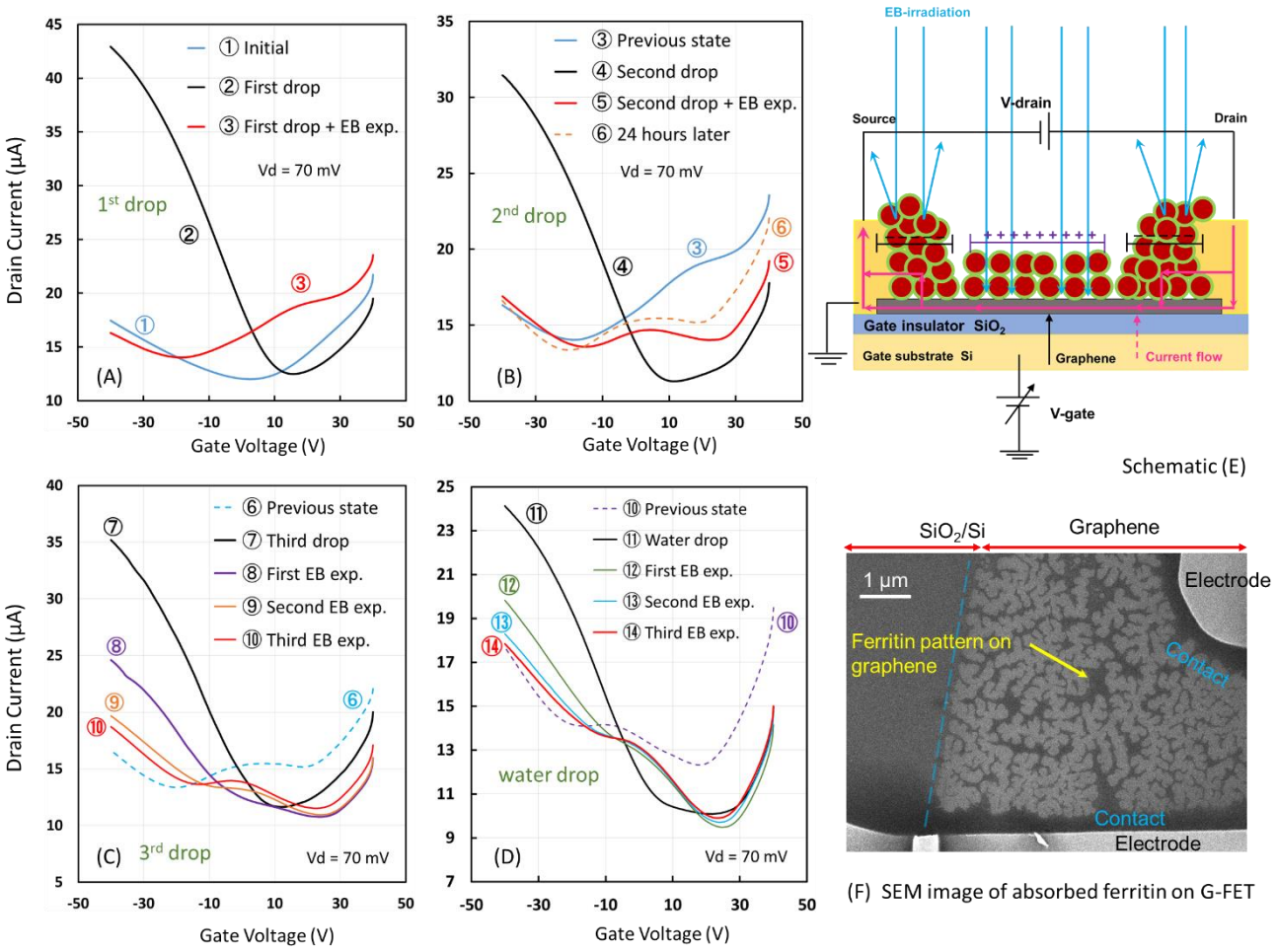

Fig. 5. Changes in ambipolar characteristics of G-FET measured in vacuum environment after adsorption of iron-cored ferritin several times **(A)** to **(C)**; and after water supply **(D)**; schematic of iron-cored ferritin adsorption and the measurement setup **(E)**. The emergence of two Dirac points can be confirmed obviously confirmed in **(A)** to **(C)**, as a signature of the formation of p-n junction. Water also had apparently an important role in restoring the ferritin electrostatic and in the formation of p-n junction as well **(D)**. SEM top view image of G-FET after 1st adsorption of iron-cored ferritin **(F)**, where it can be observed that most of the iron-cored ferritin were adsorbed around the contact regions, indicated by dark area. The areas of graphene surface which are not covered by iron-cored ferritin are brighter than that which are covered.

After conducting EB-irradiation onto the adsorbed iron-cored ferritins on the graphene layer, as shown in Fig 5-A line No. 3, similar to the changes after apoferritin adsorption, the Dirac point negatively shifted to gate-voltage Vg = -20 V, indicating that the iron-cored ferritins became positively charged. It may be reasonable to assume that most of the ferritins lost some of their electrons due to EB-irradiation and became positively charged, leading to the negative Dirac point shift. However, contrary to the apoferritin adsorption result, in the case of iron-cored ferritins, after conducting EB-irradiation the emerging of a secondary Dirac point was barely observed at gate-voltage Vg = 20 V, as displayed in Fig 5-A line No. 3. The secondary Dirac point presumably could be attributed to a certain amount of ferritins which were not completely EB-irradiated because the electron beam could not penetrate the iron cores and left the ferritins below the iron cores in the native state or negatively charged. The existence of the two Dirac points could be related to the formation of p-n junctions, as reported by Farmer, Brenner and Chiu et al. and the dip in the secondary Dirac point became more noticeable after the second drop of iron-cored ferritins displayed in Fig 5-B.[10,11,13]

After dropping aqueous solution of iron-cored ferritin for the second time, the ambipolar curve features tended to resemble those after the first drop of iron-cored ferritins. Both Dirac points merged into a single one positioned at Vg = 10 V, although the remnant of the secondary Dirac point could still be observed as the ambipolar curve slope bent at Vg = 30 V, as plotted in line No. 4. These changes suggest that after dropping the aqueous solution for the second time, presumably the positively charged ferritins accepted enough electrons from the water molecules and possibly became negatively charged like the native ferritins. In other words, the electrostatic charge of the ferritins might partially recover to the native state.

It was confirmed that a p-n junction was possibly formed on graphene after conducting electron beam irradiation onto the iron-cored ferritin adsorbed on the graphene surface. After consecutive EB-irradiation onto the adsorbed iron-cored ferritins on graphene layer, as can be clearly observed from Fig 5-B line No 5, the formations of two identical Dirac point, located at Vg = -12 V and 27 V, were confirmed. The first Dirac point located at Vg = -12 V could be attributed to the ferritins which were EB-irradiated or were penetrated by the electron beam and became positively charged, similar to the change in ambipolar curve after apoferritins adsorption. Moreover, the second Dirac point located at Vg = 27 V could be attributed to the ferritins which were not EB-irradiated or were

penetrated by electron beam because the electron beam was blocked by the iron cores stacked up above. It appears that a substantial number of iron-cored ferritins tend to pile up at the regions around the contacts between graphene and electrode metals rather than on the midsection of the graphene layer, as displayed in Fig. 5-F. It is highly probable that on those regions where the electron beam was not able to irradiate or reach, most ferritins accumulated below stacked iron-cored ferritins, contrary to the ferritins adsorbed on the midsection area where the number of layers was significantly lower and more easily EB-irradiated, as shown in section G in the appendix. These two differently-charged regions, the positively-charged midsection area and negatively-charged contact regions, seems to contribute to the formation of two Dirac points, which is a signature of the creation of p-n junctions on G-FET. By taking into consideration the equivalent depth of both Dirac points, it may be reasonable to suppose that positively-charged and negatively-charged ferritins contributed equally to the formation of the p-n junction respectively. After re-conducting the electrical characteristics 24 hours later, both Dirac points still existed as plotted in line No. 6. This suggests that the formation of p-n junctions was seemingly permanent.

Moreover, apoferritins and even the proteins cage of ferritins could not be observed through electron microscopy such as scanning electron microscope (SEM), because the

electron density of the proteins cage of ferritin is extremely low, so that even when the electron beam was focused on ferritins, it would penetrate through the proteins cage of ferritins and no secondary electrons were emitted from them, thus no images were captured. On the contrary, since the electron density of the iron core is very high, when the electron beam is focused on the iron cores, secondary electrons are emitted so that they can be observed through SEM, as shown in section G in the appendix. At the same time, this indicates a strong possibility that the electron beam could not penetrate the stacked iron cores, which left the ferritins below the iron cores un-irradiated. With an accelerating voltage of 1 kV and iron oxides density of 5.24 g/cm^3, the penetration depth of electron beam is approximately 12 nm, which is equivalent to two layers of iron core.

After dropping aqueous solution of iron-cored ferritins onto the G-FET for the third time, as shown in Fig. 5-C line No. 7, the two Dirac points merged into a single Dirac point. This suggests that the electrostatic charge of all the ferritins uniformly recovered into its native state, which was negatively charged, because the ferritins which lost their electrons due to EB-irradiation and became positively charged accepted electrons from the water molecules and eventually recovered to the native state. After consecutively conducting EB-irradiation several times, as plotted in line No. 8 - 10, it was observed that the Dirac point gradually split into two Dirac points, one located at Vg = -12 V and the

other at 27 V, which also exhibited the process of p-n junction formation. The number of ferritins in the midsection area increased after the third drop, and consequently the number of layers of adsorbed ferritin increased. Therefore, as plotted in line No. 10, the depth of the Dirac point located at Vg = -12 was narrower that the other, indicating that the ferritins in the midsection area became less positively charged.

Furthermore, to further demonstrate the involvement of water molecules in recovering the electrostatic charge of ferritin, 0.3 μL of pure water was similarly dropped onto the iron-cored ferritin adsorbed on the graphene layer. As shown in Fig. 5-D line No. 11, after dropping water molecules onto the ferritins the two Dirac points merged, suggesting that the electrostatic charge of most ferritins recovered to the native state, and after consecutively conducting EB-irradiation several times, as plotted in line No. 12 - 14, a certain amount of ferritins became positively charged and the Dirac point started to split, suggesting that a kind of p-n junction was formed similar to the results described in Fig. 5-C. This evidence also points to the strong possibility that the ferritins which lost their electrons due to EB-irradiation and became positively charged accepted electrons from the water molecules and eventually recovered to the native state.

Additionally, as can be seen from Fig. 5-A to 5-C, after dropping iron-cored ferritins the ambipolar curve slope significantly increased indicating that the electron mobility

increased and the increased electron mobility was more significant than that of apoferritin shown in Fig. 4-A to D. The primary reason for increased electron mobility is the decreased electron scattering. Electron scattering on G-FET generally occurs on the graphene layer itself and at the contact region.[33,34] In the case of apoferritin both measured in vacuum or under water-gate (Fig. 1 and 2), although the ambipolar curve slope increased, the Dirac point did not shift upward indicating that although the electron mobility increased, the conductivity did not substantially increase. This might occur because the adsorbed iron-cored ferritins seemingly formed a kind of protective layer on the top of graphene layer. This protective layer would likely reduce the electron scattering on the graphene layer which eventually increasing the electron mobility. However, in the case of iron-cored ferritin both measured in vacuum or through water-gate (Fig. 4 and 5), besides the increased slope of ambipolar curve, the Dirac point shifted upward indicating that the electron mobility and the conductivity increased. This occurred possibly because iron-cored ferritins accumulated at the contact between graphene and electrodes, (Fig. 5-F) suppressing the electron scattering at the contact and leading to the significantly increased electron mobility.[34] The iron cores accumulating at the G-FET contact also provided an alternative current path which avoids the high contact resistivity between graphene and metal,[33] thus causing the conductivity of G-FET to eventually increase.

4.4. Conclusion

In summary, we have successfully constructed a p-n junction on G-FET through iron-cored ferritin adsorption. By utilizing iron-cored ferritin, we were able to construct a stable p-n junction and a p-n junction which can also operate even the electric field was applied through the water-gate. Moreover, we also investigated the interaction between ferritin and electron beam. We found that EB-irradiation could cause ferritins to become positively charged and the electrostatic characteristic of ferritin could also be restored by supplying water making the p-n junction reversible. Furthermore, we investigated the interaction between graphene and electron beam. We found that EB-irradiation could reduce the effect of charged impurities adsorbed on a graphene layer, thus shifting the Dirac point to gate-voltage Vg = 0. This new approach in constructing p-n junctions will open up wider opportunities for investing quantum transport in graphene as well as future applications in graphene devices.

References:

(1) Bigasa, M.; Cabrujaa, E.; Forestb, J.; Salvib, J. *Microelectr. J.* **2006,** 37 (5), 433–451, DOI: 10.1016/j.mejo.2005.07.002.

(2) Huang, L.; Xu, H.; Zhang, Z.; Chen, C.; Jiang, J.; Ma, X.; Chen, B.; Li, Z.; Zhong, H.; Peng, L. -M. *Sci. Rep.* **2014**, 4, 5548, DOI: 10.1038/srep05548.

(3) Williams, J. R.; DiCarlo, L.; Marcus, C. M. *Science* **2007**, 317 (5838), 638-641, DOI: 10.1126/science.1144657.

(4) Özyilmaz, B.; Jarillo-Herrero, P.; Efetov, D.; Abanin, D. A.; Levitov, L. S.; Kim, P. *Phys. Rev. Lett.* **2007**, 99, 166804, DOI: 10.1103/PhysRevLett.99.166804.

(5) Stander, N.; Huard, B.; Goldhaber-Gordon, D. *Phys. Rev. Lett.* **2009**, 102, 026807, DOI: 10.1103/PhysRevLett.102.026807.

(6) Rycerz, A.; Tworzydlo, J.; Beenakker, C.W. J. *Nature Phys.* **2007**, 3, 172-175, DOI: 10.1038/nphys547.

(7) Silvestrov, P. G.; Efetov, K. B. *Phys. Rev. Lett.* **2007**, 98, 016802, DOI: 10.1103/PhysRevLett.98.016802.

(8) Cheianov, V. V.; Fal'ko, V.; Altshuler, B. L.; *Science* **2007**, 315 (5816), 1252-1255, DOI: 10.1126/science.1138020.

(9) Wilmart, Q.; Berrada, S., Torrin, D.; Nguyen, V. H.; Fève, G.; Berroir, J. -M.; Dollfus, P.; Plaçais, B. *2D Materials* **2014**, 1, 011006, DOI:10.1088/2053-1583/1/1/011006.

(10) Farmer, D. B.; Lin, Y. -M.; Afzali-Ardakani, A.; Avouris. P. *Appl. Phys. Lett.* **2009**, 94 (21), 213106, DOI: 10.1063/1.3142865.

(11) Brenner, K.; Murali, R. *Appl. Phys. Lett.* **2010**, 96 (6), 063104, DOI: 10.1063/1.3308482.

(12) Liu, G.; Velasco, J. Jr.; Bao, W.; Lau, C. N. *Appl. Phys. Lett.* **2008**, 92, 203103, DOI: 10.1063/1.2928234.

(13) Chiu, H. -Y.; Perebeinos, V.; Lin, Y. -M.; Avouris, P. *Nano Lett.* **2010**, 10 (11), 4634–4639, DOI: 10.1021/nl102756r.

(14) Theil, E., C. *Annu. Rev. Biochem*. **1987**, 56, 289-315, DOI: 10.1146/annurev.bi.56.070187.001445.

(15) Harrison, P. M.; Arosio, P. *BBA-Bioenergetics* **1996**, 1275 (3), 161–203, DOI: 10.1016/0005-2728(96)00022-9.

(16) Xu, D.; Watt, G. D.; Harb, J. N.; Davis, R. C. *Nano Lett.* **2005**, 5 (4), 571–577, DOI: 10.1021/nl048218x.

(17) Yamashita, I.; Iwahori K.; Kumagai S. *Biochim Biophys Acta.* **2010**, 1800 (8), 846-857, DOI: 10.1016/j.bbagen.2010.03.005.

(18) Okuda, M.; Iwahori, K.; Yamashita, I.; Yoshimura, H. *Biotech. Bioeng*. **2003**, 84 (2), 187-194, DOI: 10.1002/bit.10748.

(19) Wong, K.; Mann, S. *Adv. Mater.* **1996**, 8, 928, DOI: 10.1002/adma.19960081114.

(20) Awschalom, D. D.; Smyth, J. F.; Grinstein, G.; DiVincenzo, D. P.; Loss, D. *Phys. ReV. Lett.* **1992**, 68 (20), 3092-3095, DOI: 10.1103/PhysRevLett.68.3092.

(21) Hilty, S.; Webb, B.; Frankel, R. B.; Watt, G. D. *J. Inorg. Biochem.* **1994**, 56 (3), 173-185. DOI:10.1016/0162-0134(94)85004-6.

(22) Tejada, J.; Zhang, X. X.; del Barco, E.; Hernandez, J. M. *Phys. Rev. Lett.* **1997**, 79 (9), 1754-1757, DOI: 10.1103/PhysRevLett.79.1754.

(23) Harris, J. G. E.; Grimaldi, J. E.; Awschalom, D. D.; Chiolero, A.; Loss, D. *Phys. Rev. B* **1999**, 60 (5), 3453-3456, DOI: 10.1103/PhysRevB.60.3453.

(24) Mamiya, H.; Nakatani, I.; Furubayashi, T. *Supperlattices Microstruct.* **2002**, 32 (4-6), 179-186, DOI: 10.1016/S0749-6036(03)00018-1.

(25) Blake, P.; Hill, E. W.; Castro-Neto, A. H.; Novoselov, K. S.; Jiang, D.; Yang, R.; Booth, T. J.; Geim, A. K. *Appl. Phys. Lett.* **2007**, 91 (6), 063124, DOI: 10.1063/1.2768624.

(26) Mulyana, Y; Uenuma, M.; Ishikawa, Y.; Uraoka, Y. *J. Phys. Chem. C* **2014**, 118 (47), 27372–27381, DOI: 10.1021/jp508026g.

(27) Mulyana, Y.; Horita, M.; Ishikawa, Y.; Uraoka, Y.; Koh, S. *Appl. Phys. Lett.* **2013**, 103 (6), 063107, DOI: 10.1063/1.4818329.

(28) Kumagai, S.; Yoshii, S.; Yamada, K.; Matsukawa, N.; Fujiwara, I.; Iwahori, K.; Yamashita, I. *Appl. Phys. Lett*. **2006**, 88 (15), 153103, DOI: 10.1063/1.2189566.

(29) Ohno, Y.; Maehashi, K.; Inoue, K; Matsumoto, K. *Jpn. J. Appl. Phys.* **2011**, 50, 070120, DOI:10.1143/JJAP.50.070120.

(30) Yamada, K.; Yoshii, S.; Kumagai, S.; Fujiwara, I.; Nishio, K.; Okuda, M.; Matsukawa, N.; Yamashita, I. *Jpn. J. Appl. Phys.* **2006**, 45, 4259, DOI: 10.1143/JJAP.45.4259.

(31) Shimaya, M.; Shiono, N.; Nakajima, O.; Hashimoto, C.; Sakakibara, Y. *J. Electrochem. Soc.* **1983**, 130 (4), 945-950, DOI: 10.1149/1.2119863.

(32) Li, W. -Q.; Zhang H. -B. *Micron.* **2010**, 41 (5), 416-22, DOI: 10.1016/j.micron.2010.02.010.

(33) Chen, J. -H.; Jang, C.; Adam, S.; Fuhrer, M. S.; Williams, E. D.; Ishigami, M. *Nat. Phys.* **2008**, 4, 377 - 381, DOI:10.1038/nphys935.

(34) Nagashio, K.; Toriumi, A. *Jpn. J. Appl. Phys.* **2011**, 50, 070108, DOI: 10.1143/JJAP.50.070108.

CHAPTER 5

Graphene and Escherichia coli: Sensitivity of graphene

In this chapter the interaction between graphene and Escherichia coli (E. coli) bacteria was discussed. The changes in ambipolar characteristics of six graphene-based field effect transistors (G-FETs) before and after the adsorption of E. coli bacteria were evaluated. The Dirac point of all the devices shifted positively, indicating that E. coli was negatively charged and this particular negative charge caused the ambipolar curve to positively shift. The minimum shift of Dirac point was 20 V, which is equivalent to 2 x 10^8 V/m electric field. The maximum shift was beyond 40 V. The Dirac point shift of the remaining devices was around 30 V, which is equivalent to 3 x 10^8 V/m electric field. We expected that these data would benefit the more systematic investigation of the sensitivity of biosensors based on G-FETs.

5.1. Background

In the field of biosensors, nanomaterials offer the extremely high surface area to volume ratio. This allows the immobilization of large numbers of biomolecules per unit area results in high with the potential to increase biosensor sensitivity, response time and selectivity. A wide variety of nanomaterials have been explored for their application in biosensors due to their

unique chemical, physical and optoelectronic properties.[1-8] Moreover, electrical detection of biomolecules using nanomaterial based devices can be downsized for personal usage.

Siliconnanowire[1,2] and carbon-nanotube (CNT)-based biosensors[3-8] have been reported by many researchers over the past decade. In particular, the CNT is one of the best candidates for highly sensitive biological sensors owing to its large surface-to-volume ratio. However, CNT-based biosensors have some critical problems for sensing application. Since their electrical characteristics strongly depend on their chirality, i.e., some devices show semiconducting characteristics and other devices show metallic characteristics.[9] Graphene could solve these problems. It has an extremely high carrier mobility with a large sheet carrier concentration and is chemically stable.[12,13] Its electrical characteristics are very sensitive to its environmental conditions, and it also has a high potential for use in chemical and biological sensors. Ohno et al. have reported specific protein sensing using aptamer-modified graphene-based field effect transistor (G-FETs), which can selectively detect human immunoglobulin E (IgE) as the target protein.[14] IgE is an antibody subclass found only in mammals. However, from the perspective of ambipolar characteristics, the sensitivity of the devices were considerably low.

In this chapter, we evaluate the sensitivity of G-FETs by investigating the interaction between graphene and Escherichia coli (E. coli). Some distinct variations of E. coli can cause serious food poisoning in their hosts, and are occasionally responsible for product recalls due

to food contamination. The likely source of the e. coli is not the fruit & vegetable waste, but disposable diapers or human excretion that are poorly treated in the mixed waste stream. As a first step in developing more sophisticated bio-sensors based on G-FET that can detect harmful organisms such as E. coli, the interaction between graphene and E. coli needs to be systematically investigated. This is the objective of the investigation, which is to investigate the interaction between graphene and E. coli.

5.2. Experimental

E. coli cells were cultured in E. coli growth medium at 37 centigrade for 6 hours. Then the E. coli cells were washed with centrifugation and suspension by pure water. The cell density in pure water was set to 1.0 or 8 x 10^8 cells/ml using optical density (OD600). Next, 0.5 μL of the E. coli cell aqueous solution was dropped onto the G-FETs and the devices were left for 30 min so that the aqueous solution naturally dried and some E. coli cells were adsorbed onto the graphene layer. The change in ambipolar characteristics of the devices before and after the adsorption on E. coli cells was evaluated. Six devices of multilayer graphene were used in this experiment and the fabrication process of G-FET was described in the chapter 2 and 3. Electrical characterizations of G-FETs were performed under a vacuum condition of 4.6 x 10^{-5} Pa using NE4000 nano probing microscopy from Hitachi.

5.3. Result and discussion

The changes in ambipolar characteristics of the G-FET No. 1-2, 3-5, 6 before and after the adsorption of E. coli are shown in Fig. 1, 2, 3 respectively. The channel length of G-FET No. 1 -5 was 5 μm and that of G-FET No. 6 was 10 μm. As can be seen from Fig. The ambipolar curve of all G-FET shifted positively after the adsorption of E. coli. This indicates that the E. coli was negatively charged and this particular negative charge caused the ambipolar curve to positively shift. The positive shift in ambipolar characteristic was also consistent with experiment result reported by Ohno et al. using IgE.[14] The greatest shift was observed on device No. 4 shown in Fig. 2, where Dirac point located beyond back-gate voltage = 40 V. The smallest shift of Dirac point i.e. 20 V was observed on device No. 6 whose the channel length was 10 μm, twice as long as the rest. Since the thickness of back insulator of the devices was 100 nm, this 20 V Dirac point shift equivalent to 2 x 10^8 V/m electric field. The Dirac shift of the remaining device was around 30 V, equivalent to 3 x 10^8 V/m electric field, which could be considered great. The shift of Dirac point is related to the sensitivity of G-FET based biosensor. The sensitivity of G-FET based biosensor increases as the shift amount increases.

Although the graphene used in this experiment was multilayer, the amount of Dirac point shift of each device was considerably great, implying the high sensitivity of graphene layer. Thus, greater Dirac point shift or higher sensitivity of thinner graphene can be expected. The minimum shift of Dirac point was observed on device No. 6 as shown in Fig. 3, which is 20 V

and equivalent to 2 x 10^8 V/m electric field. The channel length of this device was 10 μm, which is twice as long as the rest. This longer channel length may contribute to the smaller Dirac point shift or the less sensitive sensing.

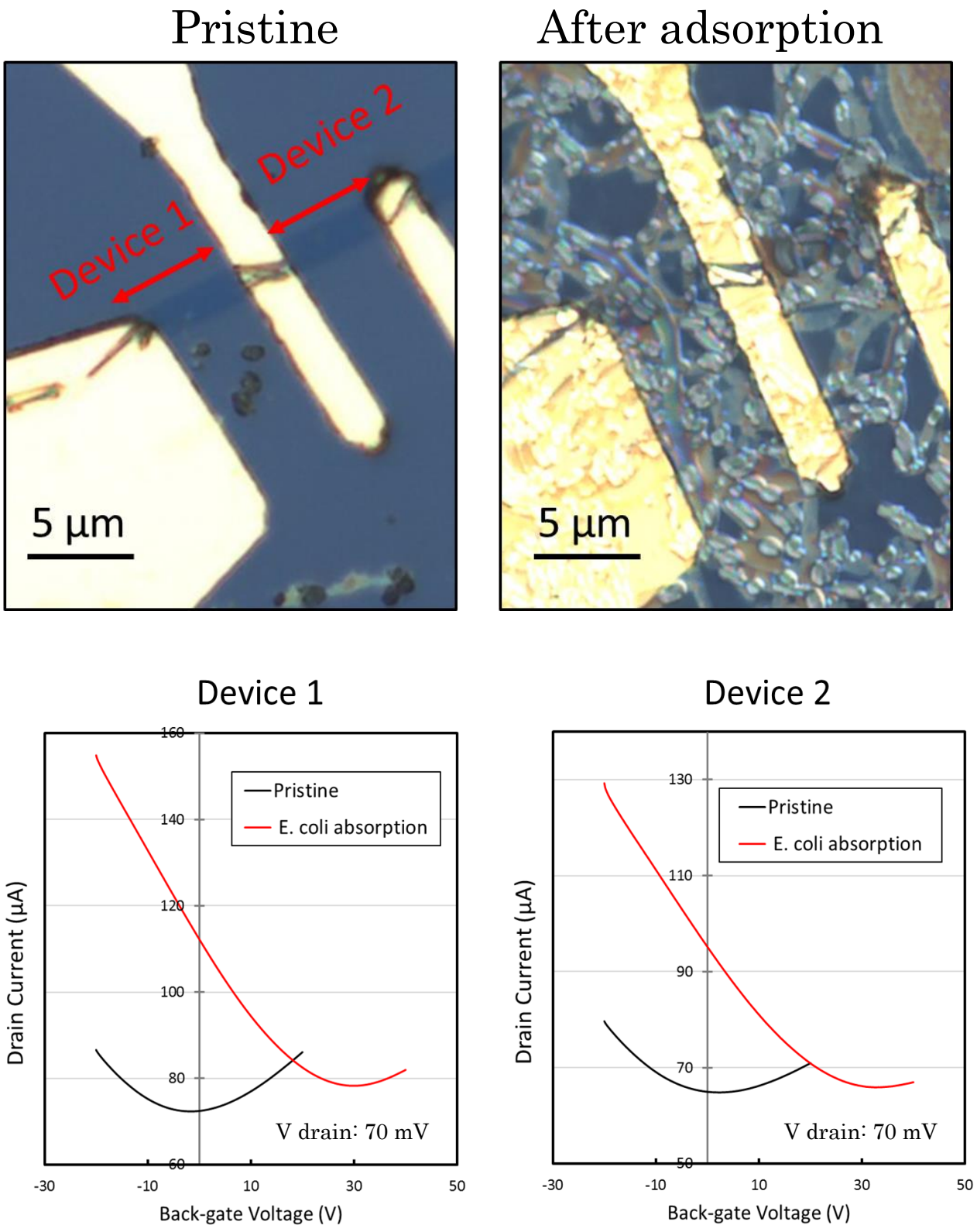

Fig. 1. Change in ambipolar characteristic of device 1 - 2 before and after adsorption of E. coli bacteria.

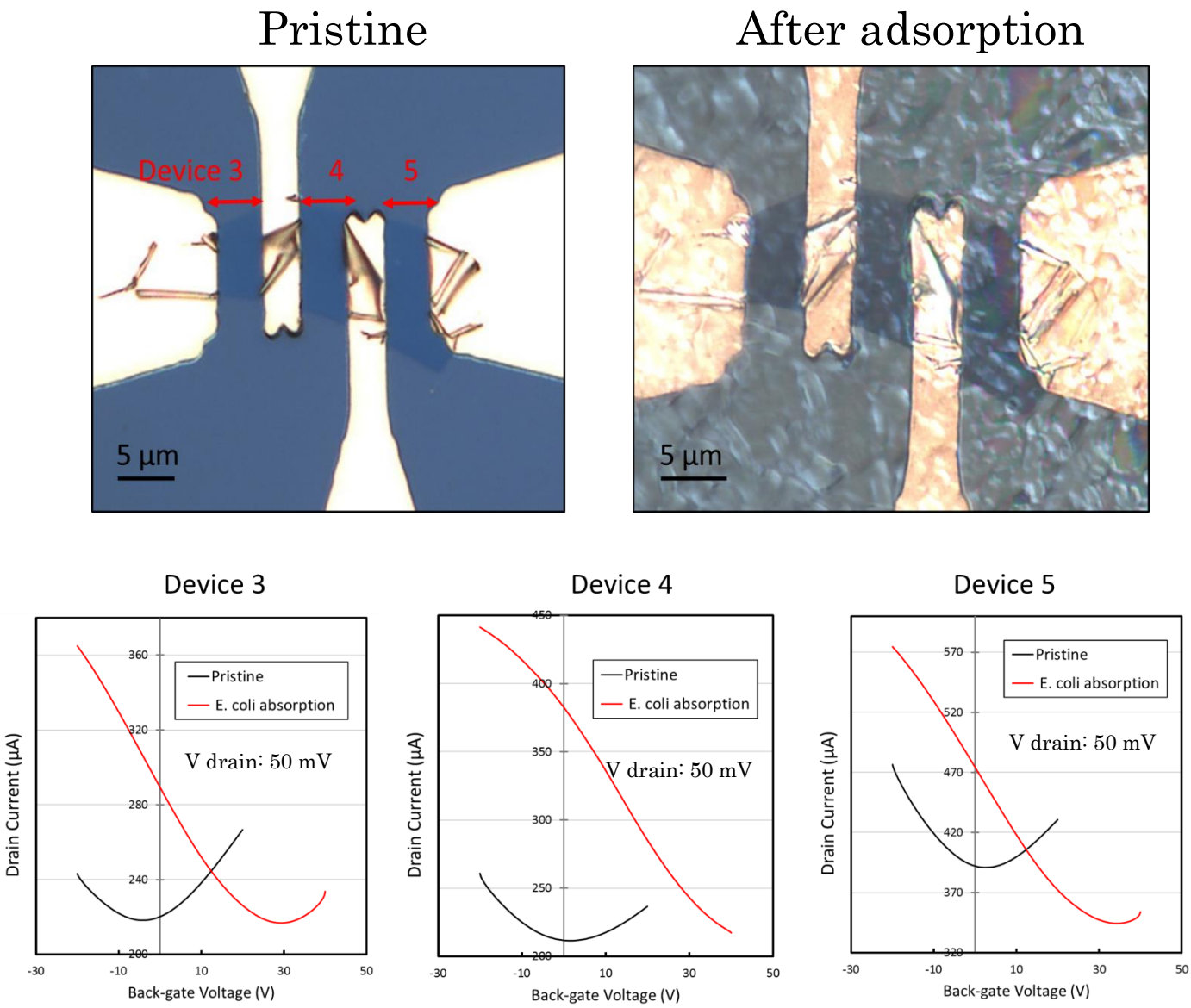

Fig. 2. Change in ambipolar characteristic of device 3 - 5 before and after adsorption of E. coli bacteria.

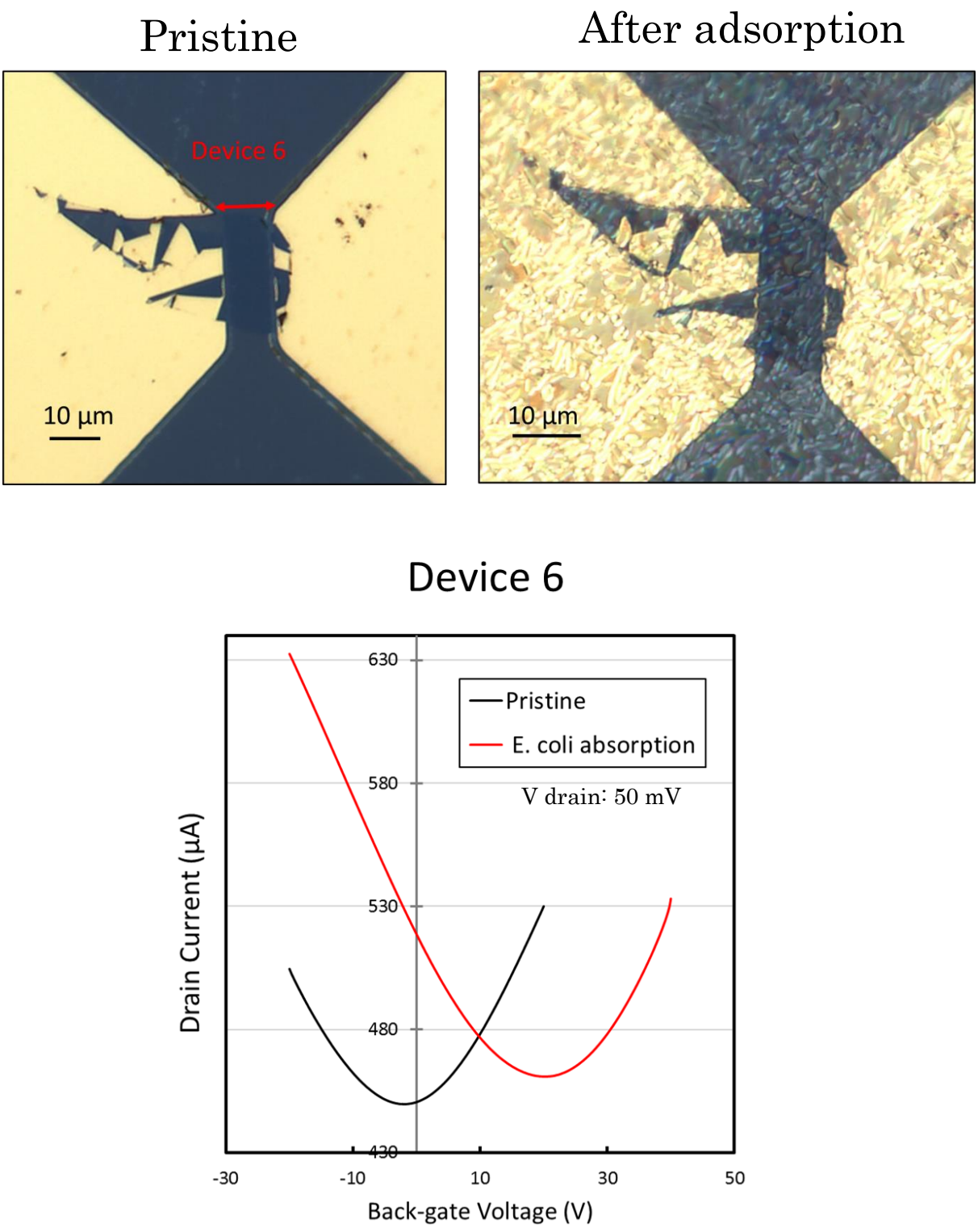

Fig. 3. Change in ambipolar characteristic of device 6 before and after adsorption of E. coli bacteria.

5.4. Comparison with ferritin

Differences in ambipolarity shift between E. coli adsorption and ferritin adsorption onto graphene layer are discussed in this section, as shown Fig. 4. In case of the adsorption of E. coli onto graphene layer, the ambipolar curve shifted positively from the pristine state plotted in the black trace with the position of Dirac point at Vg = 0 V to the red trace with the position of Dirac point at Vg = 33 V. Similarly, in case of the adsorption of ferritin onto graphene layer, the ambipolar curve shifted positively from the pristine state plotted in the grey trace with the position of Dirac point at around Vg = 0 V to the violet trace with the position of Dirac point at Vg = 5 V. This positive shift might indicate that both ferritin and E. coli were negatively charged or possibly have negative electrostatic potential. This seems reasonable since both ferritin and E. coli are entirely or mostly made of protein.

Moreover, any decline in gradient of all ambipolar curves was not observed. This indicates that the electron mobility of all devices did not decrease after the adsorption of both E. coli and ferritin. This suggests that both E. coli and ferritin did not chemically react with graphene, but merely adsorbed on graphene surface physically.

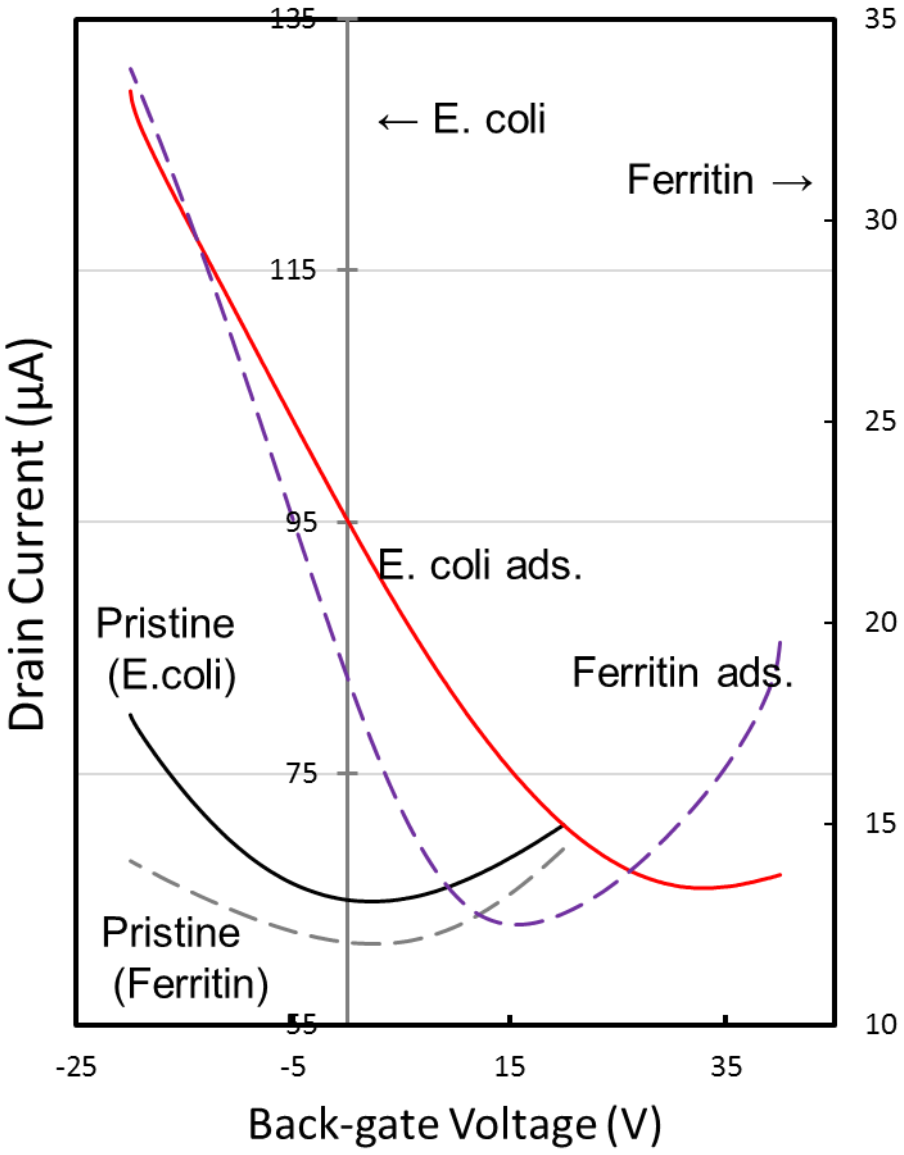

Fig. 4. Differences in ambipolarity shift between E. coli adsorption and ferritin adsorption onto graphene layer.

5.5. Comparison with radical oxygen

Differences in ambipolarity change between E. coli adsorption and radical oxygen doping onto graphene layer are discussed in this section, as shown Fig. 5. Contrary to the case of E. coli and ferritin explained in the previous section, in case of radical oxygen doping, a significant decline in gradient of the ambipolar curve was observed. This indicates that the electron mobility of the device significantly decrease after the radical oxygen doping. This suggests that the radical oxygen chemically reacted with graphene and caused the possibility of electron scattering to increase which eventually lead to the decrease in electron mobility.

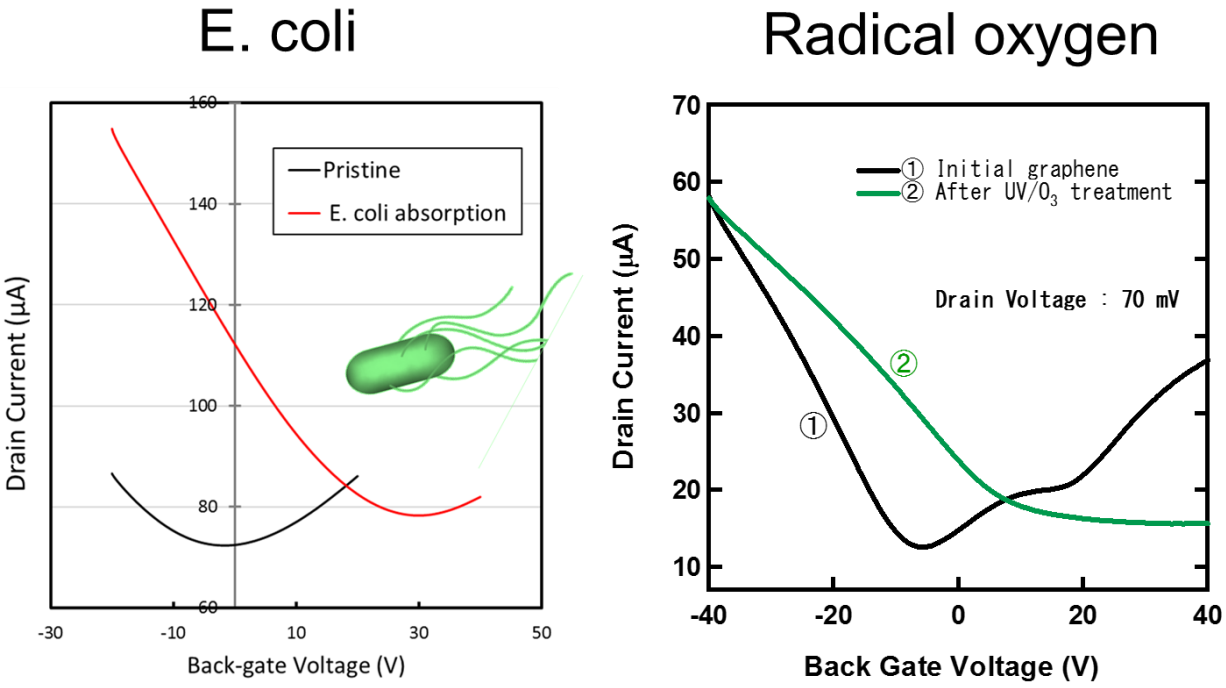

Fig. 5. Differences in ambipolarity change between E. coli adsorption and radical oxygen doping on graphene layer.

5.6. Effect of electron beam irradiation

Shift in ambipolarity of G-FET with E. coli-adsorbed onto its graphene layer after EB-irradiation is discussed in this section. SEM image of E. coli adsorbed onto graphene layer is shown in Fig. 6. As can be understood from this SEM image that was taken under a vacuum condition of 10^{-5} Pa, it is clear that E. coli was still adsorbed onto the graphene layer even in a vacuum environment. E. coli was not also rinsed out even after pure water cleanses.

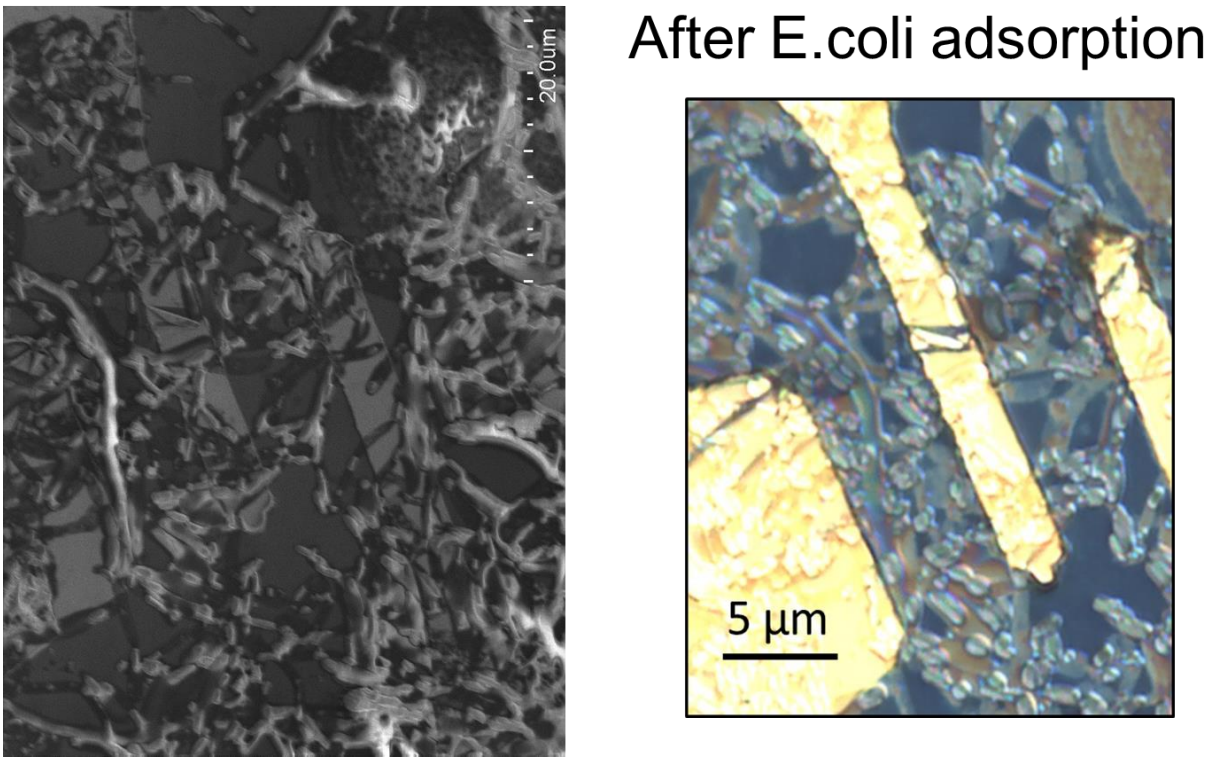

Fig. 6. SEM image of E. coli-adsorbed onto graphene layer.

Shift in ambipolarity of G-FET with E. coli-adsorbed onto its graphene layer after EB-irradiation is shown in Fig. 7. As can be understood from the figure, the ambipolar curve did not show any shift after EB-irradiation. This may indicate that even if the condition of the upper surface of E. coli had changed due to EB-irradiation, as long as the condition of the lower surface of E. coli, which was directly connected with the graphene layer, did not change the ambipolar curve would not shift. This seems reasonable since the thickness of E. coli was around 1 μm order and since the electron density of E. coli was much higher than that of ferritin, the electron beam could not penetrate until the lower surface of E. coli.

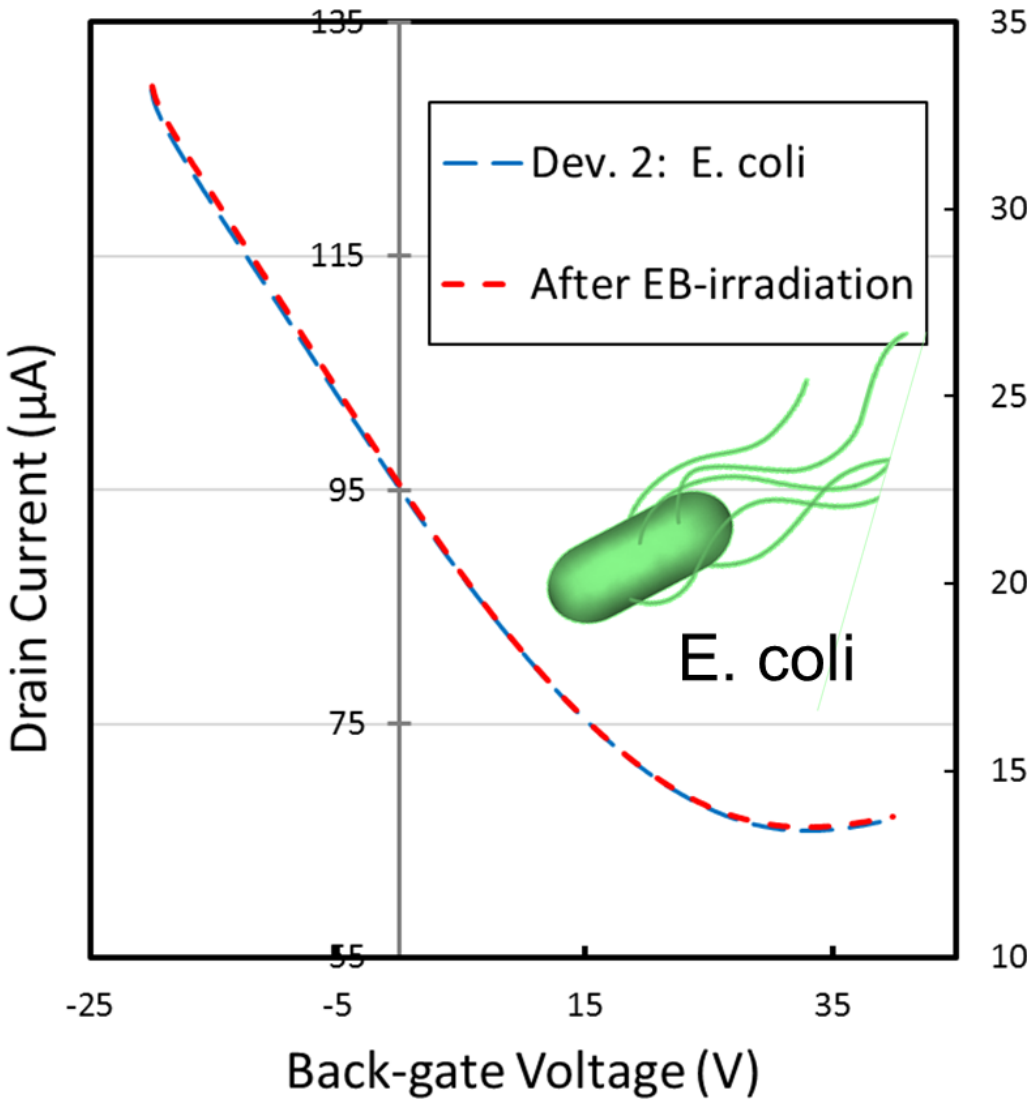

Fig. 7. Shift in ambipolarity of G-FET with E. coli-adsorbed onto its graphene layer after electron beam irradiation.

5.7. Conclusion

We found that even for multilayer G-FETs, the Dirac point of ambipolar curve shifted positively in a considerably great amount, exhibiting the real possibility of high sensitivity in G-FET based biosensor. This positive shift of Dirac point indicates that E. coli was negatively

charged and this particular negative charge caused the ambipolar curve to positively shift. The minimum shift of Dirac point was 20 V, which is equivalent to 2 x 10^8 V/m electric field. The maximum shift was beyond 40 V. The Dirac point shift of the remaining devices was around 30 V, which is equivalent to 3 x 10^8 V/m electric field. We expected that these data would benefit the more systematic investigation of the sensitivity of biosensors based on G-FETs.

Reference:

1) Y. Cui, Q. Wei, H. Park, and C. M. Lieber: Science 293 (2001) 1289.
2) G. Zheng, F. Patolsky, Y. Cui, W. U. Wang, and C. M. Lieber: Nat. Biotechnol. 23 (2005) 1294.
3) C. Li, M. Curreli, H. Lin, B. Lei, F. N. Ishikawa, R. Datar, R. J. Cote, M. E. Thompson, and C. Zhou: J. Am. Chem. Soc. 127 (2005) 12484.
4) R. J. Chen, S. Bangsaruntip, K. A. Drouvalakis, N. W. S. Kam, M. Shim, Y. Li, W. Kim, P. J. Utz, and H. Dai: Proc. Natl. Acad. Sci. U.S.A. 100 (2003) 4984.
5) A. Star, J. C. P. Gabriel, K. Bradley, and G. Gru¨ner: Nano Lett. 3 (2003) 459.
6) K. Besteman, J. O. Lee, F. G. M. Wiertz, H. A. Heering, and C. Dekker: Nano Lett. 3 (2003) 727.
7) K. Maehashi, T. Katsura, K. Kerman, Y. Takamura, K. Matsumoto, and E. Tamiya: Anal. Chem. 79 (2007) 782.
8) F. N. Ishikawa, H.-K. Chang, M. Curreli, H.-I. Liao, C. A. Olson, P.-C. Chen, R. Zhang, R. W. Roberts, R. Sun, R. J. Cote, M. E. Thompson, and C. Zhou: ACS Nano 3 (2009) 1219.
9) R. Saito, M. Fujita, G. Dresselhaus, and M. S. Dresselhaus: Phys. Rev. B 46 (1992) 1804.
10) Y. Hakamata, Y. Ohno, K. Maehashi, S. Kasai, K. Inoue, and K. Matsumoto: J. Appl. Phys. 108 (2010) 104313.
11) A. Palaniappan, W. H. Goh, J. N. Tey, I. P. M. Wijaya, S. M. Moochhala, B. Liedberg, and S. G. Mhaisalkar: Biosens. Bioelectron. 25 (2010) 1989.
12) K. S. Novoselov, A. K. Geim, S. V. Morozov, D. Jiang, Y. Zhang, S. V. Dubonos, I. V. Grigorieva, and A. A. Firsov: Science 306 (2004) 666.
13) A. K. Geim and K. S. Novoselov: Nat. Mater. 6 (2007) 183.
14) Y. Ohno, K. Maehashi, K. Inoue, and K. Matsumoto: Jpn. J. Appl. Phys. 50 (2011) 070120.

CHAPTER 6

General conclusion

After being exposed to chemically reactive materials such as radical oxygen and high energy ultraviolet lights, the crystalline of graphene lattice was massively modified and the ambipolarity was heavily altered. However, those alterations could be restored to the near pristine level after recovery. Judging from the chemically robust behavior of graphene ambipolarity and its crystalline, it may suggest that graphene possess a promising chemical stability. Moreover, after the adsorption of ferritin and E. coli onto the graphene layer, the position of Dirac point positively shifted, but in the same time, no decrease in electron mobility was observed. This may indicate that graphene possess high bio-sensitivity and in the same time high bio-compatibility. From all the results of these experimental investigations, it seems reasonable conclude that graphene possess a great chemical stability; and a high bio-sensitivity and bio-compatibility in the same time, which are very important criteria in realizing graphene-based sensing devices in the future.

6.1. Interaction with radical oxygen

The changes in electrical properties of graphene after being oxidized through UV/O_3 treatment were investigated. Reactive oxygen atoms chemically reacted with carbon atoms of

graphene, which was confirmed from the XPS spectra. The electron mobility of the graphene layer decreased as a result of oxidation. The electrical characteristics such as carrier mobility recovered to the level before oxidation after conducting reduction of the oxidized graphene with thermal and non-thermal treatment through UV-irradiation. This suggests that the oxidation of graphene with UV/ O_3 treatment is both thermally and non-thermally reversible. Thus, we also concluded that UV/O_3-treatment and UV-irradiation might be prominent candidates to be used in oxidation and reduction, and furthermore on more advance chemical functionalization of graphene.

6.2. Interaction with ferritin

We have successfully constructed a p-n junction on G-FET through iron-cored ferritin adsorption. By utilizing iron-cored ferritin, we were able to construct a stable p-n junction and a p-n junction which can also operate even the electric field was applied through the water-gate. Moreover, we also investigated the interaction between ferritin and electron beam. We found that EB-irradiation could cause ferritins to become positively charged and the electrostatic characteristic of ferritin could also be restored by supplying water making the p-n junction reversible. We hope that these findings would contribute to research on controlling electrical properties of graphene and development of graphene-based information processing and storage technology as well as sensing devices.

6.3. Interaction with E. coli

We found that even for multilayer G-FETs, the Dirac point of ambipolar curve shifted positively in a considerably great amount after the adsorption of E. coli bacteria, exhibiting the real possibility of high sensitivity in G-FET based biosensor. This positive shift of Dirac point indicates that E. coli was negatively charged and this particular negative charge caused the ambipolar curve to positively shift. The minimum shift of Dirac point was 20 V, which is equivalent to 2 x 10^8 V/m electric field. The maximum shift was beyond 40 V. The Dirac point shift of the remaining devices was around 30 V, which is equivalent to 3 x 10^8 V/m electric field. We expected that these data would benefit the more systematic investigation of the sensitivity of biosensors based on G-FETs.

6.4. Future task

Graphene is very sensitive to any charged materials, including charged targets and charged impurities. That is why, when utilizing G-FETs similar to one used in this study as a base of bio-sensor, the target material need to be separated from the charged impurities through the process of filtration. Otherwise, a form of selectivity function needs to be incorporated to the G-FETs. Ueno et al. from NTT corp. proposed a biomolecular probe for highly sensitive protein detection by modifying an aptamer with a DNA spacer. The spacer controls the distance

between a fluorescence dye and a quencher, which is crucial for FRET-based sensors. Ueno et al. demonstrated an improvement in the sensitivity and selectivity of an on-chip graphene oxide aptasensor.[1]

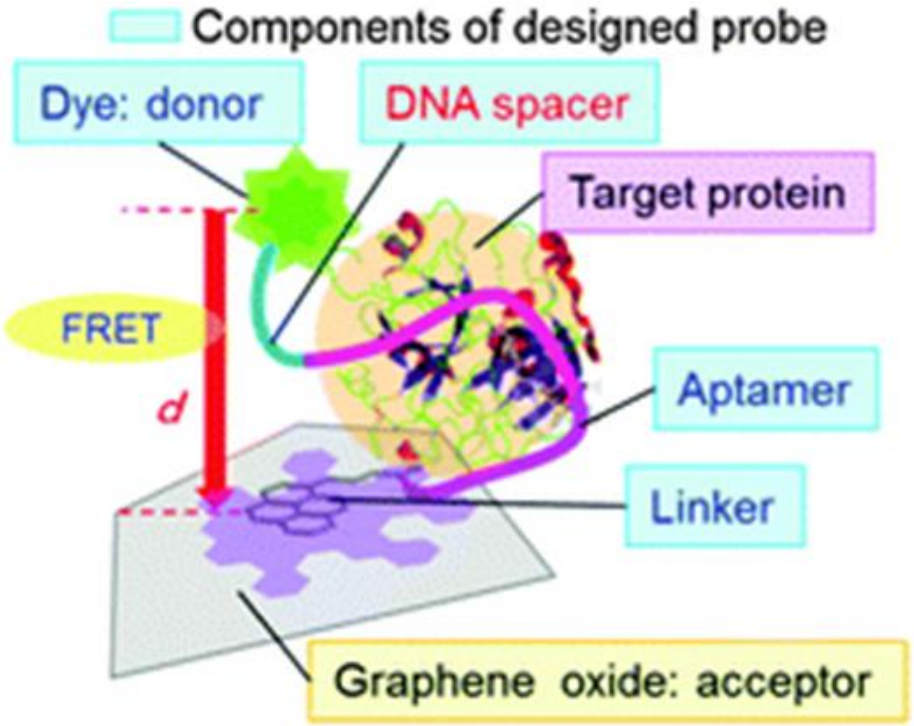

Fig. 1. Biomolecular probe for highly sensitive protein detection by modifying an aptamer with a DNA spacer proposed by Ueno et al.[1]

Reference:

1. Ueno, Y.; Furukawa, K.; Matsuo, K.; Inoue, S.; Hayashi, K.; Hibino, H. Molecular design for enhanced sensitivity of a FRET aptasensor built on the graphene oxide surface. *Chem. Commun.* **2013**, 49, 10346.

Appendix

Section A: STM Measurement 3

Section B: XPS Measurement 9

UV/O_3 treatment time dependence 11

UV/O_3 treatment number dependence 14

Reduction through UV-irradiation 17

Section C: Electrical Characterization 20

P type electron mobility of graphene-FETs 20

N type electron mobility of graphene-FETs 21

Raman spectra of graphene-FETs 22

Section D: Raman Spectroscopy Measurement 25

Data aggregation 25

Note 28

Section E: 6-min UV/O_3-treatment on Exfoliated Graphene (Additional Experiment) 29

Data aggregation 29

Note 30

Section F: Ambipolar characteristics for various metal contacts 32

Ni metal contact 32

Au/Cr metal contact 33

Au/TiN metal contact 34

Section G: SEM images of adsorbed ferritin 35

Section H: K-AFM images of EB-irradiated ferritin 38

Section A:

STM Measurement

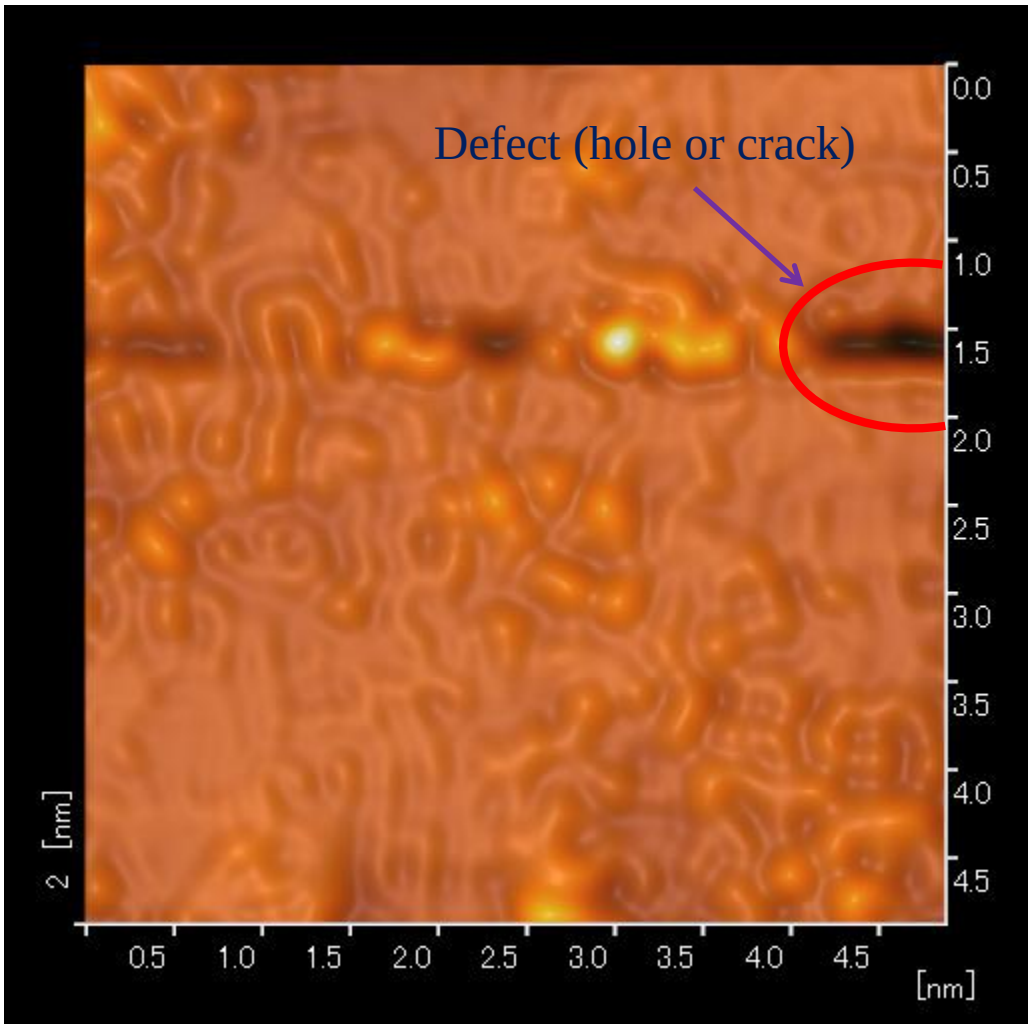

Fig. A-1(a) Top view STM image of defect on spot No. 1 on graphene lattice.

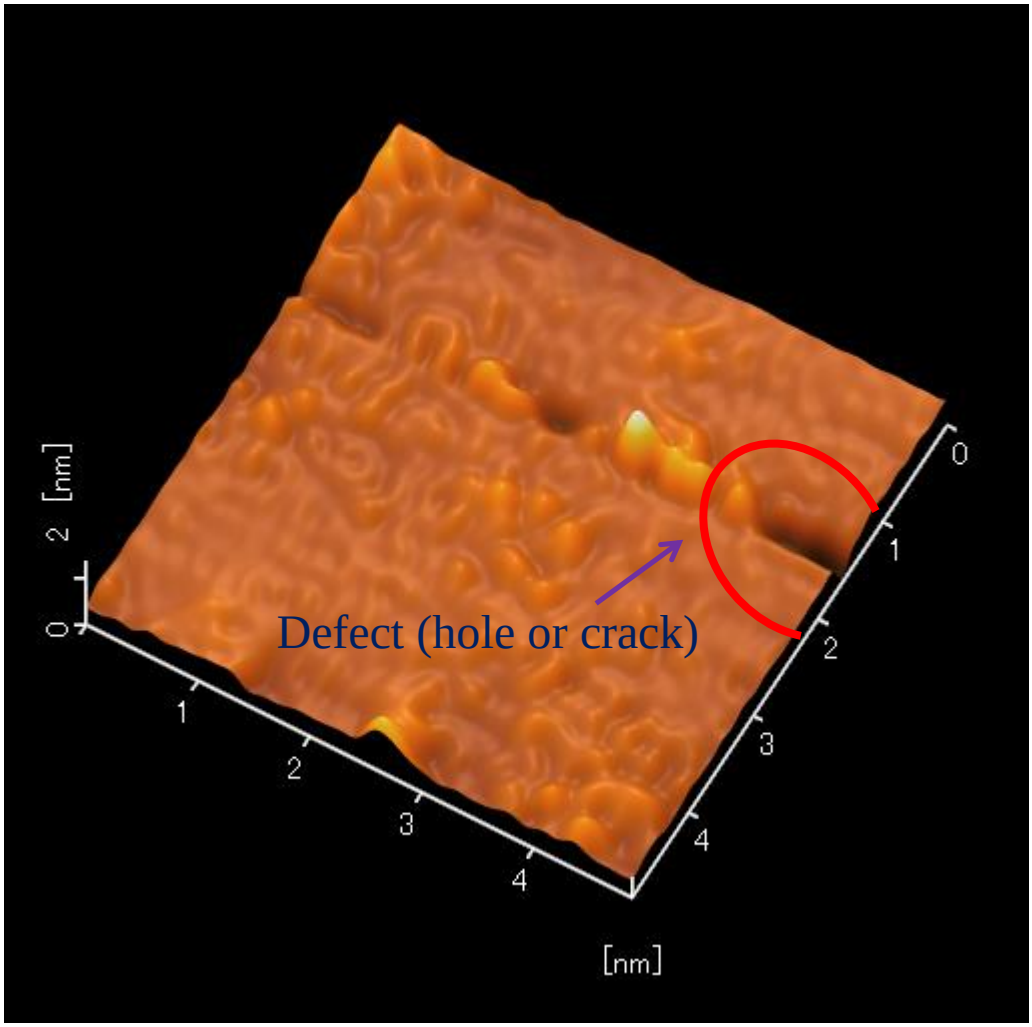

Fig. A-1(b) STM image of defect on spot No. 1 on graphene lattice (tilt angle: 45°).

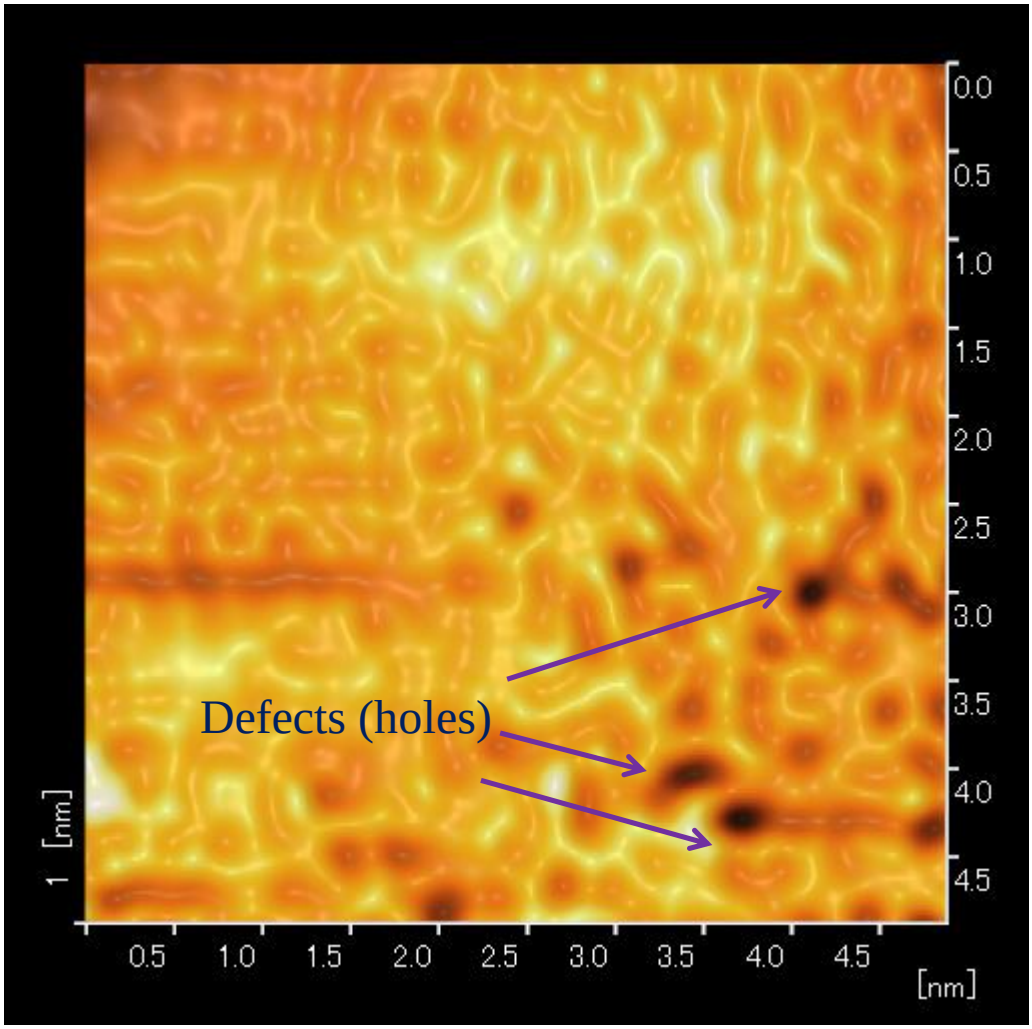

Fig. A-2 Top view STM image of defect on spot No. 2 on graphene lattice.

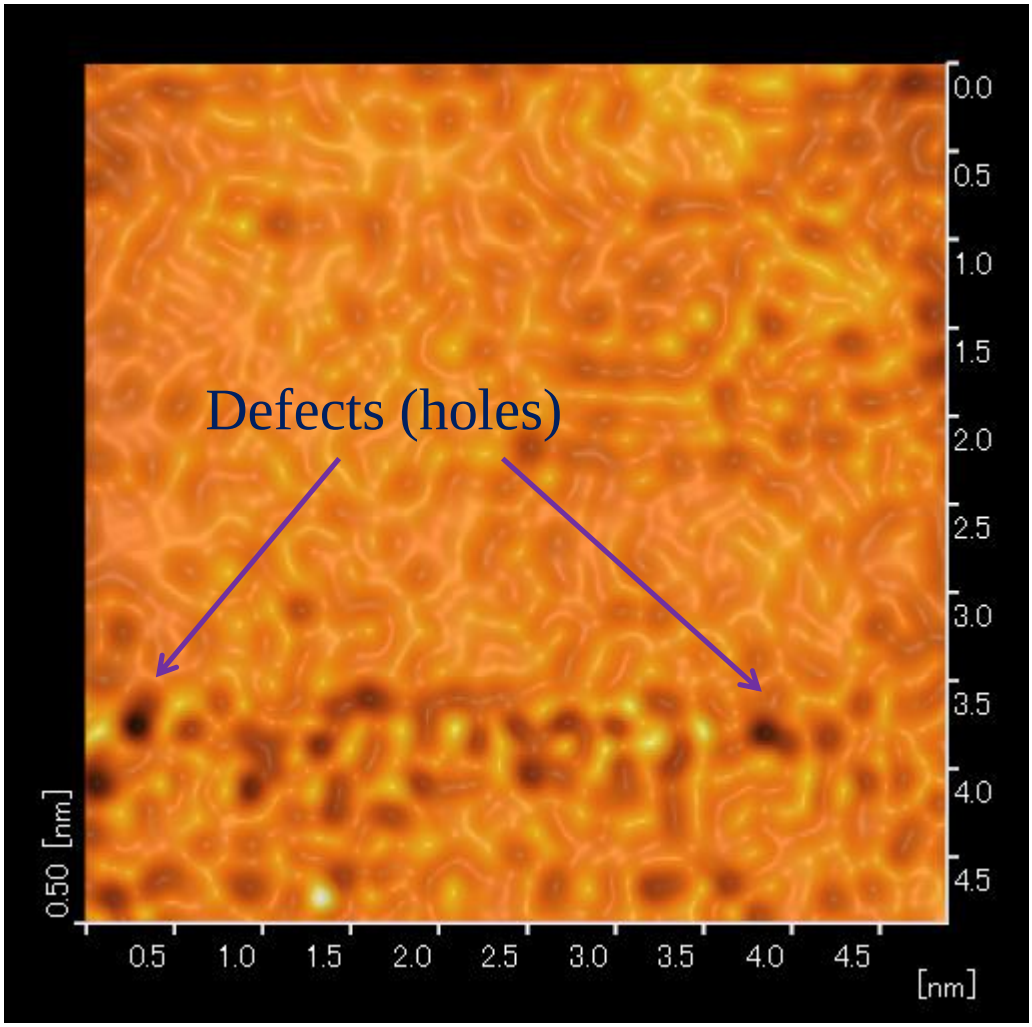

Fig. A-3 Top view STM image of defect on spot No. 3 on graphene lattice.

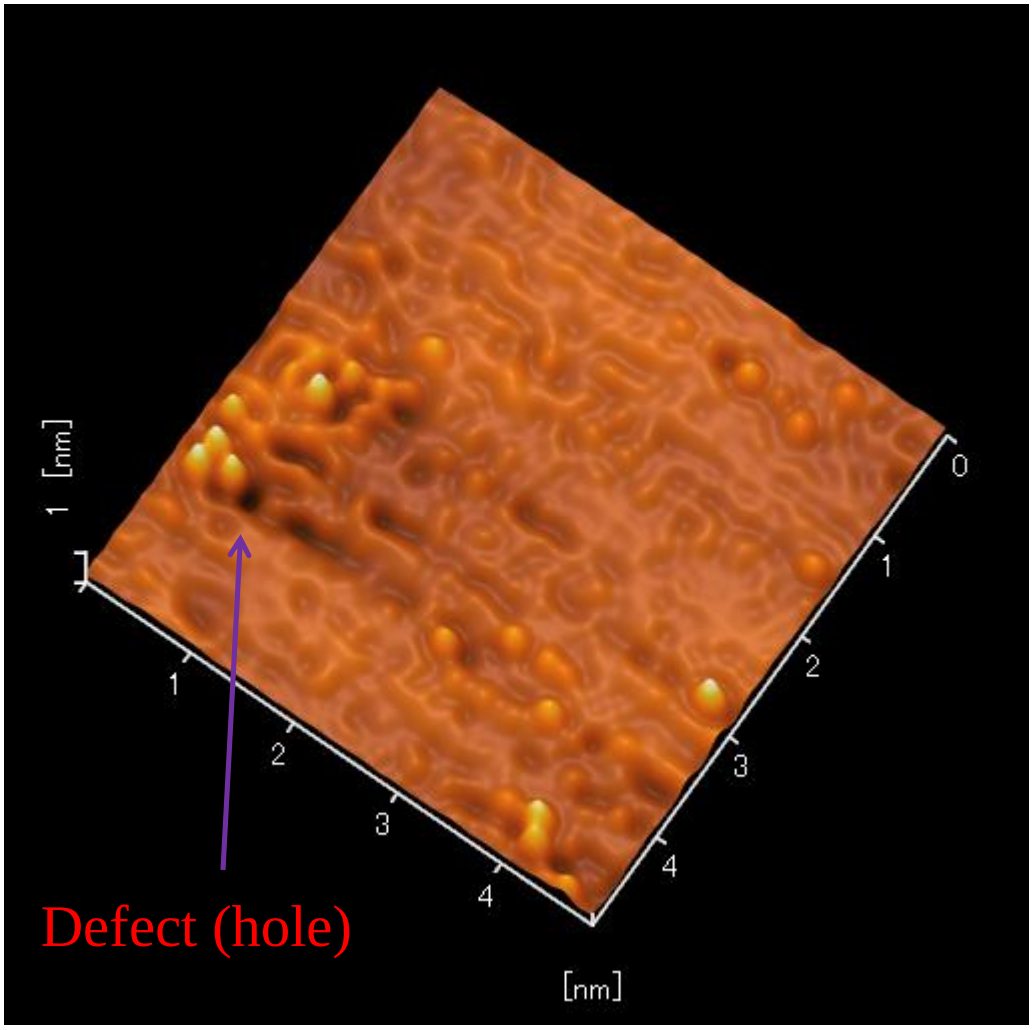

Fig. A-4 STM image of defect on spot No. 4 on graphene lattice (tilt angle: 60°).

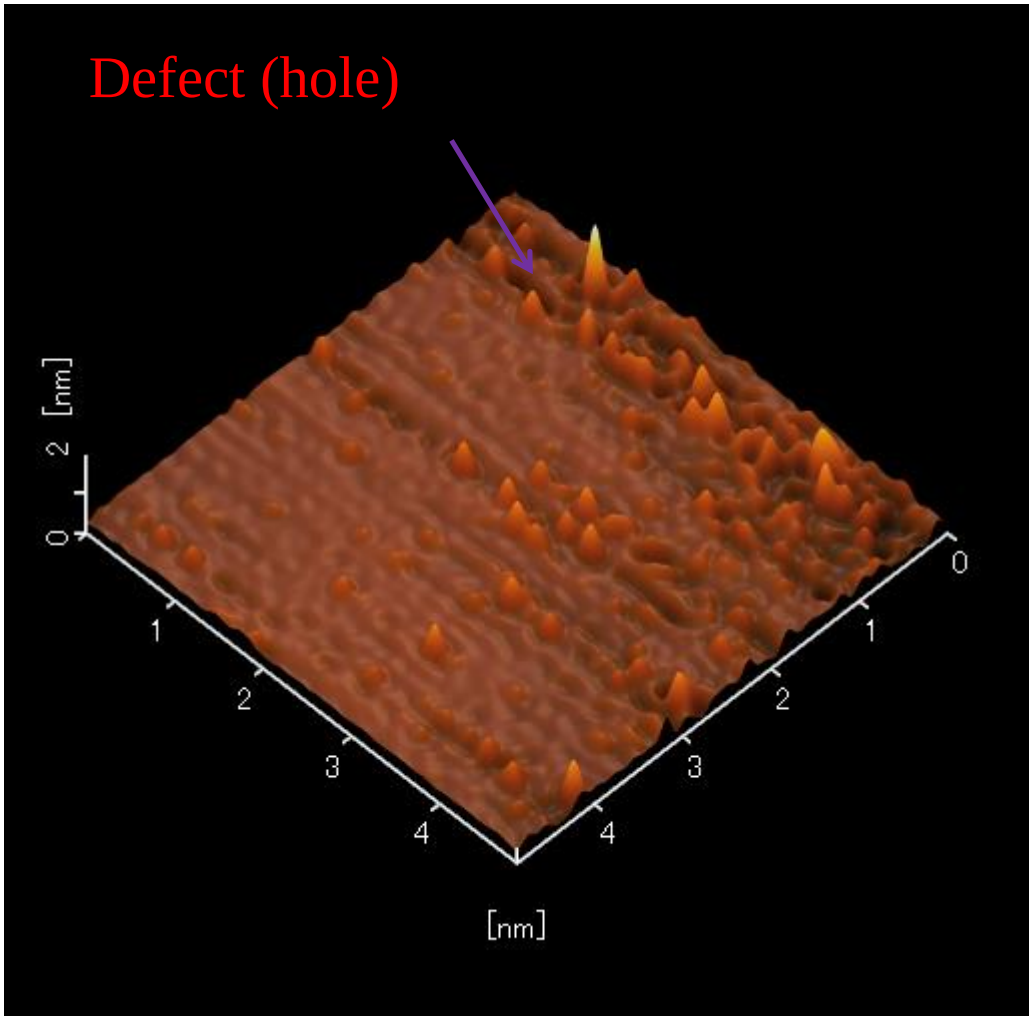

Fig. A-5 STM image of defect on spot No. 5 on graphene lattice (tilt angle: 45°).

Section B:

XPS Measurement

All results of XPS measurements and detailed analysis results, including error estimation, are presented in this section. Error estimation of each calculation was implied using coefficient of variation of the root mean square error (CV-RMSE), statistically expressed in percentage. CV-RMSE is also well-known as an indicator of goodness of fit. The less great the CV-RMSE is, the more accurate the fitting is.

All XPS spectra of pristine graphene are shown in Figure B-01. XPS spectra related to UV/O_3-treatment time dependence of doped oxygen quantity, where the treatment time was arranged from 3 to 30 min, are shown in Figure B-02 to B-03, and changes in the quantity of doped oxygen are summarized in Figure B-04.

All XPS spectra related to UV/O_3-treatment number dependence of doped oxygen quantity, where a 3-min UV/O_3-treatment time was conducted for six times, are shown in Figure B-05 to B-06 and changes in the quantity of doped oxygen are summarized in Figure B-07.

All XPS spectra after each UV/O_3-treatment and UV-irradiation during two cycles of redox processes are shown in Figure B-08 to B-09 and changes in the quantity of doped oxygen are summarized in Figure B-10. UV/O_3-treatment and UV-irradiation were conducted for 3 min.

Pristine graphene

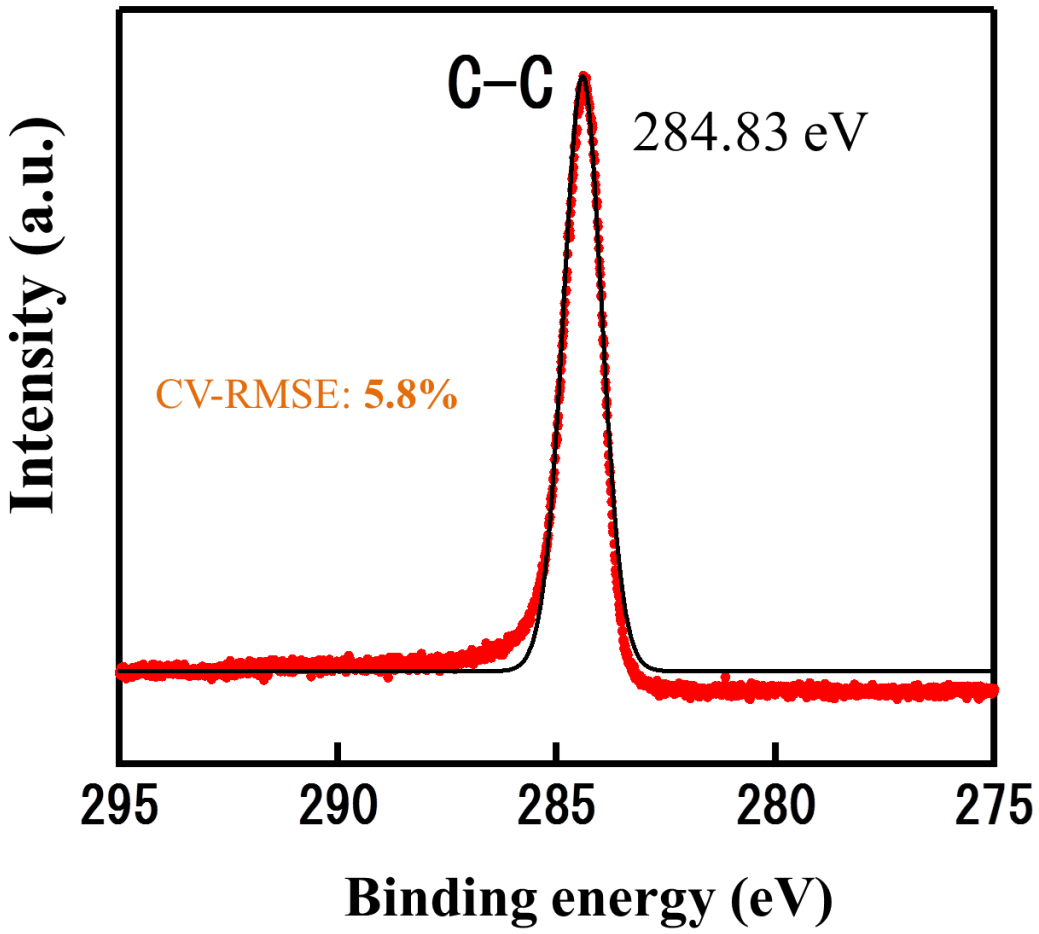

Fig. B-01 XPS spectra of pristine graphene.

UV/O_3 treatment time dependence (3 to 15 min)

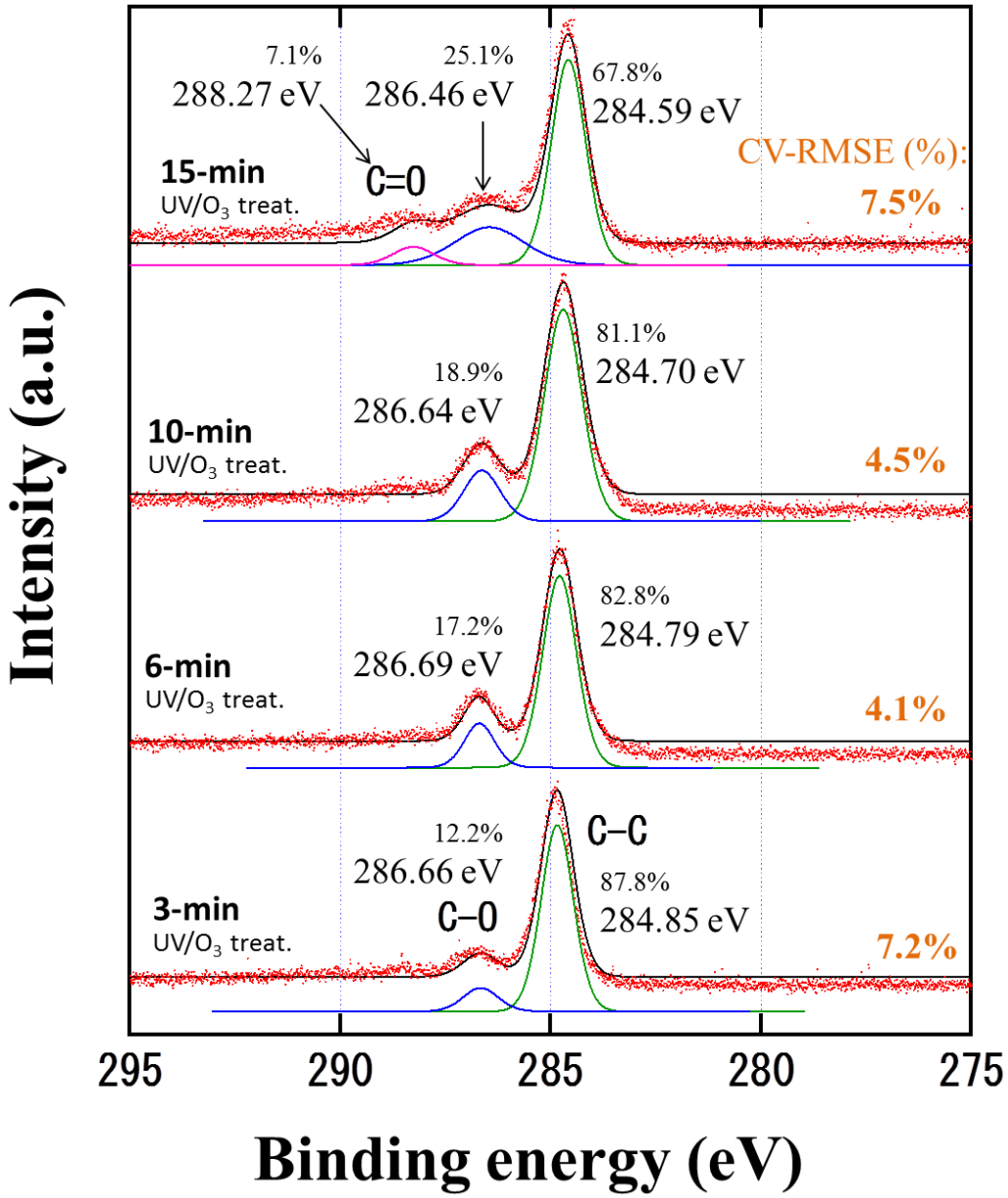

Fig. B-02 UV/O_3-treatment time dependence of doped oxygen quantity (treatment time ranged from 3 min to 15 min).

UV/O_3 treatment time dependence (10 to 30 min)

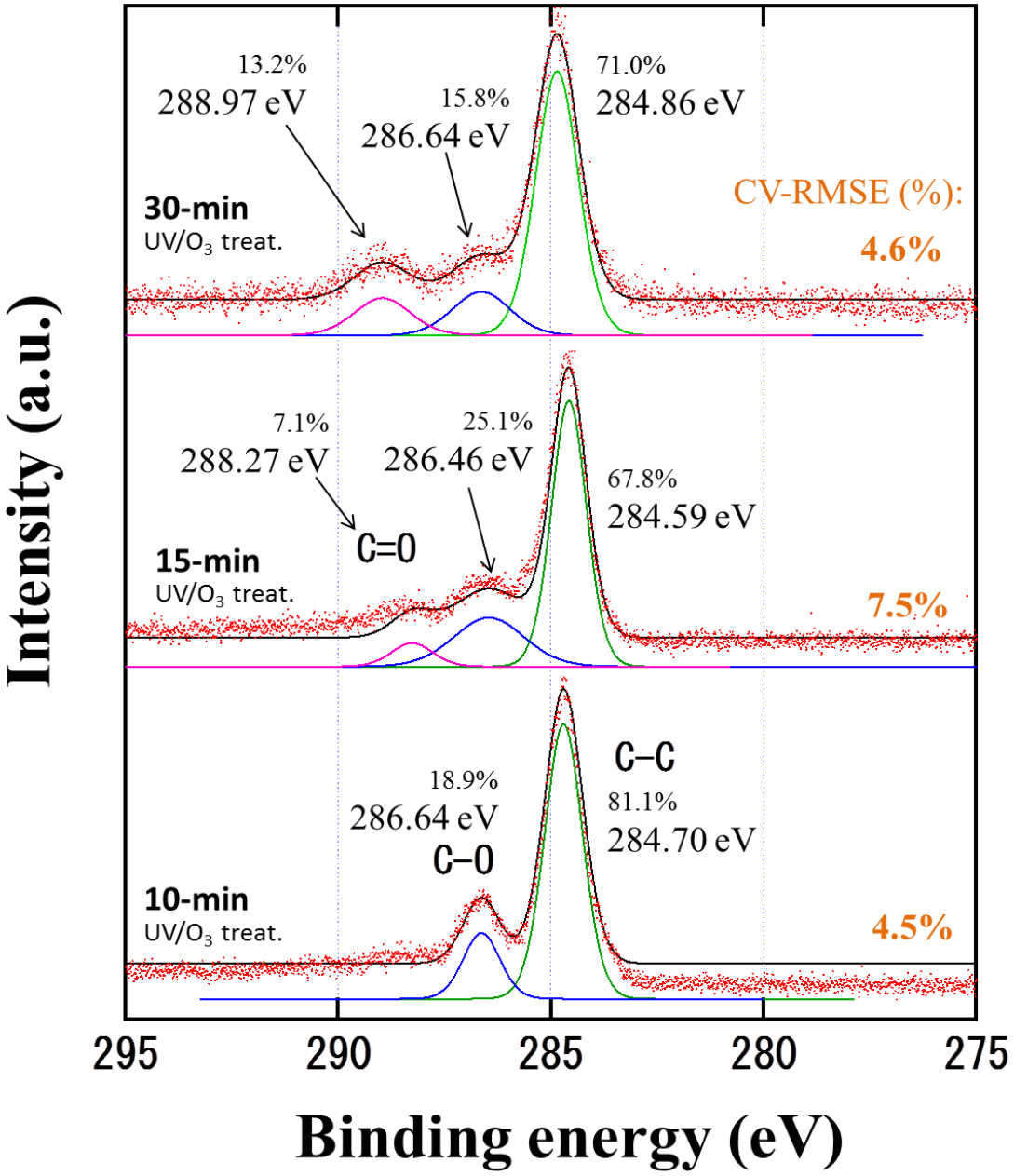

Fig. B-03 UV/O_3 treatment time dependence of doped oxygen quantity (treatment time ranged from 10 min to 30 min).

UV/O_3 treatment time dependence of oxygen quantity (0 to 30 min)

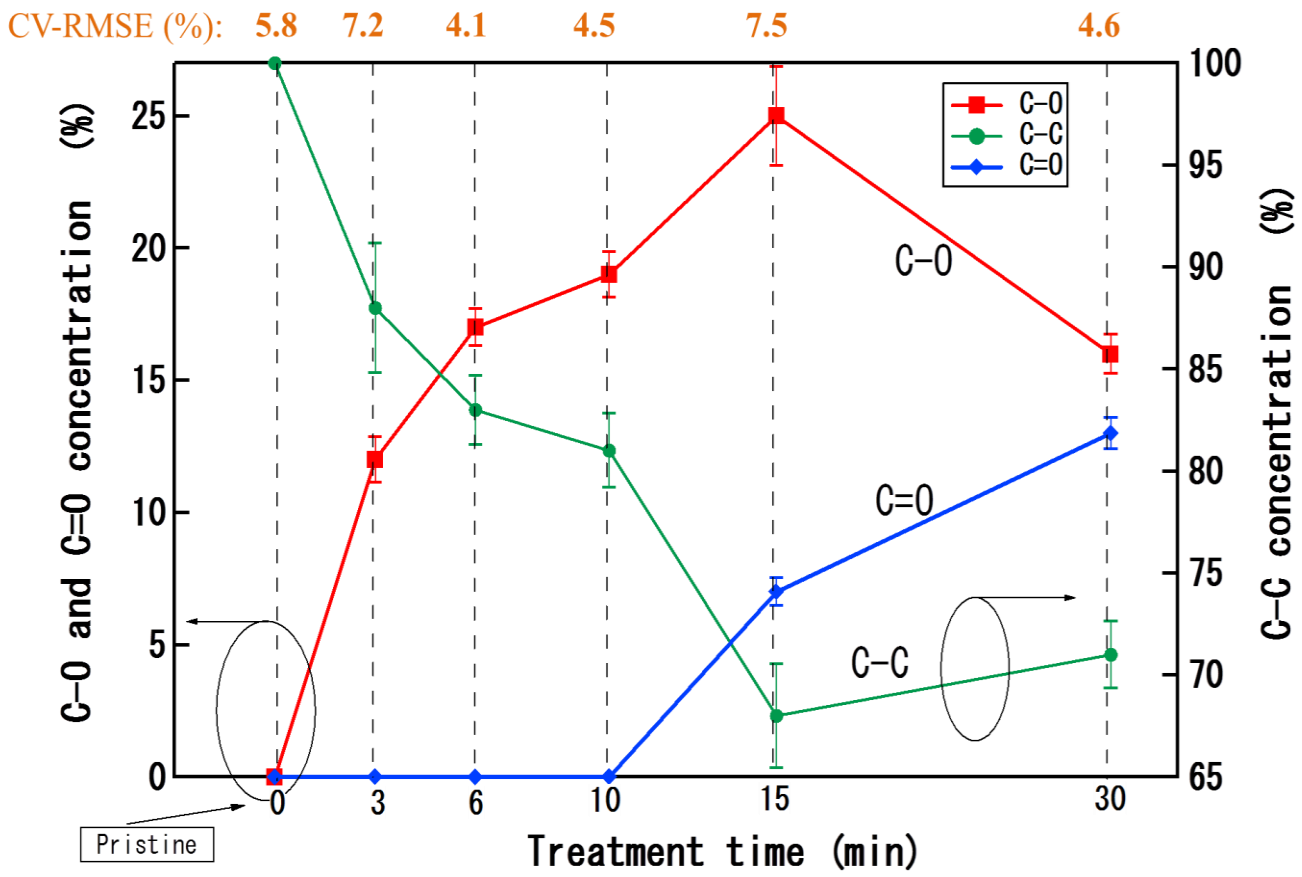

Fig. B-04 UV/O_3 treatment time dependence of doped oxygen quantity (treatment time ranged from 0 to 30 min).

UV/O_3 treatment number dependence (one to three times)

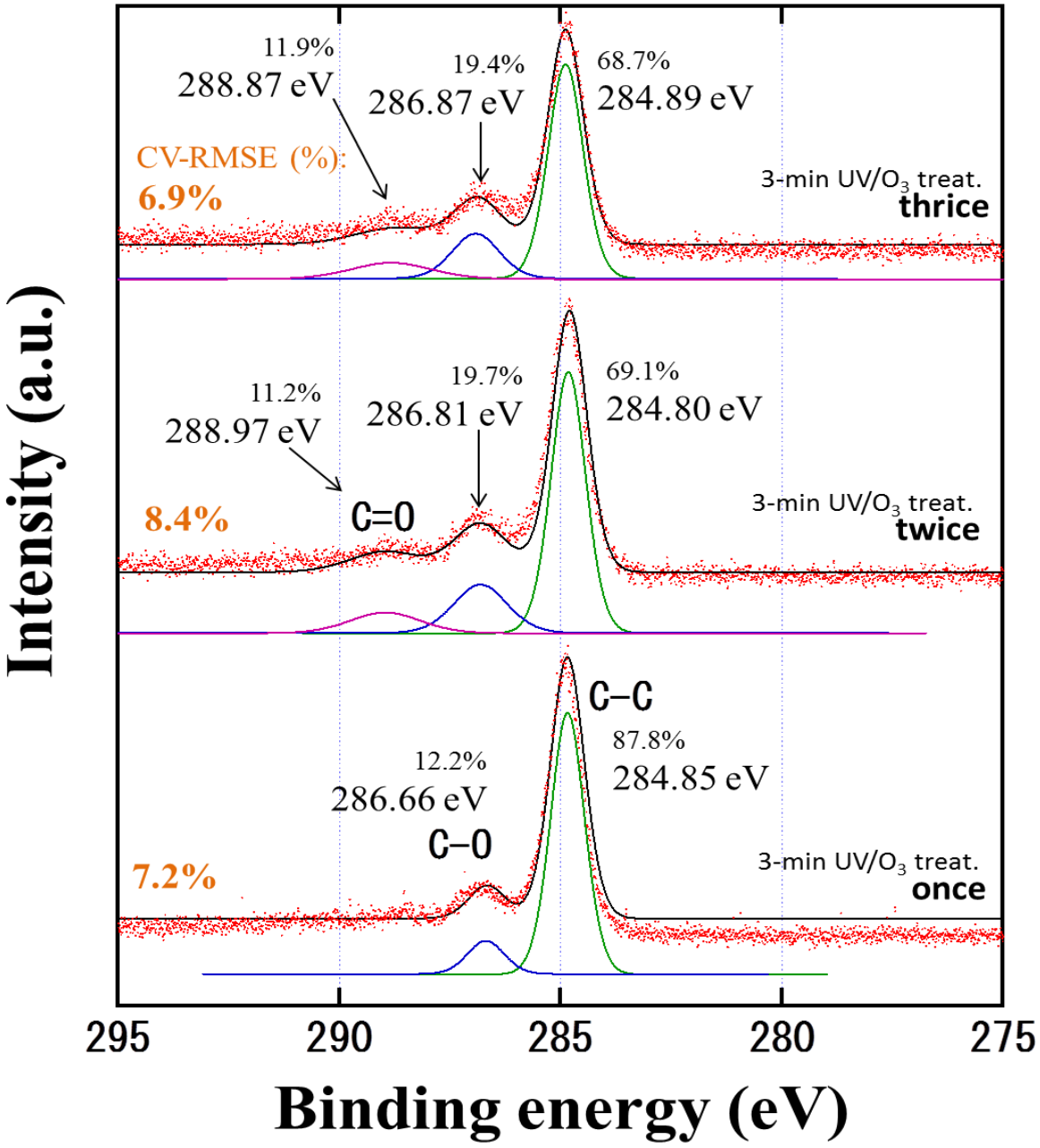

Fig. B-05 UV/O_3 treatment number dependence of doped oxygen quantity (treatment number ranged from one to three times, and treatment time for each UV/O_3-treatment was 3 min).

UV/O_3 treatment number dependence (four to six times)

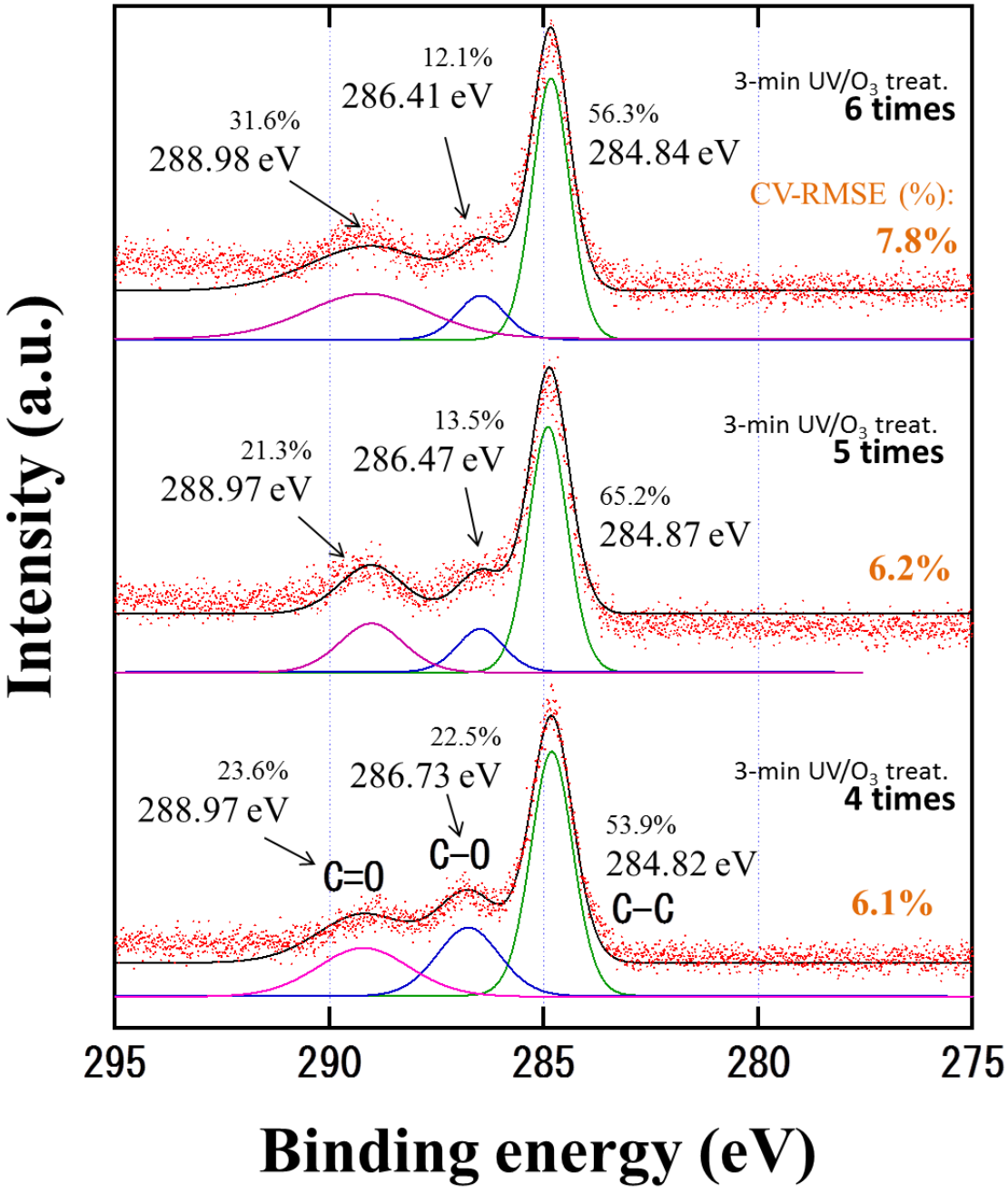

Fig. B-06 UV/O_3 treatment number dependence of doped oxygen quantity (treatment number ranged from four to six times, and treatment time for each UV/O_3-treatment was 3 min).

UV/O_3 treatment number dependence (one to six times)

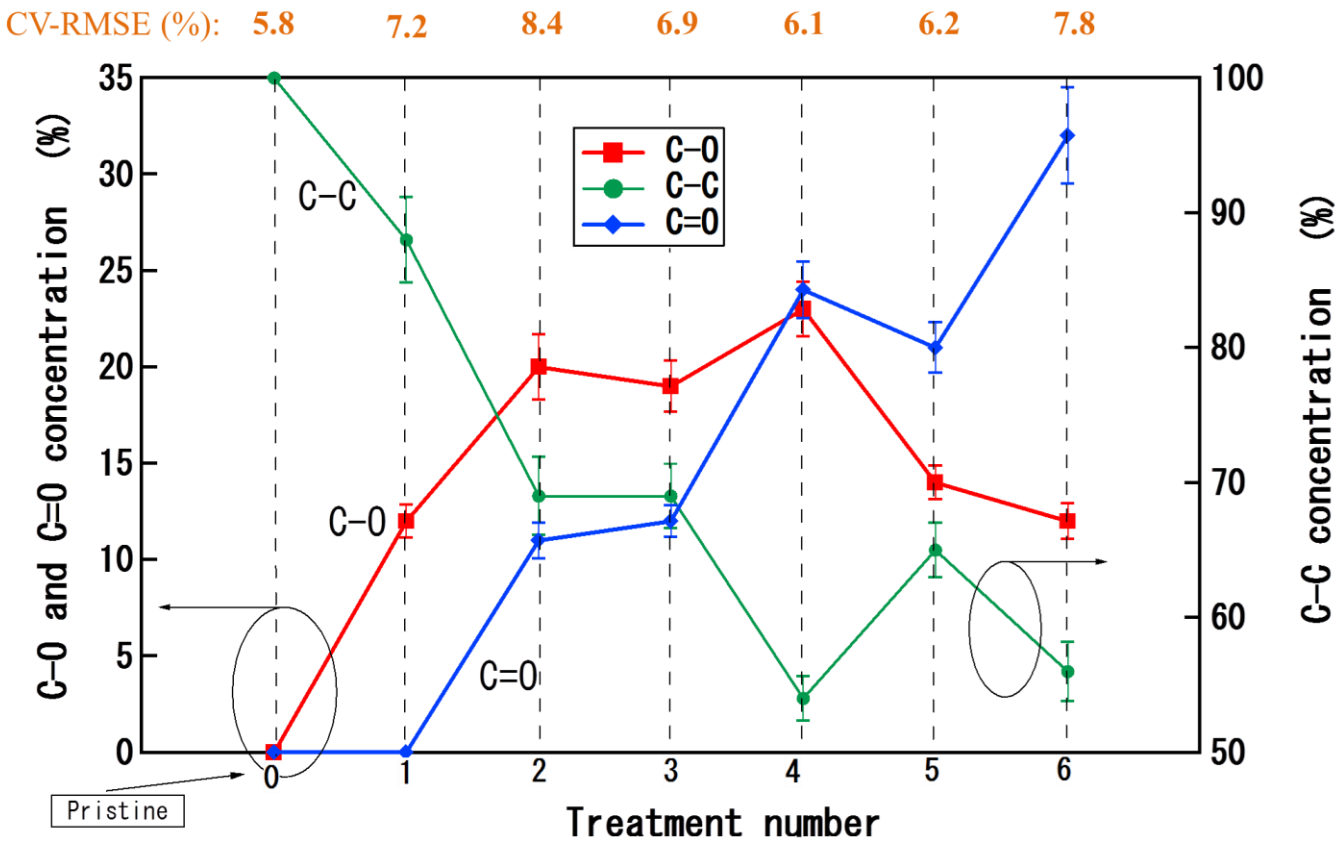

Fig. B-07 UV/O_3 treatment number dependence of doped oxygen quantity (treatment number ranged from 0 to 6 times, and treatment time for each UV/O_3-treatment was 3 min).

Reduction through UV-irradiation (first cycle)

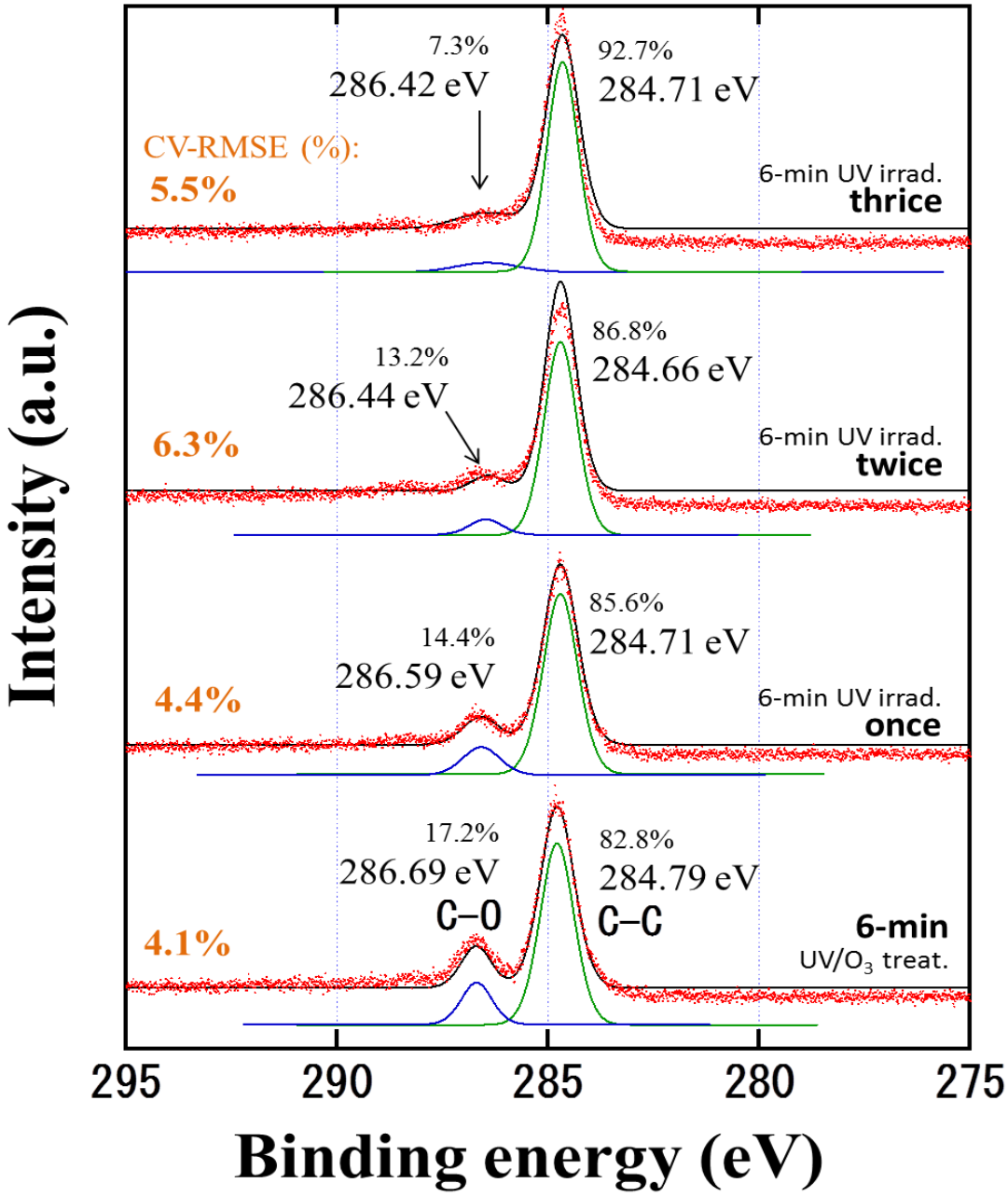

Fig. B-08 XPS spectra of graphene oxide after conducting 6-min UV-irradiation several times.

Reduction through UV-irradiation (second cycle)

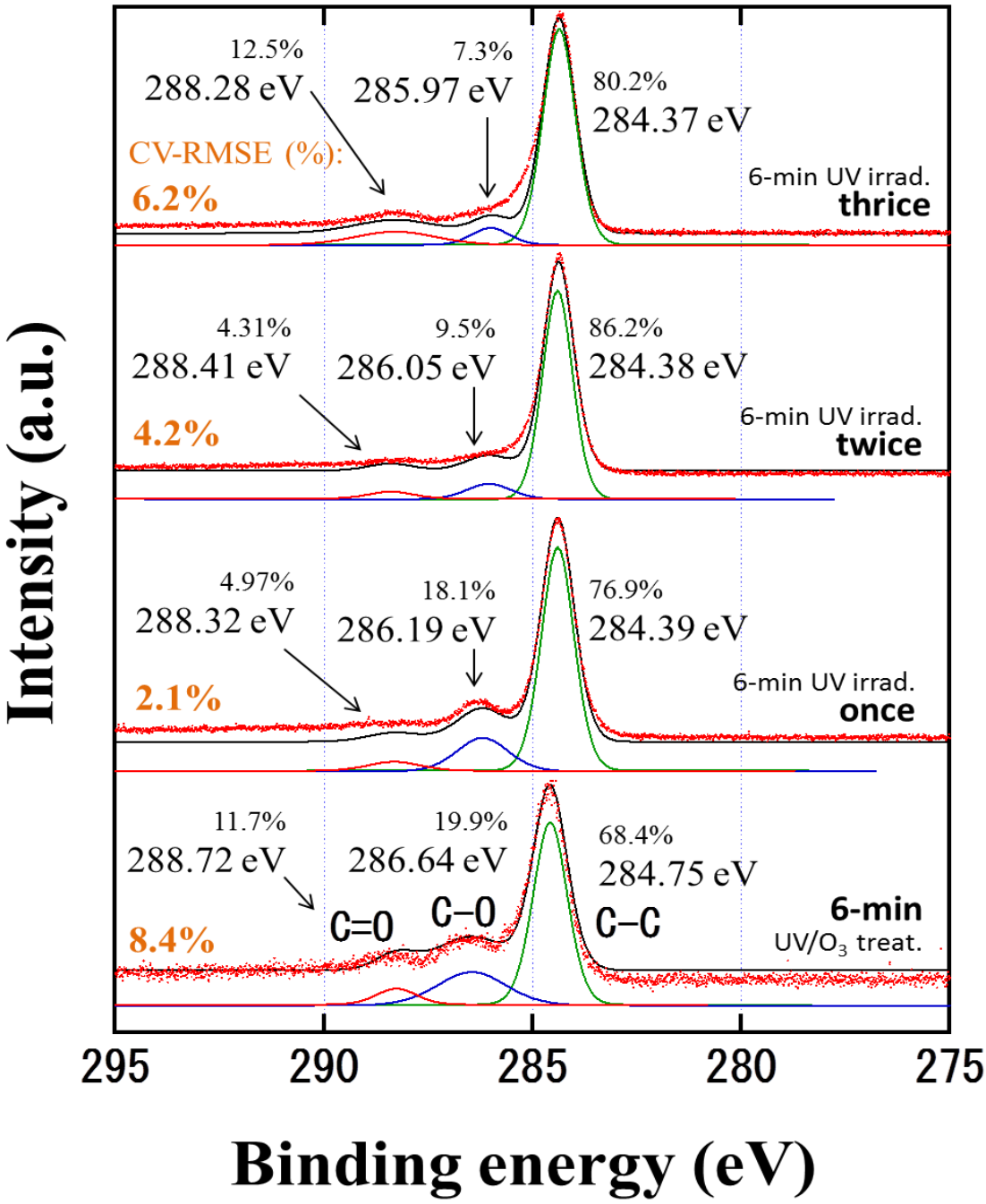

Fig. B-09 XPS spectra of graphene oxide after conducting 6-min UV-irradiation several times.

Two cycles of redox processes

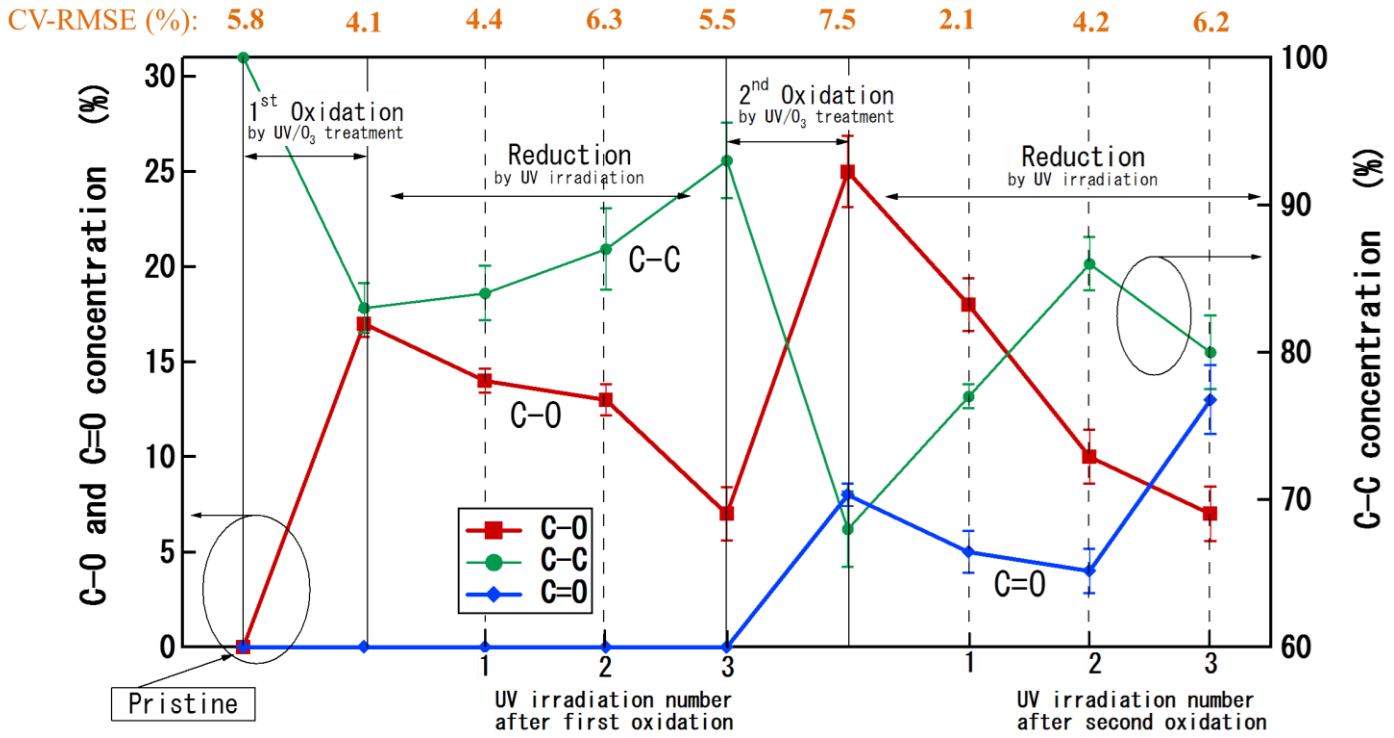

Fig. B-10 Quantity of doped oxygen after two cycles of oxidation and reduction process.

Section C:

Electrical Characterization

Exact values of electron mobility and changes in Raman spectra of graphene-FETs after redox process are shown in this section. P type and N type electron mobility of three identical graphene-FETs after two cycles of redox processes are shown in Table C-I and C-II. Values stated in the tables are manifested in Figure 6 in the main paper. Changes in Raman spectra of three identical graphene-FETs after redox process are shown in Figure C-1 to C-2. The intensity of defect-derived D band increased after two cycles of redox process, however the sharpness of 2D band, which indicates that the graphene film is one layer, remained unchanged.

Table C-I P type electron mobility of three identical graphene-FETs after two cycles of redox processes

Process / Device No.	P type mobility ($cm^2/V \cdot s$)								
	1			2			3		
	mean	SE*	SD**	mean	SE*	SD**	mean	SE*	SD**
Initial graphene	4463	52	525	4428	40	450	4238	46	467
First redox:									
$UV/0_3$-treatment	3241	50	618	3821	42	520	3531	71	767
1^{st} UV-irradiation	4537	39	476	3688	44	315	3453	48	485
2^{nd} UV-irradiation	3857	38	427	3890	34	284	4056	23	166
Second redox:									
$UV/0_3$-treatment	2186	23	302	2200	30	365	2277	28	298
1^{st} UV-irradiation	3002	37	561	3190	39	390	3149	24	210
2^{nd} UV-irradiation	3446	53	535	3477	27	271	3446	53	535
3^{rd} UV-irradiation	3527	47	526	3830	29	253	4192	23	162
4^{th} UV-irradiation	3714	21	181	3797	19	172	3809	25	237

*) SE is standard error.
**) SD is standard deviation.

Table C-II N type electron mobility of three identical graphene-FETs after two cycles of redox processes

Process / Device No.	N type mobility ($cm^2/V \cdot s$)								
	1			2			3		
	mean	SE*	SD**	mean	SE*	SD**	mean	SE*	SD**
Initial graphene	3165	40	287	3043	39	337	2946	38	329
First redox:									
$UV/0_3$-treatment	1498	71	713	1495	53	536	2061	63	453
1^{st} UV-irradiation	2455	48	418	2281	40	350	2414	66	335
2^{nd} UV-irradiation	2122	42	364	2149	35	286	2584	49	348
Second redox:									
$UV/0_3$-treatment	40	21	181	96	8	98	134	13	133
1^{st} UV-irradiation	417	25	286	431	26	259	444	16	179
2^{nd} UV-irradiation	596	35	396	543	27	233	587	30	375
3^{rd} UV-irradiation	628	28	279	780	14	142	846	16	157
4^{th} UV-irradiation	727	25	181	827	15	108	843	30	213

*) SE is standard error.
**) SD is standard deviation.

Raman spectra of device No. 1

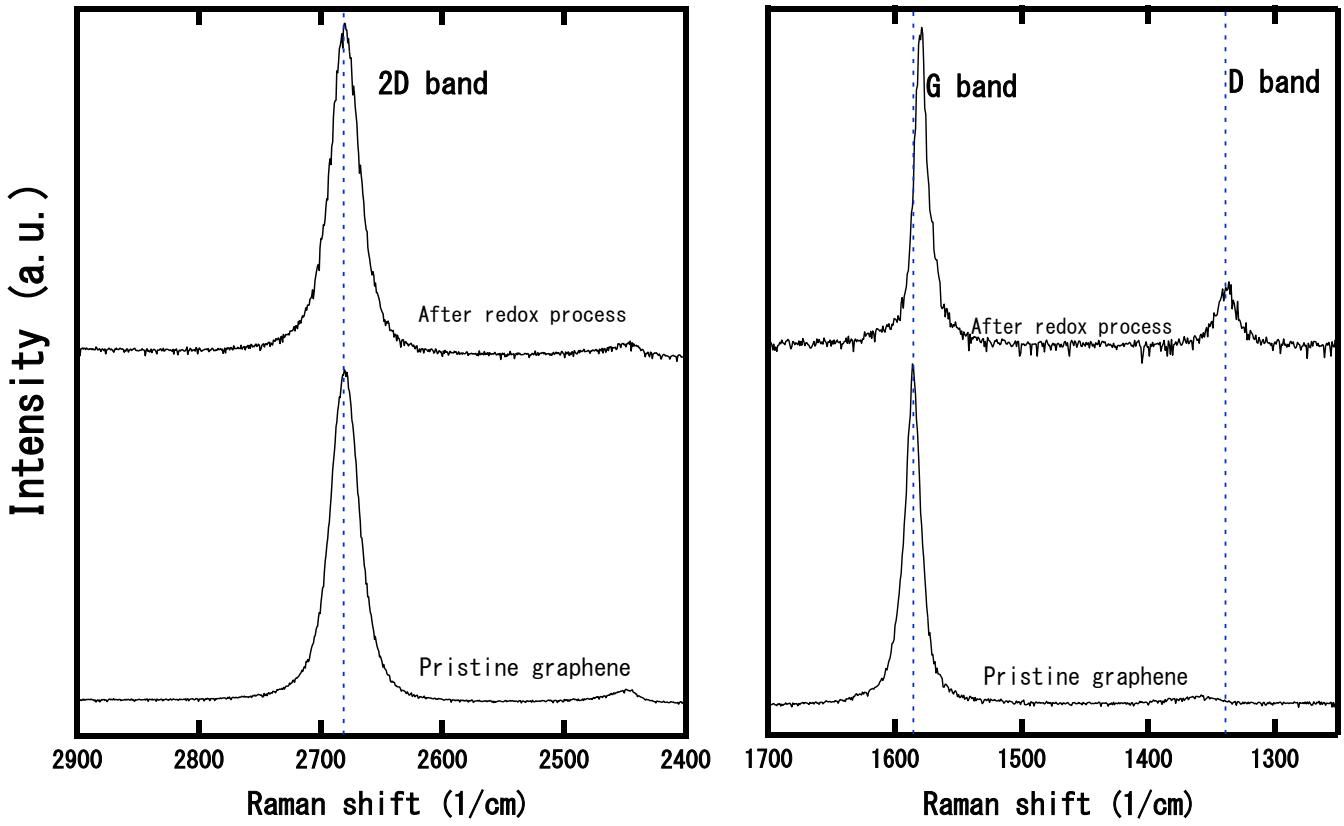

Fig. C-1(a) Raman spectra of device No. 1 after two cycles of oxidation and reduction process.

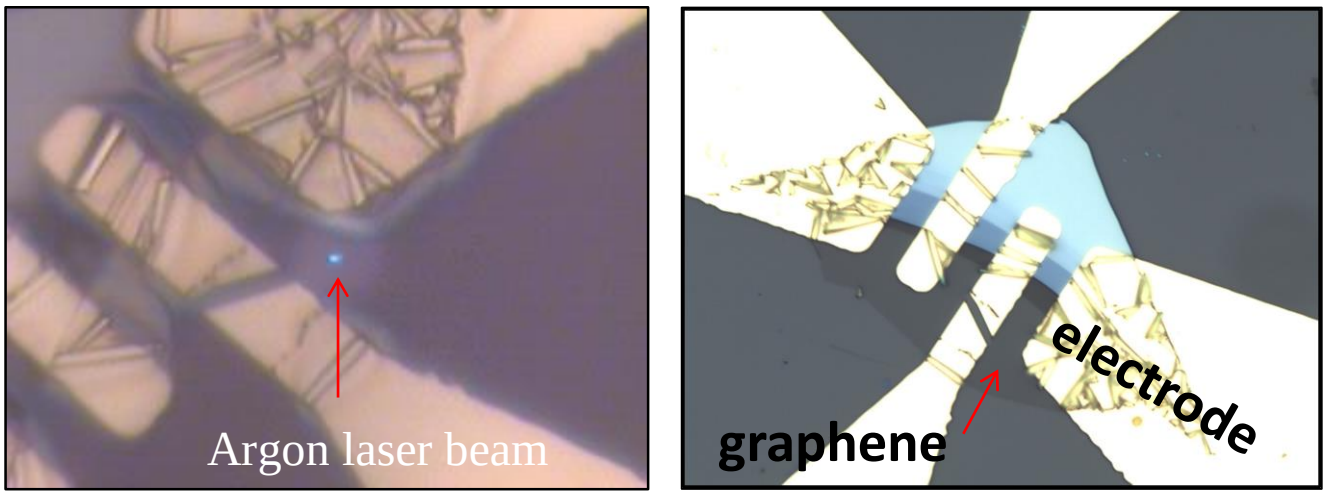

Fig. C-1(b) Raman spectroscopy measurement of device No. 1

Raman spectra of device No. 2

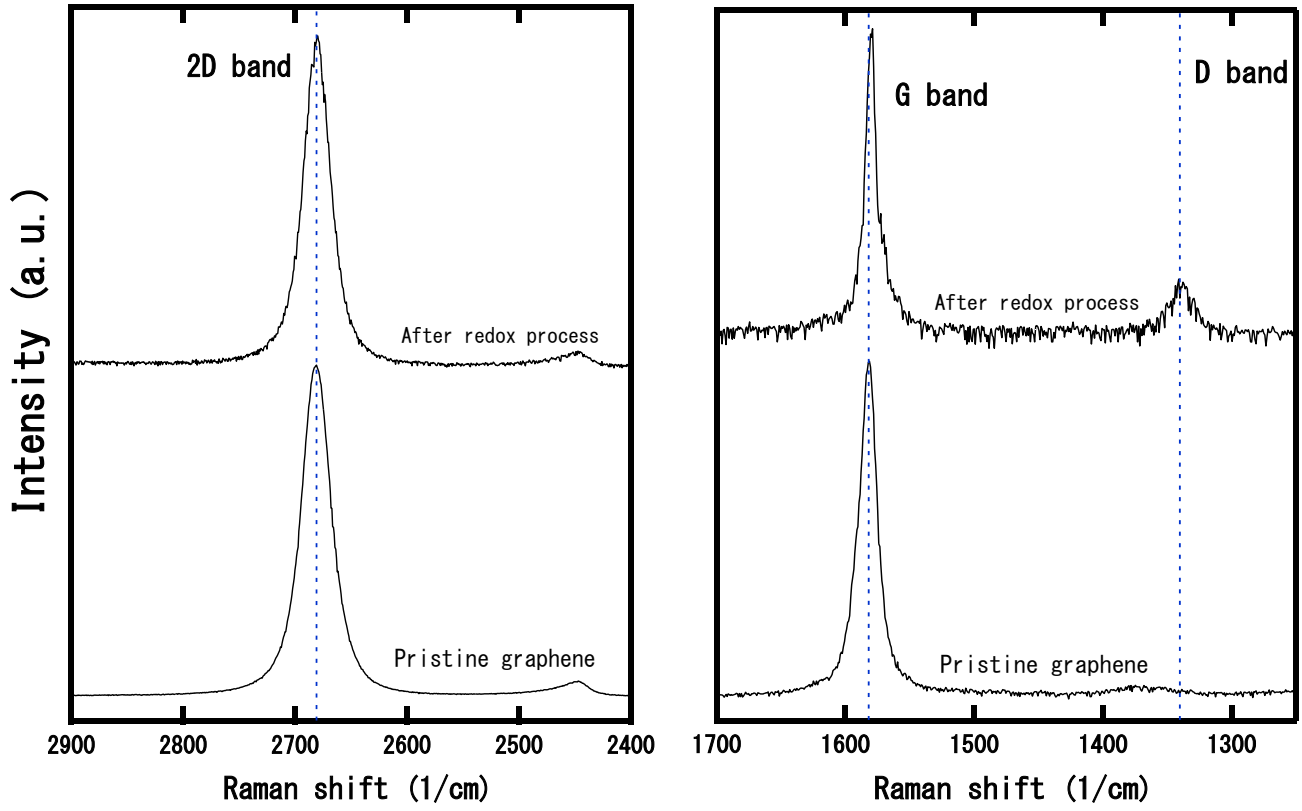

Fig. C-2(a) Raman spectra of device No. 2 after two cycles of oxidation and reduction process.

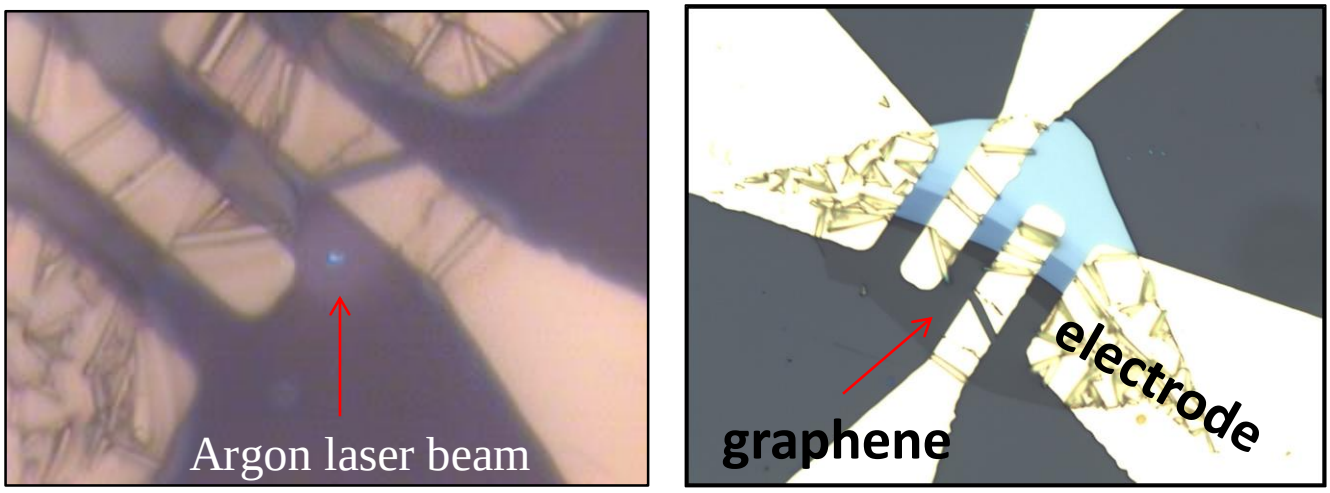

Fig. C-2(b) Raman spectroscopy measurement of device No. 2

Raman spectra of device No. 3

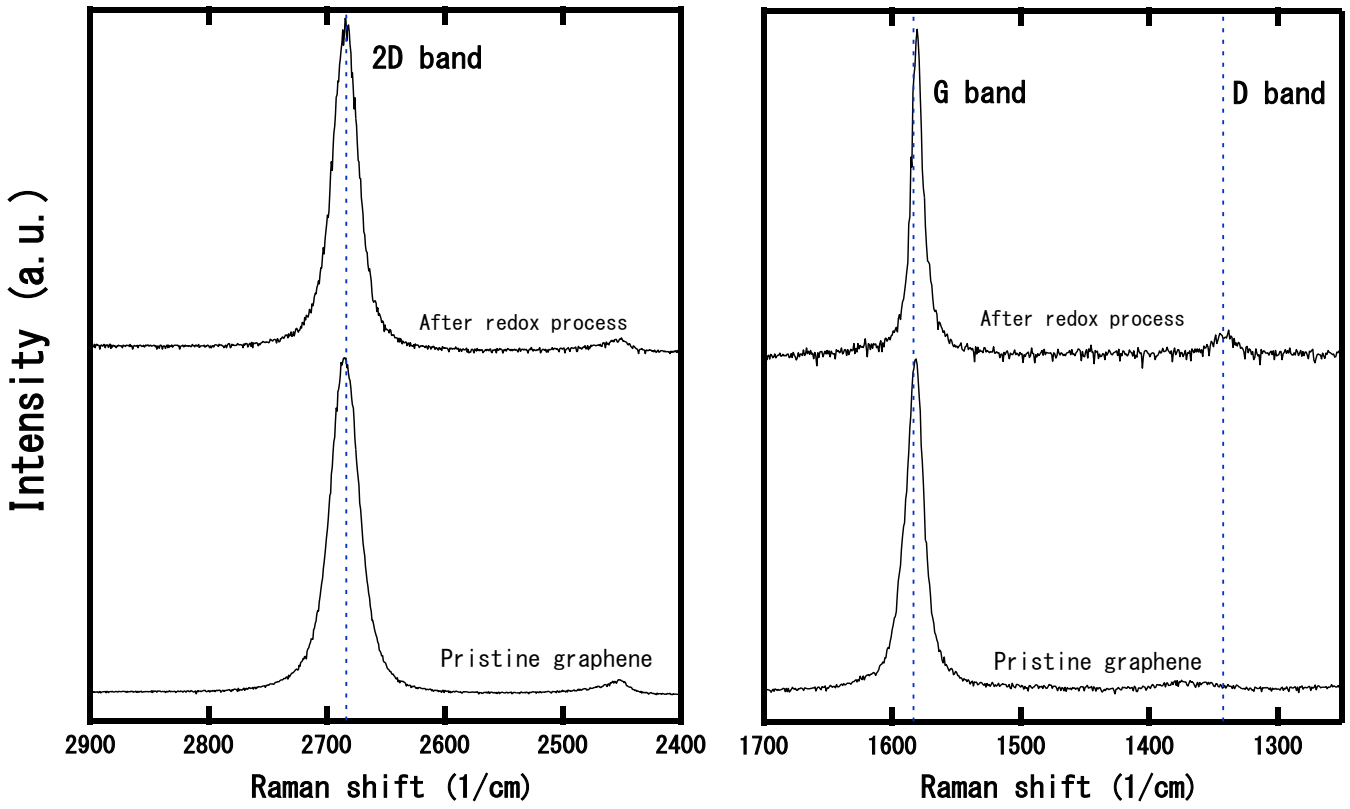

Fig. C-3(a) Raman spectra of device No. 3 after two cycles of oxidation and reduction process.

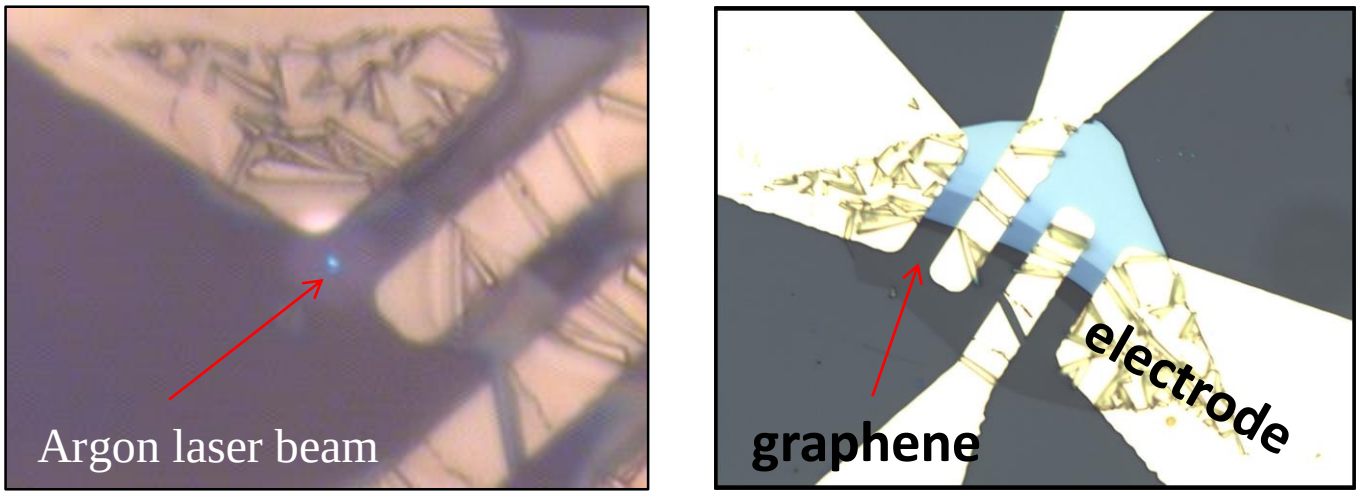

Fig. C-3(b) Raman spectroscopy measurement of device No. 3

Section D:

Raman Spectroscopy Measurement

Raman spectra of three exfoliated graphene films after each treatment during two cycles of redox processes are presented in this section. Detailed features such as full width at half maximum of each band (FWHM), peak position of G band and D/G band intensity ratio are summarized in Table D-I to D-V. Exact values of D/G band intensity ratio plotted in Figure 7 in the main paper are shown in Table D-I.

Table D-I D/G band intensity ratio of Raman spectroscopy of three exfoliated graphene layers after two cycles of redox processes

Process / Graphene No.	D/G band intensity ratio		
	1	2	3
First redox			
Initial graphene	0.029 ± 0.003	0.13 ± 0.01	0.11 ± 0.01
UV/0_3-treatment	0.120 ± 0.010	0.25 ± 0.02	0.25 ± 0.02
1^{st} UV-irradiation	0.039 ± 0.012	0.16 ± 0.02	0.19 ± 0.02
2^{nd} UV-irradiation	0.009 ± 0.005	0.11 ± 0.01	0.19 ± 0.01
3^{rd} UV-irradiation	0.019 ± 0.006	0.14 ± 0.03	0.18 ± 0.02
Second redox			
UV/0_3-treatment	0.139 ± 0.008	0.47 ± 0.02	0.40 ± 0.01
1^{st} UV-irradiation	0.041 ± 0.003	0.27 ± 0.02	0.27 ± 0.03
2^{nd} UV-irradiation	0.044 ± 0.007	0.35 ± 0.02	0.31 ± 0.01
3^{rd} UV-irradiation	0.042 ± 0.002	0.30 ± 0.02	0.32 ± 0.03

Table D-II Full width at half maximum of G band of three exfoliated graphene layers after two cycles of redox processes

Process / Graphene No.	G band FWHM (1/cm)		
	1	2	3
First redox			
Initial graphene	8.78 ± 0.01	8.82 ± 0.01	8.61 ± 0.01
UV/0_3-treatment	10.92 ± 0.01	10.62 ± 0.02	10.83 ± 0.03
1st UV-irradiation	10.96 ± 0.01	9.92 ± 0.02	9.77 ± 0.03
2nd UV-irradiation	8.52 ± 0.01	7.23 ± 0.01	7.46 ± 0.01
3rd UV-irradiation	6.97 ± 0.02	6.40 ± 0.02	8.62 ± 0.02
Second redox			
Initial graphene	6.97 ± 0.02	6.40 ± 0.02	8.62 ± 0.02
UV/0_3-treatment	12.85 ± 0.07	13.86 ± 0.02	13.50 ± 0.03
1st UV-irradiation	9.96 ± 0.02	11.03 ± 0.03	11.35 ± 0.06
2nd UV-irradiation	11.12 ± 0.01	14.03 ± 0.01	11.84 ± 0.03
3rd UV-irradiation	11.18 ± 0.01	12.43 ± 0.06	12.03 ± 0.02

Table D-III Position of G band of three exfoliated graphene layers after two cycles of redox processes

Process / Graphene No.	G band position (1/cm)		
	1	2	3
First redox			
Initial graphene	1584.68	1592.75	1591.94
UV/0_3-treatment	1582.25	1584.67	1583.06
1st UV-irradiation	1583.06	1583.87	1585.48
2nd UV-irradiation	1586.29	1586.29	1585.48
3rd UV-irradiation	1590.33	1591.13	1590.32
Second redox			
Initial graphene	1591.94	1591.13	1590.32
UV/0_3-treatment	1582.25	1587.10	1587.10
1st UV-irradiation	1588.71	1588.71	1587.90
2nd UV-irradiation	1587.94	1587.90	1587.90
3rd UV-irradiation	1588.71	1587.10	1587.90

Table D-IV Full width at half maximum of 2D band of three exfoliated graphene layers after two cycles of redox processes

Process / Graphene No.	2D band FWHM (1/cm)		
	1	2	3
First redox			
Initial graphene	25.76 ± 0.01	26.35 ± 0.02	26.38 ± 0.04
UV/0_3-treatment	26.43 ± 0.03	26.83 ± 0.07	26.59 ± 0.03
1st UV-irradiation	26.85 ± 0.07	26.51 ± 0.02	26.03 ± 0.02
2nd UV-irradiation	26.87 ± 0.01	25.95 ± 0.01	25.86 ± 0.05
3rd UV-irradiation	26.11 ± 0.14	25.89 ± 0.01	26.74 ± 0.05
Second redox			
Initial graphene	26.11 ± 0.14	25.89 ± 0.01	26.74 ± 0.05
UV/0_3-treatment	28.46 ± 0.03	26.76 ± 0.03	26.53 ± 0.03
1st UV-irradiation	26.59 ± 0.02	26.01 ± 0.02	25.79 ± 0.45
2nd UV-irradiation	26.74 ± 0.03	26.05 ± 0.02	26.81 ± 0.04
3rd UV-irradiation	26.44 ± 0.01	26.33 ± 0.02	25.61 ± 0.03

Table D-V Full width at half maximum of D band of graphene No. 2 and 3 after two cycles of redox processes

Process / Graphene No.	D band FWHM (1/cm)	
	2	3
First redox		
Initial graphene	15.99 ± 0.19	19.23 ± 0.09
UV/0_3-treatment	15.91 ± 0.33	16.55 ± 0.33
1st UV-irradiation	14.32 ± 0.34	14.30 ± 0.13
2nd UV-irradiation	10.56 ± 0.09	16.64 ± 0.04
3rd UV-irradiation	13.85 ± 0.03	16.71 ± 0.18
Second redox		
Initial graphene	13.85 ± 0.03	16.71 ± 0.18
UV/0_3-treatment	16.10 ± 0.11	15.44 ± 0.07
1st UV-irradiation	15.34 ± 0.03	15.90 ± 0.07
2nd UV-irradiation	14.30 ± 0.01	15.06 ± 0.19
3rd UV-irradiation	16.32 ± 0.11	16.11 ± 0.07

Note: (regarding 3-min UV/O_3-treatment and 3-min UV-irradiation on exfoliated graphene)

Besides the changes in D/G band intensity ratio, FWHM and peak position of G band obviously changed correspondingly with the oxidation and reduction process. As stated in Table D-II, there is a tendency that the FWHM of G band became wider after oxidation through UV/O_3-treatment, and then gradually recovered after several reductions through UV-irradiation. As seen in the G band spectra and Table D-III, there is a tendency that the position of G band peak apparently shifted to the lower wavelength, and then shifted back to the initial position after several reductions through UV-irradiation.

We observed that there are changes in the FWHM of 2D band, as stated in Table D-IV. However, since the degree of changes was very small, we were not able to draw any conclusion regarding the changes in FWHM of 2D band.

The changes in FWHM of D band are shown in Table D-V. Because the D band of graphene No. 1 was very small, the spectra processing machine was not able to accurately compute the FWHM of D band of graphene No. 1. Although the peak intensity or area of D band noticeably decreased after reduction process, we found that the FWHM of D band did not change correspondingly with oxidation and reduction process.

However, the overall degree of change in FWHM and peak position was relatively small, except for changes in D/G band intensity ratio which were relatively apparent. Therefore, to reproduce statistically more reliable data some improvement on measurement, such as conducting the Raman spectroscopy measurement on several spots or using as many graphene films as possible or even using Raman spectrometer with higher resolution, could be implied.

Section E:

6-min UV/O_3-treatment on Exfoliated Graphene

(Additional Experiment)

An additional experiment where an exfoliated graphene film was UV/O_3-treated for 6 min are shown in this section. This treatment time (6 min) is twice longer than treatment time of the experiment of three exfoliated graphene films shown in previous section (3 min). After conducting UV/O_3-treatment for 6 min, oxidized graphene was reduced by performing 6-min UV-irradiation several times. Raman spectra obtained from the measurement (Figure E-1) are shown in Figure E-2 to E-3. D band spectra where the greatest difference in band intensity or area observed are presented in Figure E-4. Changes in D/G band intensity ratio after each oxidation and reduction process are plotted in Figure E-5. Detailed features such as full width at half maximum of each band, peak position of G band are summarized in Table E-I to E-II.

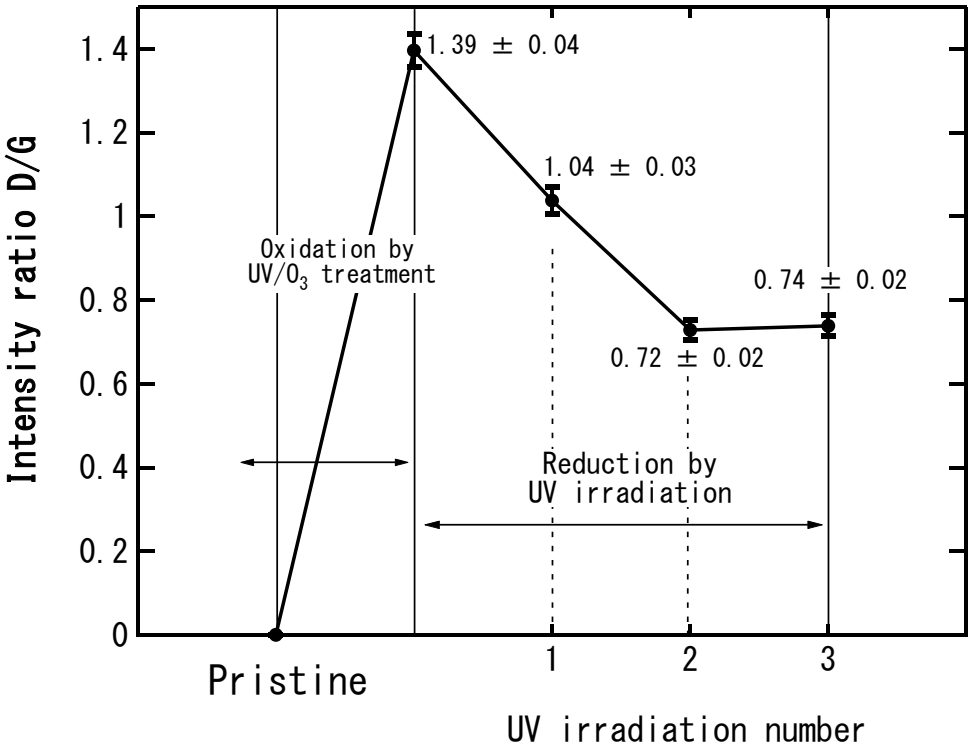

Fig. E-5 D/G band intensity ratio of graphene No. 4 during redox process.

Table E-I Full width at half maximum of G band, D band and 2D band of graphene No. 4 during redox process

Process	FWHM (1/cm)		
	G band	D band	2D band
Initial graphene	14.25 ± 0.12	none	30.77 ± 0.04
UV/0_3-treatment	15.74 ± 0.03	28.30 ± 0.04	50.89 ± 0.03
1st UV-irradiation	13.72 ± 0.12	28.43 ± 0.19	52.50 ± 0.02
2nd UV-irradiation	16.47 ± 0.03	26.26 ± 0.07	50.76 ± 0.05
3rd UV-irradiation	15.56 ± 0.01	26.31 ± 0.03	52.33 ± 0.05

Table E-II Position of G band peak of graphene No. 4 during redox process

Process	G band peak position (1/cm)
Initial graphene	1586.29
UV/0_3-treatment	1578.28
1st UV-irradiation	1579.02
2nd UV-irradiation	1581.45
3rd UV-irradiation	1581.45

Note: (regarding 6-min UV/O_3-treatment and 6-min UV-irradiation on exfoliated graphene)

The D/G band intensity ratio increased from zero to 1.39 ± 0.04 after conducting UV/O_3-treatment for 6 min, meaning that the D band had larger area than the G band as shown in Figure E-3. This may indicate that by conducting UV/O_3-treatment for 6 min the quantity of doped oxygen were greater than 3-min UV/O_3-treatment. We also confirmed the existence of a small peak located near the G band known as the D' band, which is also derived

from lattice disorder or defects. This existence of D' band together with a huge area of D band may point to the possibility that after conducting UV/O_3-treatment for 6 min, besides doped oxygen, a certain degree of defects or hole (as shown in section A) might probably introduced. The formation of holes may not be recovered by only performing reduction through UV-irradiation. That may be a reason why the reversibility is not 100%.

Nevertheless, the D/G band intensity ratio decreased after performing 6-min UV-irradiation several times, indicating that the oxidized graphene was successfully reduced. Along with that, the FWHM of D band also slightly decreased after conduction UV-irradiation.

There might be also a tendency that the FWHM of G band slightly increased after oxidation and decreased after reduction. However, since the magnitude of changes was relatively small, additional research is required to verify the change in the FWHM of G band. The FWHM of 2D band significantly increased after conducting UV/O_3-treatment for 6 min, however it did not show any substantial recovery after performing 6-min UV-irradiation several times.

Section F:

Ambipolar characteristics for various metal contacts

Ni metal contact:

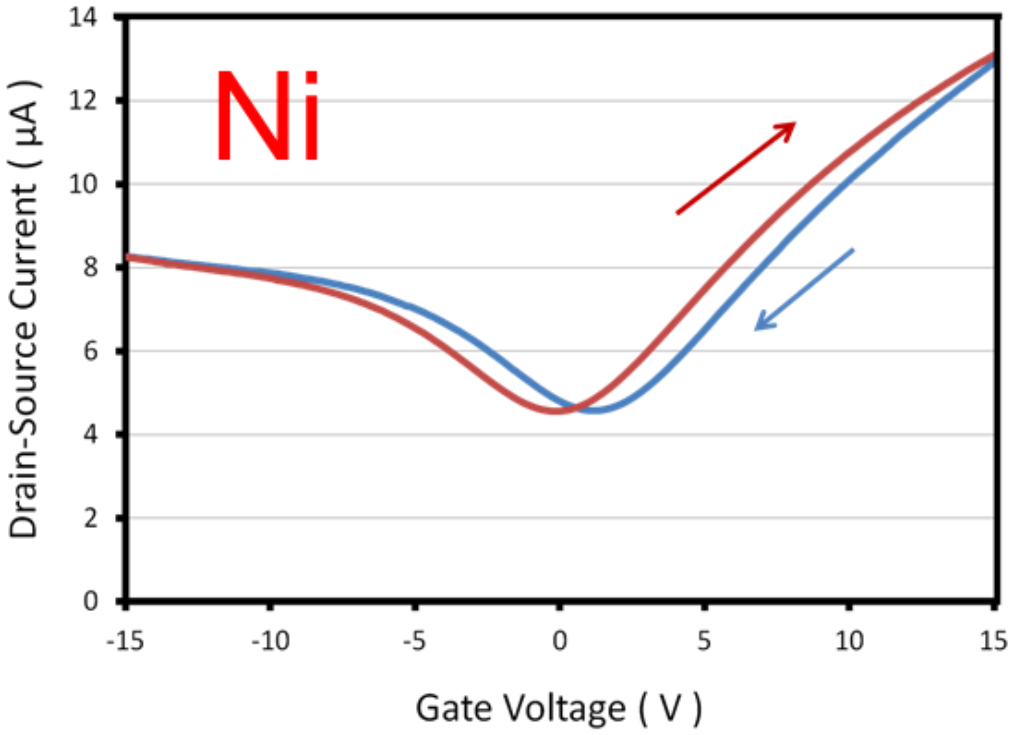

Fig. F-1. Ambipolar characteristics of G-FET with Ni metal contact.

Au/Cr metal contact:

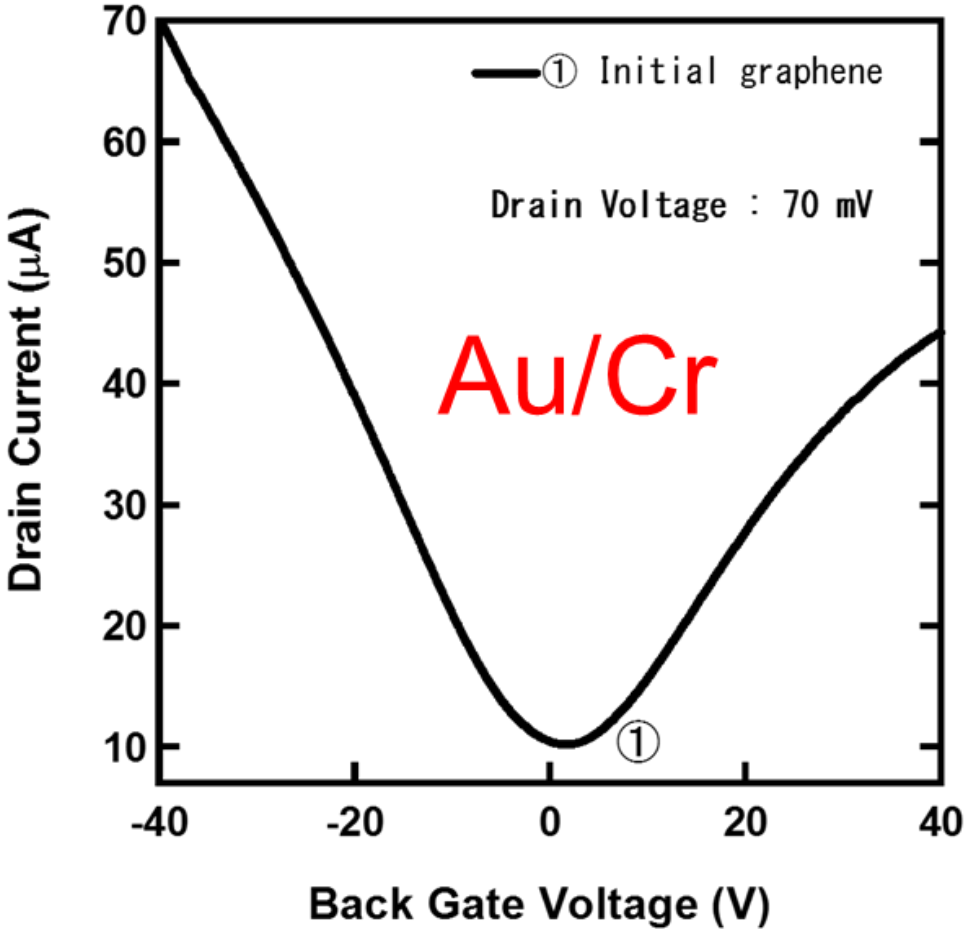

Fig. F-2. Ambipolar characteristics of G-FET with Au/Cr metal contact.

Au/TiN metal:

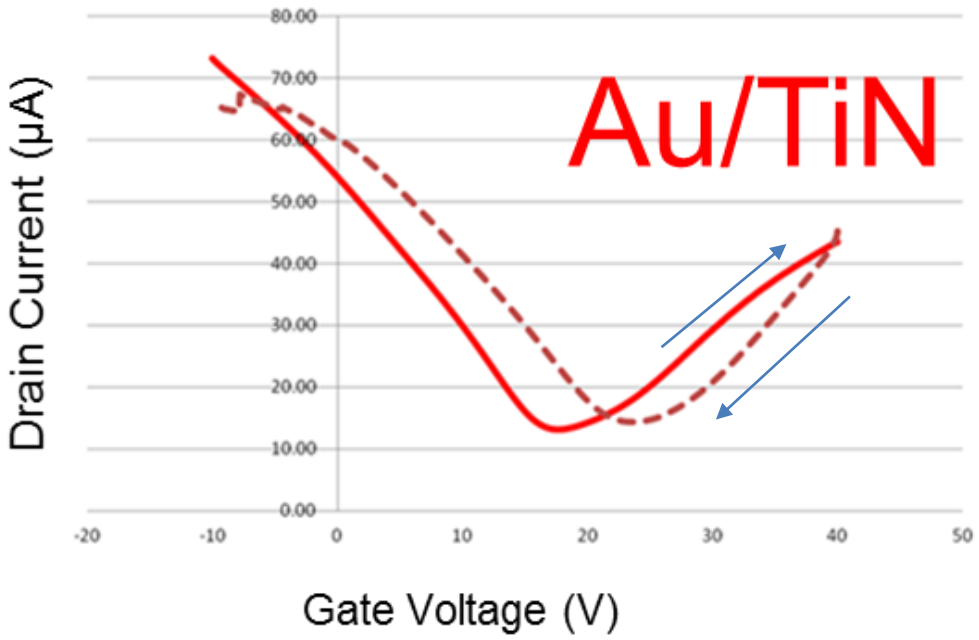

Fig. F-3. Ambipolar characteristics of G-FET with Au/TiN metal contact.

Section G:

SEM images of adsorbed ferritin

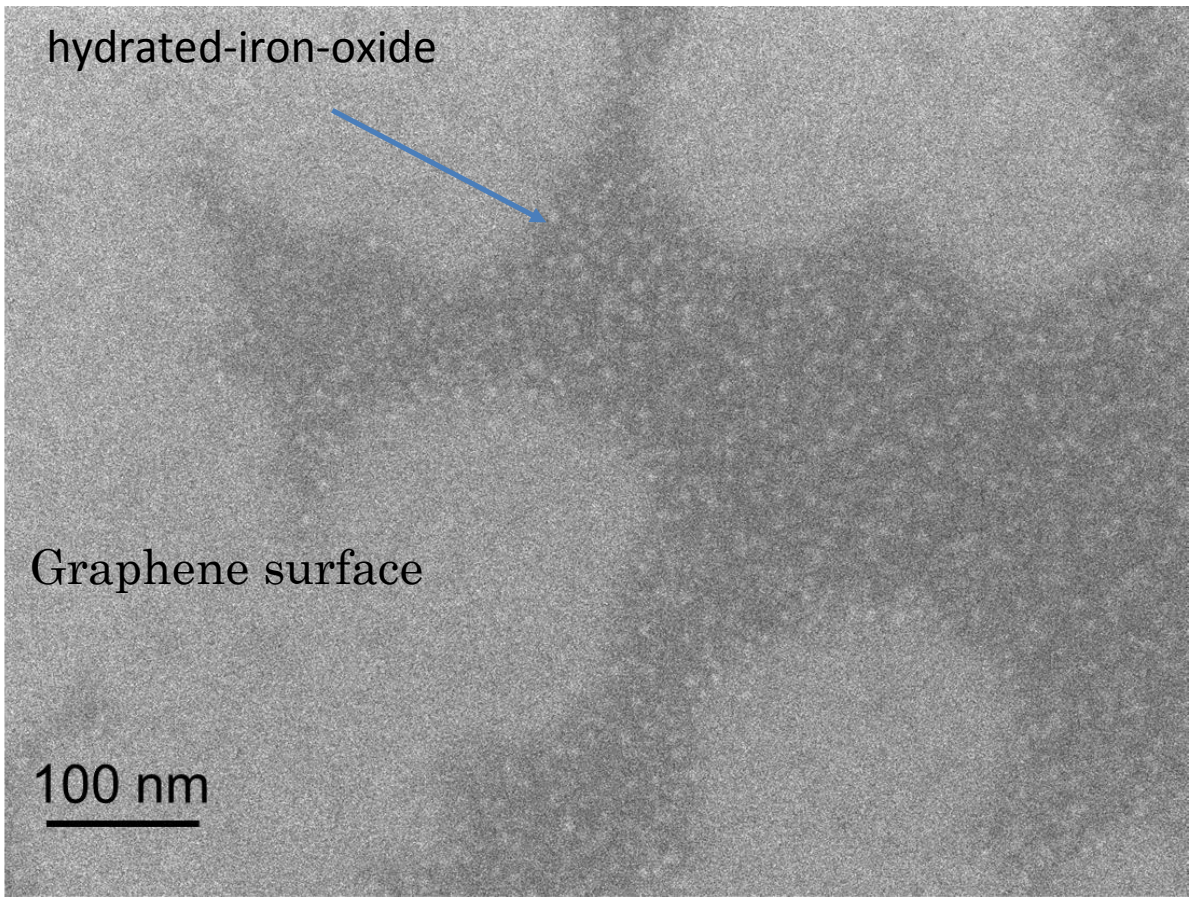

Figure G-1. SEM image of ferritin on graphene surface after first adsorption of ferritin aqueous solution. The white particles are the hydrated-iron-oxide inside the ferritin.

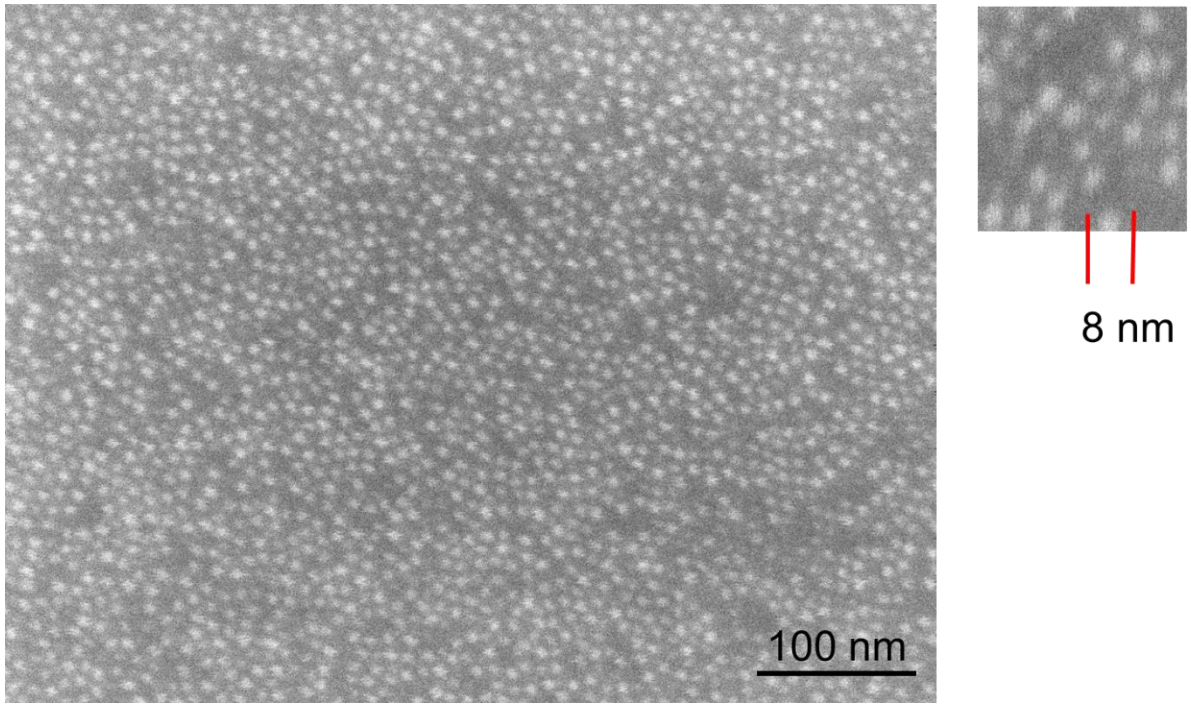

Figure G-2. SEM image of ferritin on graphene surface after second adsorption of ferritin aqueous solution. The white particles are the hydrated-iron-oxide inside the ferritin. The size of the iron-oxide was around 7 - 8 nm.

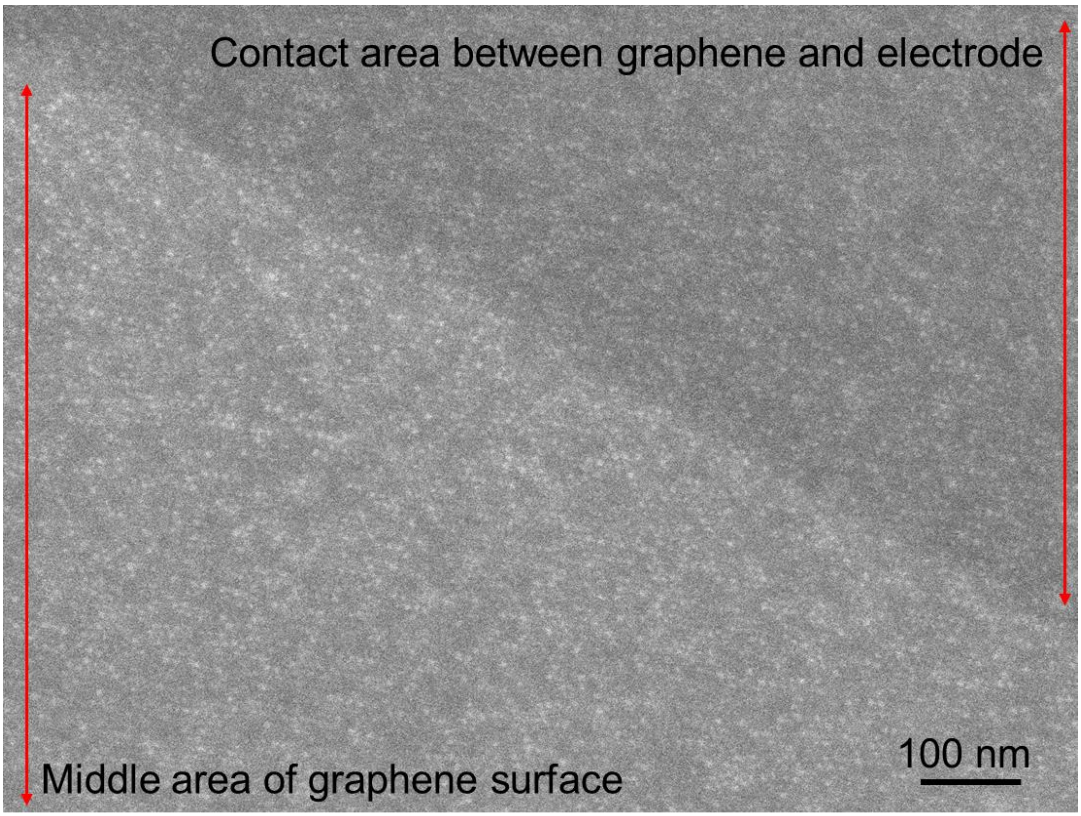

Figure G-3. SEM image of ferritin adsorbed around contact area between graphene and electrode after second adsorption of ferritin aqueous solution. The contact area is darker, indicating that a significant number of ferritins are stacked up or accumulated.

Section H:

K-AFM images of EB-irradiated ferritin

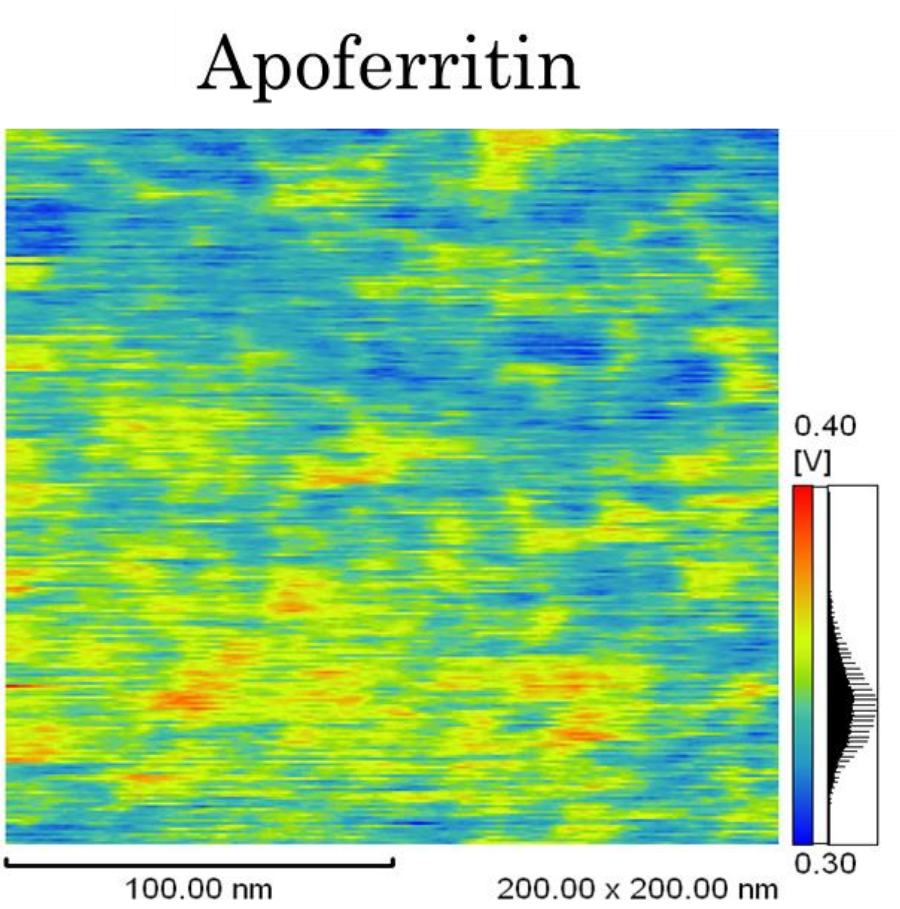

Figure H-1. K-AFM image of EB-irradiated ferritin